Aus dem Zentrum für Neurochirurgie der Universität zu Köln
Klinik für Allgemeine Neurochirurgie
Direktor: Universitätsprofessor Dr. med. R. Goldbrunner

Functional Reorganization of the Somatosensory System in Degenerative Cervical Myelopathy

Inaugural-Dissertation zur Erlangung der Doktorwürde
der Medizinischen Fakultät
der Universität zu Köln

vorgelegt von
Leonie Hams
aus Köln

promoviert am 18. Dezember 2023

Gedruckt mit Genehmigung der Medizinischen Fakultät der Universität zu Köln

2024

Dekan: Universitätsprofessor Dr. med. G. R. Fink

1. Gutachterin: Privatdozentin Dr. med. C. Weiß Lucas
2. Gutachter: Privatdozent Dr. med. M. B. Sommerauer

Erklärung

Ich erkläre hiermit, dass ich die vorliegende Dissertationsschrift ohne unzulässige Hilfe Dritter und ohne Benutzung anderer als der angegebenen Hilfsmittel angefertigt habe; die aus fremden Quellen direkt oder indirekt übernommenen Gedanken sind als solche kenntlich gemacht.

Bei der Auswahl und Auswertung des Materials sowie bei der Herstellung des Manuskriptes habe ich Unterstützungsleistungen von folgenden Personen erhalten:

Frau Priv.-Doz. Dr. Carolin Weiß Lucas
Frau Dr. rer. nat. Charlotte Nettekoven

Weitere Personen waren an der Erstellung der vorliegenden Arbeit nicht beteiligt. Insbesondere habe ich nicht die Hilfe einer Promotionsberaterin/eines Promotionsberaters in Anspruch genommen. Dritte haben von mir weder unmittelbar noch mittelbar geldwerte Leistungen für Arbeiten erhalten, die im Zusammenhang mit dem Inhalt der vorgelegten Dissertationsschrift stehen.

Die Dissertationsschrift wurde von mir bisher weder im Inland noch im Ausland in gleicher oder ähnlicher Form einer anderen Prüfungsbehörde vorgelegt.

Die im Rahmen dieser Arbeit präsentierten Daten entstanden im Rahmen eines lokalen Spin-Off-Projektes der prospektiven, multizentrischen CReMe Studie (Cerebral Reorganization in Cervical Myelopathy Measured by Navigated Transcranial Magnetic Stimulation multicenter study, registriert unter clinicaltrials.gov, Nr.: 898 30 535).

Die Projekt-Idee, die funktionelle Reorganisation des somatosensiblen Systems bei DCM-Patienten zu untersuchen, wurde von mir selbst eingebracht; die Integration der Idee in ein Studiendesign erfolgte maßgeblich durch Frau Priv.-Doz. Dr. Carolin Weiß Lucas und Frau Dr. rer. nat. Charlotte Nettekoven.

Die Rekrutierung von Teilnehmern für die Studie erfolgte durch mich mit Unterstützung von Frau Priv.-Doz. Dr. Carolin Weiß Lucas und Frau Sophia Kochs.

Die dieser Arbeit zugrunde liegenden fMRT-Messungen sind nach entsprechender Anleitung unter meiner Mitwirkung im Team mit Frau Priv.-Doz. Dr. Carolin Weiß Lucas, Frau Dr. rer. nat. Charlotte Nettekoven, Herrn Phillip Keil und Frau Claudia Müller (medizinisch-technische Assistentin) durchgeführt worden.

Die Durchführung der neurologischen Untersuchungen erfolgte gemeinsam mit Frau Priv.-Doz. Dr. Carolin Weiß Lucas, Frau Dr. Catharina Schröter und Frau Dr. Julia Pieczewski.

Messungen von somatosensibel evozierten Potentialen (SSEPs) wurden durch Irina Sommer (neurophysiologisch-technische Assistentin) und Frau Dr. rer. nat. Charlotte Nettekoven durchgeführt.

Die klinischen Funktionstests (z.B. Gangtest, Finger Tapping Test) und Befragungen wurden nach entsprechender Einarbeitung in der Regel von mir allein durchgeführt.

Die Auswertung und Analyse der klinischen sowie der fMRT-Daten erfolgte durch mich.

Erklärung zur guten wissenschaftlichen Praxis:

Ich erkläre hiermit, dass ich die Ordnung zur Sicherung guter wissenschaftlicher Praxis und zum Umgang mit wissenschaftlichem Fehlverhalten (Amtliche Mitteilung der Universität zu Köln AM 132/2020) der Universität zu Köln gelesen habe und verpflichte mich hiermit, die dort genannten Vorgaben bei allen wissenschaftlichen Tätigkeiten zu beachten und umzusetzen.

Köln, den 28.08.2023

Unterschrift: .....

Danksagung

Zuerst möchte ich Frau Priv.-Doz. Dr. Carolin Weiß Lukas für ihre fachliche wie persönliche Betreuung und Förderung in den vergangenen Jahren meiner Promotion danken. Vielen Dank für deine Korrekturen und Ideen und die zahlreichen Möglichkeiten, die du mir während der Promotionszeit geboten hast.

Weiterhin gilt mein ausgesprochener Dank den Mitgliedern der Arbeitsgruppe Funktionelle Bildgebung, Neuromodulation und klinisch-experimentelle Neurophysiologie. Danke für den netten Austausch und die gute Zusammenarbeit. Besonderer Dank gilt Frau Dr. Charlotte Nettekoven für ihre Anleitung und ihre Betreuung. Ebenso möchte ich Claudia Müller (MFA), Sophia Kochs (Study Nurse) und Phillip Keil für ihre zuverlässige und engagierte Unterstützung und für die schöne gemeinsame Zeit danken.

Ein großer Dank gilt Prof. Dr. Roland Goldbrunner für die Möglichkeit, diese Promotion in seiner Klinik für Allgemeine Neurochirurgie durchzuführen sowie für seine Unterstützung unserer Forschungsvorhaben.

Ebenso gilt mein ausgesprochener Dank unseren Projektpartner:innen der CReME Studie, insbesondere den Initiator:innen Frau Dr. Anna Zdunczyk und Prof. Dr. Peter Vajkoczy von der Klinik für Neurochirurgie der Charité Berlin sowie der Deutschen Wirbelsäulengesellschaft (DWG) für die Förderung des multizentrischen Projekts. Vielen Dank für den Austausch und die Kooperation!

Ganz besonders danken möchte ich meiner Familie und meinen Freunden, die an mich geglaubt haben und mich bisher in allem unterstützt haben, was ich begonnen habe. Und ich möchte meinem Freund sehr dafür danken, dass er mich so oft motiviert und aufgebaut hat. Ohne euren Rückhalt hätte diese Arbeit nicht entstehen können.

Content

Abbreviations

6MWT Six-Minute Walk Test

AMPA α-amino-3-hydroxy-5-methyl-4-isoxazolepropionic acid

BA Brodmann area

BOLD blood oxygenation level dependent

CoV coefficient of variation

CReMe Cerebral Reorganization in Cervical Myelopathy Measured by Navigated Transcranial Magnetic Stimulation

CSF cerebrospinal fluid

CSM cervical spondylotic myelopathy

CSS cervical spinal stenosis

CST contralateral corticospinal tract

CV cervical vertebra

DASH Disabilities of the Arm, Shoulder and Hand

DCM degenerative cervical myelopathy

DCML dorsal column medial lemniscus

DTI diffusion tensor imaging

DWI diffusion weighted imaging

ED Euclidean distance

EMG electromyography

EPI echo-planar imaging

EPs evoked potentials

FA fractional anisotropy

FDR false discovery rate

FID free induction decay

fNIRS functional near-infrared spectroscopy

FoV field of view

FTT Finger Tapping Test

FWE family-wise error

FWHM full width at half maximum

GE gradient echo

GE-EPI gradient-echo echo-planar-imaging

GLM general linear model

GM gray matter

HHD Hand-Held Dynamometry

HRF hemodynamic response function

ISI interstimulus interval

ITI intertrial interval

JOA Japanese Orthopaedic Association

LI lateralization index

M1 primary motor cortex

mITI mean intertap interval

MNI Montreal Neurological Institute

MPM maximum probability map

MR magnetic resonance

MRC Medical Research Council

MRI magnetic resonance imaging

NCS nerve conduction studies

NHPT Nine-Hole Peg Test

NMR nuclear magnetic resonance

nTMS navigated transcranial magnetic stimulation

RF radiofrequency

ROI region of interest

rTMS repetitive transcranial magnetic stimulation

S1 primary somatosensory cortex

S2 secondary somatosensory cortex

SCI spinal cord injury

SD standard deviation

SF-12 Short Form 12

SF-36 Short Form 36

SMA supplementary motor area

SPM statistical parametric map

SSEPs somatosensory evoked potentials

T1FTE T1 turbo field echo

TE echo time

TR repetition time

TTP time-to-peak

VOA volume of activation

VPL ventral posterior lateral thalamic nucleus

WM white matter

1. Zusammenfassung / Abstract

Hintergrund: Die degenerative zervikale Myelopathie (DCM) ist die häufigste Ursache erworbener Rückenmarksschäden im Erwachsenenalter und ihre Prävalenz steigt infolge der demographischen Entwicklung. Allerdings ist die Entscheidung über die Operationsindikation noch immer eine Herausforderung, da ausreichend reliable Prädiktoren für den klinischen Spontanverlauf und das Outcome fehlen. Unlängst wurde ein kompensatorisches Potential durch Neuroplastizität innerhalb des zerebrospinalen motorischen Netzwerks diskutiert. Somatosensible Einschränkungen als frühes, wenn auch häufig unbeachtetes Symptom der DCM waren bisher nicht im Mittelpunkt der Forschung. In vorliegender Arbeit wurde die Anpassung des somatosensiblen Systems bei DCM-Patienten mittels blood oxygenation level dependent (BOLD) funktioneller Magnetresonanztomographie (fMRT) untersucht.

Material und Methoden: 18 rechtshändige Teilnehmer, darunter 9 DCM-Patienten (Alter 56 ± 12 Jahre, 7 männlich) und 9 Kontrollen (Alter 57 ± 12 Jahre, 7 männlich) entsprechenden Alters und Geschlechts nahmen an einer fMRT-Untersuchung (3 Tesla) mit Block-Design teil. Das fMRT-Protokoll bestand aus alternierender, passiver somatosensibler Stimulation der Hand- und Fußrücken mit einem Filzstab. Mithilfe von MATLAB® 2019a und dem SPM12 Software Paket erfolgte eine Region of Interest (ROI)-weise Analyse der BOLD-Antwort auf Gruppen-Ebene durch eine dreifaktorielle Varianzanalyse (ANOVA) mit den Faktoren „Gruppe“ (Patienten/Kontrollen), „Extremität“ (Hand/Fuß) und „Seite“ (links/rechts). Die funktionelle hemisphärische Lateralisierung wurde durch Berechnung ROI-spezifischer Lateralisierungsindices untersucht. Ergänzend erfolgte eine umfassende klinische Beurteilung einschließlich klinischer Tests und Scores, neurologischer Untersuchung und somatosensibel evozierter Potentiale (SSEPs) des Nervus tibialis. Korrelationen zwischen BOLD-Aktivierung und klinischer Beeinträchtigung wurden mittels SPM-Multipler-Regressionsanalyse untersucht.

Ergebnisse: Sowohl Patienten als auch Kontrollen zeigten bei somatosensibler Stimulation der rechten (dominanten) Hand eine stark links-lateralisierte kortikale Antwort in S1 und S2 ($p \leq 0{,}05$, family-wise error (FWE)-korrigiert). Die Aktivierung war bei Patienten verglichen mit Kontrollen reduziert ($p \leq 0{,}001$, unkorrigiert). Für die anderen Tasks wiesen Kontrollen signifikante Antworten im somatosensiblen Kortex auf ($p \leq 0{,}05$, FWE-korrigiert); insbesondere eine konsistente Aktivierung im ipsilateralen S2. Im Gegensatz dazu ergab sich für die Patienten nur eine schwache Aktivierung in S1 ($p \leq 0{,}001$, unkorrigiert) sowie eine deutlich unbeständigere Beteiligung ipsilateraler Areale. Bezüglich der hemisphärischen Lateralisierung fanden sich keine signifikanten Unterschiede zwischen DCM-Patienten und Kontrollen. Die multiple Regressionsanalyse lieferte erste Hinweise in Richtung einer geringeren BOLD-Aktivierung im somatosensiblen Kortex bei stärker klinisch beeinträchtigten Patienten.

Schlussfolgerung: Zusammenfassend zeigten die Ergebnisse bei DCM-Patienten eine reduzierte kortikale Antwort auf periphere Stimuli, wobei die kortikale Repräsentation der

rechten (dominanten) Hand robuster gegen Abweichungen durch die DCM zu sein schien als die Repräsentationen der anderen getesteten Extremitäten. Insgesamt schienen degenerative Prozesse hinsichtlich der somatosensiblen Funktion im untersuchten Patientenkollektiv vorzuherrschen, abweichend von berichteten Kompensationsmechanismen im Bereich des motorischen Systems. Auf Basis longitudinaler Daten bleibt zu untersuchen, inwieweit klinische Beeinträchtigungen und reduzierte BOLD-Antworten sich nach einer operativen Dekompression reversibel zeigen können.

Background: Degenerative cervical myelopathy (DCM) is the most common cause of spinal cord dysfunction in adults and shows growing prevalence due to demographic trends. Nevertheless, the surgical decision-making is still challenging due to the lack of sufficiently reliable predictors of disease progression and surgical outcome. Recently, the compensatory potential of reorganization processes within the cerebrospinal motor network has been discussed. Somatosensory impairment as an early but often overlooked symptom of DCM, however, was not in the main focus of research so far. In this thesis, the functional adaptation of the somatosensory system in DCM patients was investigated using blood oxygenation level dependent (BOLD) functional magnetic resonance imaging (fMRI).

Materials and Methods: 18 right-handed participants, including 9 DCM patients (age 56 ± 12 years, 7 male) and 9 age- and gender-matched healthy control subjects (age 57 ± 12 years, 7 male) underwent a block design fMRI (3 Tesla) session. The fMRI procedure consisted of alternating, passive somatosensory stimulation of the subjects' dorsal hands and feet using a wooden stick with a felt tip. By means of MATLAB® 2019a and the SPM12 software package, a region of interest (ROI)-wise analysis of BOLD-response was performed at the group level using a three-way analysis of variance (ANOVA), including the factors “group” (patients/controls), “limb” (hand/foot) and “side” (left/right). Functional hemispheric lateralization was assessed by calculating lateralization indices for individual ROIs. Furthermore, a comprehensive clinical assessment including clinical tests and scores, neurological examination, and somatosensory evoked potentials (SSEPs) of the tibial nerve was performed. An SPM multiple regression analysis was performed to determine correlations between BOLD signal change and clinical impairment.

Results: Both, patients and controls featured a strongly left-lateralized cortical response in S1 and S2 ($p \leq 0.05$, family-wise error (FWE)-corrected) regarding the somatosensory stimulation of the right (dominant) hand. However, activation in patients was lower than in control subjects ($p \leq 0.001$, uncorrected). Regarding the other task conditions, controls showed significant responses within the somatosensory cortex ($p \leq 0.05$, FWE-corrected) including a consistent activation within the ipsilateral S2. In contrast, patients showed only weak activation in S1 ($p \leq 0.001$, uncorrected) and a much scarcer involvement of ipsilateral areas. Regarding hemispheric lateralization, no significant differences were found between DCM patients and healthy controls. Multiple regression analysis provided first evidence of less BOLD activation in the somatosensory cortex in more clinically impaired patients.

Conclusion: In summary, the results showed a reduced cortical responsiveness to peripheral stimuli in DCM patients, whereby the cortical representation of the right (preferred) hand appeared to be more robust to deviations due to DCM than the representations of the other tested extremities. Overall, degenerative processes with respect to somatosensory function appeared to predominate in the patient collective studied, which differs from reported evidence

of compensatory mechanisms within the motor system. It remains to be investigated based on longitudinal data to what extent clinical impairment and reduced BOLD responses may be reversible after surgical decompression.

2. Introduction

Neural plasticity is one of the ground-breaking discoveries in modern brain research. Recent studies of the 21st century have substantiated this principle as the foundation of adaptability in the nervous system in conditions such as learning and memory[1–3], stroke recovery[4–6], or even mental disorders[7,8]. These findings contributed to the contemporary concept of a dynamic and flexible nervous system, which is capable of persisting even into advanced old age[9–11].

This thesis focuses on cortical adaptation in degenerative cervical myelopathy (DCM), which can be referred to as a complex type of pathology, in which neither the functionality, nor the potential of neural network reorganization has been investigated sufficiently yet. DCM shows growing prevalence in the industrial nations due to the demographic development[12,13]. However, the lack of sufficiently reliable predictors of both disease progression and surgical outcome causes challenges regarding the surgical decision making[14,15]. DCM can cause a variety of symptoms and impairment of body functions[13,16], which involve afferent as well as efferent neural pathways[17]. Previous studies predominantly investigated cortical adaptation in the motor system[14,15,18–20], while reorganization of somatosensory networks was usually neglected or encompassed as a side aspect[18]. However, this subject deserves greater attention, since a loss of sensory function like paresthesia is a frequent but often overlooked early symptom of DCM[21].

The aim of the present thesis is therefore to contribute to the understanding of the behavior of the somatosensory system in DCM. In this framework, fMRI is used to investigate cortical adaptation processes resulting from spinal cord lesion. Beyond the mere scientific gain of differentiated findings about the cortical correlates of DCM, this thesis also addresses potential benefits for clinical practice. A mid-term objective is to improve the surgical decision making, i.e., to strengthen the scientific grounding for the indication of surgical decompression of cervical spinal stenosis (CSS), and the optimal choice of the time point for surgery.

2.1. Cervical Spinal Stenosis and Degenerative Cervical Myelopathy

A pronounced understanding of the spinal pathology itself is the necessary basis of further investigation and interpretation of cortical adaptation processes. Hence, fundamental aspects of CSS and of the resulting DCM regarding the pathogenesis, symptoms, and treatment options, will be introduced.

2.1.1. Pathogenesis and Symptoms

CSS usually occurs as a consequence of degenerative processes of the cervical spine, which is the most flexible and vulnerable section of the spinal column[16]. The normal sagittal diameter of the cervical spinal canal in adults ranges from 13 to 20 mm while diameters below 12 mm

can lead to spinal cord damage[22]. Factors determining pathogenesis are of statical, dynamical as well as histopathological nature[21], as visualized in Figure 1.

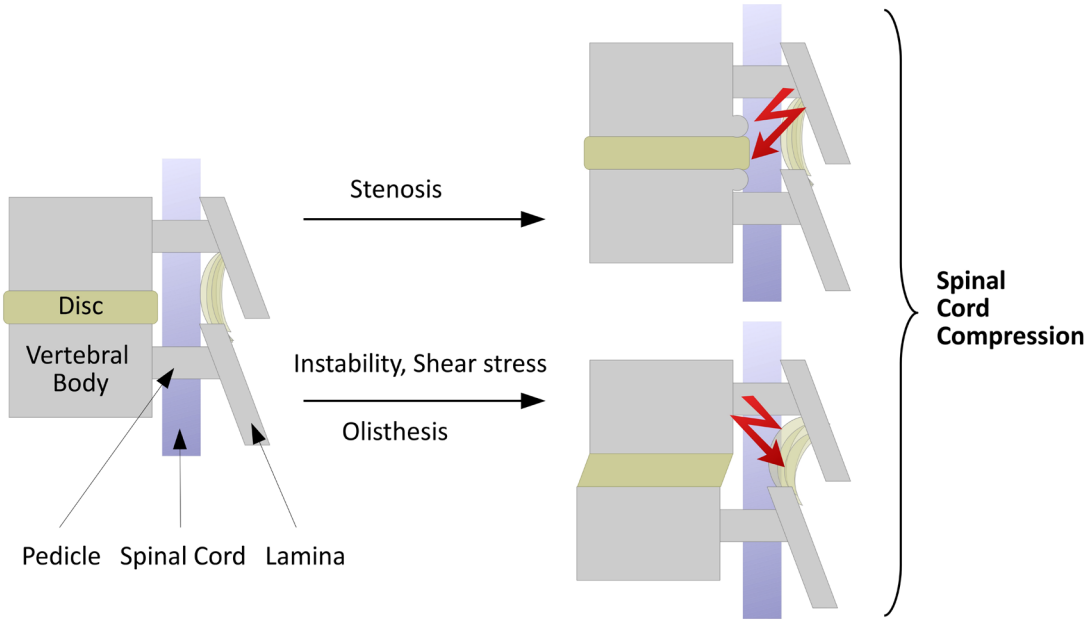

Figure 1: Pathophysiology of cervical spinal stenosis. Static as well as dynamic powers contribute to pathogenesis. Adapted from Meyer, Börm and Thomé, 2008[23].

First, the mere narrowing of the spinal canal can cause myelon compression and injury[24]. Stenosis can be caused by disc protrusion, prolapse[13] or formation of posterior marginal osteophytes evoked by mechanical strain on the endplates, which can ensue from disc collapse due to degenerative dehydration[22] (see Figure 2). In addition, ossification of the posterior longitudinal ligament and likewise hypertrophy of the ligamentum flavum can contribute to CSS[25,26]. Second, in prevailing spinal canal stenosis, the spinal cord can suffer damage due to movement[22]. Dynamic strain of the cervical spinal column, e.g., hyperextension, can transiently cause shear stress and a deterioration of stenosis[21,22,27,28]. Instability and olisthesis can intensify these pathomechanisms[29]. And third, spinal cord compression can result in hypoperfusion, inflammation and loss of neurons which contributes to further clinical impairment[21,27,28].

If these stressors induce spinal cord injury (SCI), patients can display a variety of symptoms and signs described as symptomatic DCM, as well referred to as cervical spondylotic myelopathy (CSM)[25,30,31]. Aiming at a uniform terminology, only the term "DCM" will be used in this thesis. Symptoms vary in severity and can affect motoric, sensory and autonomous functions[32].

Common signs of DCM are gait disturbance, clonus and hyperreflexia in the extremities[30]. On neurologic examination, DCM patients may also present with spasticity, motor weakness and pathologic Hoffmann and Babinski signs[21]. Possible accompanying radiculopathy due to

additional degenerative stenosis of the neuroforamina may frequently also cause hyporesponsive or even absent muscle reflexes[22,33,34]. Therefore, a mixed clinical picture of upper and lower motor neuron symptoms may result[34].

Dys- and paresthesia of one or more limbs can also occur, as well as radicular pain of the upper extremities[21]. In severe cases, even a loss of bladder function is possible[21,32].

DCM has a progressive character[13,21,22]. In most cases, symptoms appear gradually at onset and increase over a long period of time while spontaneous remission is very rare[22]. Exacerbation, also secondary to trauma, is possible and eventually leads to spastic para- or quadriparesis[22,22,32].

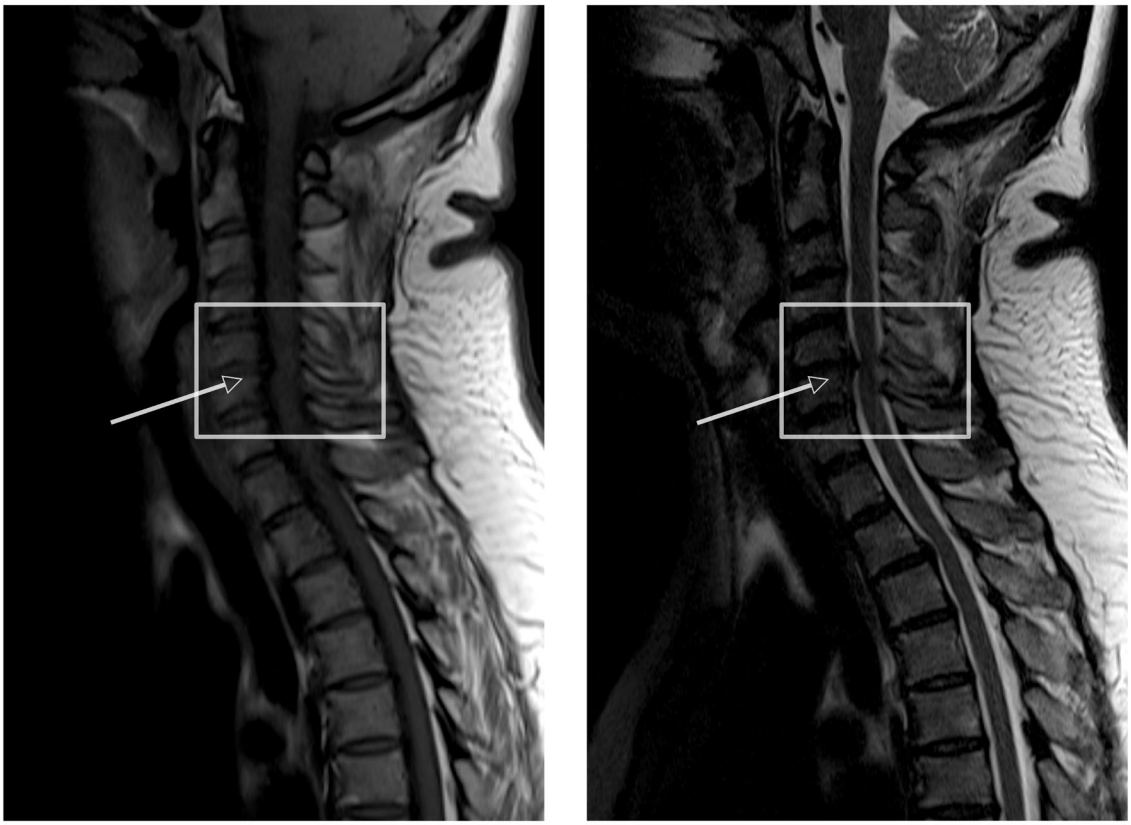

Figure 2: Cervical spinal stenosis in magnetic resonance imaging. The T1-weighted (left) and T2-weighted (right) images show spinal cord compression mainly caused by a disc protrusion at the level between cervical vertebra (CV) 5 and 6.

2.1.2. Treatment Options

Primary conservative therapy as well as a surgical decompression are the major, competing treatment strategies of DCM[35]. Due to insufficient data availability regarding the spontaneous course of DCM[36,37] and issues of delimitation between comorbidities, the decision between

both treatment options is often challenging and needs to be considered carefully for each individual case[35].

Factors that are taken into account to inform the treatment decisions are age, clinical symptoms, disease progression and radiological findings[35]. Severity of clinical impairment can be categorized by means of the Japanese Orthopaedic Association (JOA) score[38], which is described in detail in section 4.2. Based on the current state of research, conservative treatment can be considered in patients of advanced age, with mild clinical impairment (JOA > 13 - 14) and slight or missing progression, while clinical follow-up visits and reevaluation of the recommended therapy are indispensable[35,37]. According to literature, patients of younger age without a severe impairment or long preexisting DCM benefit the most from surgery, whereas older patients with comorbidities or severe symptoms (JOA < 7) might expect poorer surgical outcomes[35,39]. Prognosis of surgery could worsen in older patients with comorbidities and severe symptoms (JOA < 7)[35]. Therefore, it seems to be a crucial task of the physician, not to miss the decisive point in the course of disease when the patient can still benefit from surgery.

According to the S1 guidelines for DCM of the German Neurological Society (DGN)[35], the following treatment principles are valid: If a conservative treatment seems to be appropriate, a cervical collar may be considered in the acute stage in order to moderate the pathogenetic factors caused by motion. The collar should be worn at night in the first place, and it self-evidently can only be a temporary option. Moreover, physiotherapy can contribute to a stabilization of the cervical spine. Pharmacotherapy is reasonable in case of radicular symptoms, myalgia and spasms. It is based on analgesics, antiphlogistics, muscle relaxants and antispasmodic agents. A surgical treatment is indicated, if symptoms proceed rapidly and acute, if autonomous functional disorders occur or if symptoms proceed under conservative treatment of mild DCM.

Surgery aims to stop progress and prevent remaining neurological impairment by decompressing the spinal cord, e.g., via discectomy or vertebrectomy[35]. If nerve roots are also affected, these can additionally be treated surgically by a foraminotomy[35].

2.2. The Sensory System

An overview on how reception and processing of sensory information works will be given within this section, focusing on the epicritic component of the sensory system, which has high relevance in this thesis.

2.2.1. Qualities of Sensory Perception

Sensory perception means getting access to information about the environment as well as of the own body of an individual[40]. The instrument of sensory perception are sensory organs and their receptors, which are highly specialized for definite (environmental) stimuli[40]. As a product of evolution, the sensory organs do not serve the purpose of grasping the environment and the individual in their entirety, but of catching information, which is necessary for survival[41,42]. For instance, pain is an important warning signal which can protect from injury[40].

The specific somatosensory modalities such as vision, olfaction, taste, hearing, and balance are not considered in this elaboration because their processing does not occur primarily in the spinal cord[43] and therefore they cannot be damaged by CSS.

Similarly, visceral sensibility, which is mediated by the autonomic nervous system consisting of the sympathetic and the parasympathetic nerve fibers[44] and may indeed be injured in CSS[32], will merely play a subordinate role in this thesis.

Instead, the focus is set on somatosensation, which can be categorized as follows: Based on function as well as on anatomical structures, we can distinguish the protopathic sensibility including sensation of pain and temperature from the epicritic sensibility[43]. The epicritic sensibility means both proprioception of the locomotor system and exteroception of the skin, which is basically the sensation of touch[43].

2.2.2. Somatosensation of the Skin

In the present study, data is collected about the different components of somatosensibility with a key focus on the sensation of touch. The following subsection provides an outline about the procession of somatosensory information and the anatomy of the tactile sense.

In each segment of the spine, a pair of spinal nerves (one for each side of the body) enters the spinal cord[44]. Most of them carry the sensory information from a defined skin area (dermatome)[43]. Based on this fact, a map of the human body can be created, depicting the dermatomes of the cervical (C2 - C8), thoracic (T1 - T12), lumbar (L1 - L5) and sacral (S1 - S5) spinal nerves[43]. An exception are the dermatomes of the face, which do not belong to spinal nerves but the trigeminal nerve (fifth cranial nerve)[44]. It is important to note, that due to an overlap of innervation, every single point of the skin belongs to at least two contiguous dermatomes[44].

A variety of specialized cutaneous receptors enables the human organism to experience complex and diverse tactile sensations[45]. Aside from free nerve endings and thermoreceptors, there are cutaneous receptors of surface sensitivity responding to different qualities of tactile stimuli[46]. These so-called mechanoreceptors include Pacinian and Meissner corpuscles for sensation of deep pressure, shear and vibration, Merkel discs for sensation of contact and Ruffini endings for reception of tension[44]. Each receptor type can be characterized by a

particular speed of signal transduction and propagation as well as the size of its receptive field[46].

The signals of mechanoreceptors are transmitted via large afferent Aβ or group II fibers[44] according to the classification of nerve fibers established by Joseph Erlanger and Herbert Spencer Gasser[47], who were honored with the Nobel Prize in 1944, or the classification scheme of David P. C. Lloyd and Carlton C. Hunt[48,49]. Since both classification systems have been developed on the basis of an animal model, their applicability to humans is limited to a rather imprecise categorization of fiber diameter and transmission rate[50].

The cell bodies of the afferent neurons are localized in the dorsal root ganglia, which are ordered parallel to the spine[43]. Afferent fibers from cutaneous receptors enter the dorsal horn of the spinal cord and form the so-called dorsal columns (fasciculi gracile and cuneate)[44]. The gracile fasciculus comprises mainly afferents of the lower extremity, while the cuneate fasciculus comprises afferents of the higher spinal segments including the fibers of the upper extremity[44]. These afferent fibers ascend ipsilaterally and terminate in the nuclei gracile and cuneate, which are localized in the medulla oblongata of the brain stem[44].

From here, somatosensory information is projected via the medial lemniscus, a fiber tract, which crosses to the contralateral side and is joined at the level of the pons by the fibers of the trigeminal nerve, which carry somatosensory information of the face[43], before reaching the ventral posterior lateral thalamic nucleus (VPL)[46]. After synaptic switching, information is finally transmitted via the posterior limb of the internal capsule to the primary somatosensory cortex (S1) and can now reach consciousness[43]. Named after the fiber tracts, the nerve pathway of proprioception and tactile sensation is also called dorsal column medial lemniscus (DCML) system[51].

It is important to note that sensory information of the left side of the body is processed in the right hemisphere of the brain and vice versa. Throughout their entire course, fiber tracts of the somatosensory system retain organized according to anatomy, i.e., they have a somatotopic arrangement[43]. For instance, the inner part of the posterior columns contains fibers from the lower spinal segments, while the outer part is built from sensory fibers of the thoracal and cervical level[43].

Likewise, S1, which is localized in the parietal lobe, more precise the postcentral gyrus, shows somatotopic organization[51]. According to density of somatosensory receptors in distinct areas of the skin, some individual body parts such as the hand or the lips have a larger cortical representation in S1 than others[43]. The construction of a somatosensory "homunculus", a sketch of the human with size relations adapted to cortical somatotopy and somatosensory representation, stems from the pioneering neurosurgeons Wilder Penfield and Theodore Rasmussen from Montreal, who applied electrical stimulations systematically to the cortex with the objective of identifying the specific functions of brain regions, in order to save them during

surgeries[52,53]. Decades before this, Korbinian Brodmann already had established a cortical map solely based on the cytoarchitecture (see Figure 3), which he analyzed in histological samples of different cortical areas without knowing about their specific function in detail[54]. To an extent, his map holds true until nowadays. S1 can be subdivided in areas 1, 2 and 3 according to Brodmann[43,54], while Brodmann area (BA) 3 can be more precisely differentiated in BAs 3a and b[46]. The cortical areas, which have been defined histologically in the first place, can furthermore be differentiated on the basis of their specific function: BA 1 receives afferent fibers, mainly transmitting information from mechanoreceptors of the skin, BA 2 receives proprioceptive signals, while sensory information from muscle spindles reach area 3a and signals of pain and temperature reach BA 3b[43]. BA 3b has especially strong interconnections to BAs 1 and 2[51]. This is why in non-human primates, lesions in area 3b lead to a loss of any type of tactile sensation, whereas lesions in BAs 1 or 2 lead to a deficit in their predominant quality of somatosensory input, which can manifest in an incapacity of identifying surface textures or estimating size relations of objects[51].

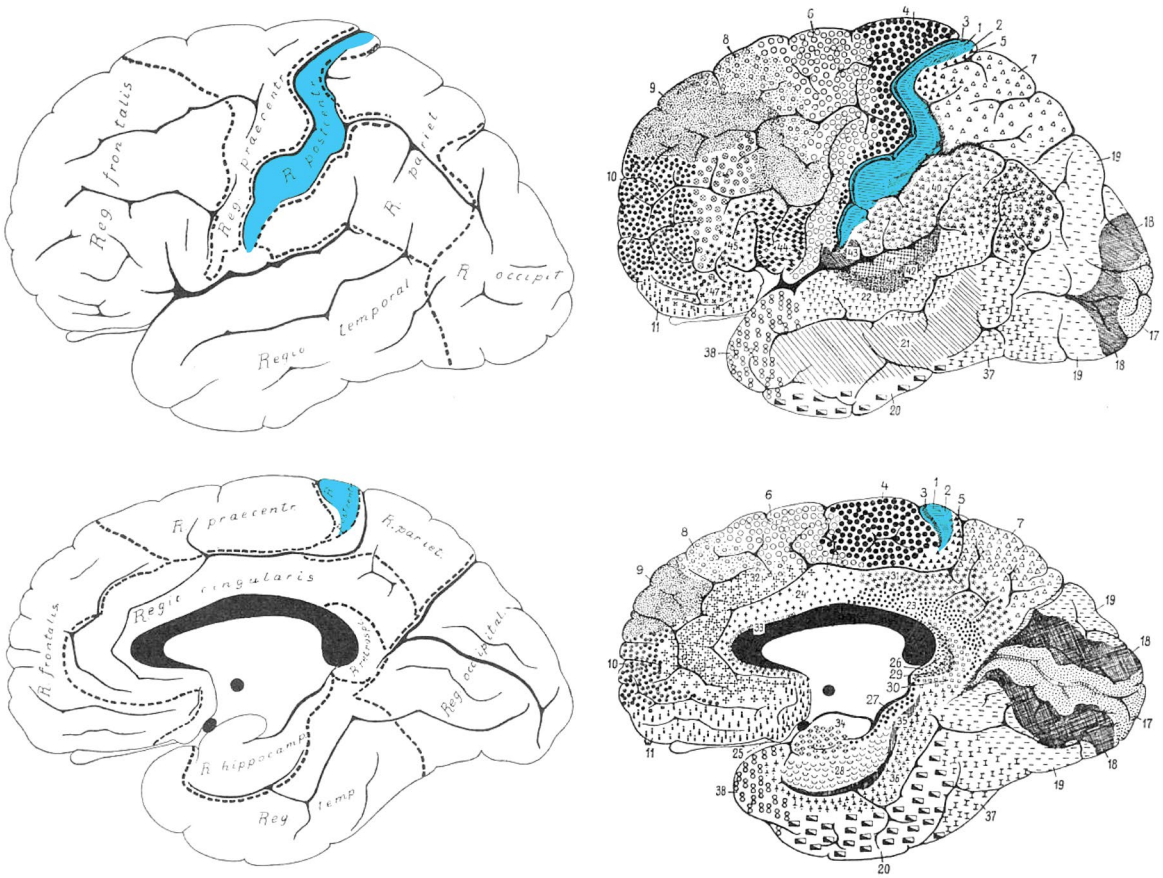

Figure 3: Cytoarchitectonic regions and areas according to Brodmann. This figure shows the main cortical cytoarchitectonic regions on the left and the distinct Brodmann Areas (BAs) on the right. The areas belonging to the primary somatosensory cortex (S1) are colored in blue. Adapted from Brodmann, 1909[54].

Aside from epicritic and protopathic signals, S1 receives afferent fibers from the vestibular nuclei and via commissural and association fibers from other cortical regions, e.g., the somatomotor cortex[43]. By means of efferent projections, S1 furthermore contributes somatosensory input to information processing in other brain regions[51]. For instance, efferent input reaches the adjacent secondary somatosensory cortex (S2) above the lateral sulcus[43,51], which is involved in higher-level cortical processing and receives somatosensory signals from both sides of the body via, inter alia, the callosal commissure[44]. From here, information can further be transmitted to structures of the limbic system, which may be important for learning processes and memory of somatosensory information[51].

Furthermore, S1 sends projections to areas 5a and 7b in the posterior parietal cortex, where an integration with information from the motor and premotor cortical areas occurs, which is essential for the coordination of voluntary motor function[51]. The posterior parietal cortex additionally receives input of other sensory qualities such as visual, vestibular and auditive projections which contribute to orientation in three-dimensional space[43]. Beyond that, descending fibers from S1 to the VPL, the principal trigeminal nucleus, the dorsal column nuclei and the dorsal horn of the spinal cord can have an intensifying or inhibiting effect on the somatosensory input from the thalamus, the brainstem and the spinal cord[43,51].

2.3. Underlying Concepts of Functional Magnetic Resonance Imaging

Its well spatial resolution makes blood oxygenation level dependent (BOLD) fMRI a method of choice for analyzing the somatotopy of the human brain[55]. In the following, the basic principles of this imaging method as well as the methods of data acquisition and fMRI design applied in this study will be described.

2.3.1. Principles of Magnetic Resonance Imaging

In 1938, Isidor Rabi was the first one to witness the phenomenon of nuclear magnetic resonance (NMR) in a beam of molecules (Nobel Prize 1944), when he presented a new method capable of measuring the magnetic moment of a large quantity of various nuclei[56]. Eight years later, both Edward Mills Purcell and Felix Bloch separately applied the NMR method to solid state material and established the theoretical basis for the whole field of NMR, which was honored with the Nobel Prize in 1952[57–60]. The groundbreaking findings for the application of NMR in modern medical imaging methods are based on the work of Paul Christian Lauterbur and Peter Mansfield (Nobel Prize 2003). In 1973, they showed independently of each other, that NMR may be used for the identification of three-dimensional structures in solids by applying magnetic field gradients[61].

Analogous to the authors Moore, Graves and McRobbie, who explained magnetic resonance imaging (MRI) quite concisely[62], the basics are pointed out here: The MRI technique is based on the magnetic properties of fundamental particles. Commonly, nuclei of hydrogen atoms are used, since the human body consists of about 75 % water. Apart from their plentiful supply, their electromagnetic behavior qualifies hydrogen nuclei – which are nothing else than protons – for MRI. These particles generate a magnetic field of very low intensity, their so-called magnetic moment, which results from their charge and their spin properties. A simplified illustration is, that the protons literally spin around their axis. When placed in the external static magnetic field of an MRI-Scanner (B_0), the proton's magnetic moment experiences a torque which makes it tend to align with the external field. Due to the laws of quantum mechanics, the proton does not align exactly with the main field, but it precesses around the direction of the main field. The totality of protons in the magnetic field precesses at the same frequency known as the Larmor frequency. With regard to their orientation in the main field, protons can be in two different spin states. Their orientation can either be nearly parallel to the main field (spin-up) or anti-parallel (spin-down), while the parallel spin state is slightly favored because it requires a bit less energy[62].

The energy difference between those two spin states is directly proportional to the strength of the main magnetic field of the scanner. The frequency of electromagnetic radiation needed to switch between these two states is the Larmor frequency. In state of equilibrium, the average of multiple protons is out of phase and produces a net magnetization M_0, which is the vector sum of all spins. The vector component in the xy-plane resulting from the precession of single protons is averaged out in the mass of protons. Due to the slight preference to the parallel spin state, the resulting net magnetization M_0 is aligned precisely with B_0 in z direction and is in the range of microtesla (see Figure 4). In order to cause a significant magnetization, that deviates from B_0, a radiofrequency (RF) pulse is applied. The RF pulse generates a magnetic field, which is varying at the Larmor frequency and orientated perpendicular to B_0. Two effects of the RF pulse may be obtained: For one thing, it brings all the spins into phase, and for another, it makes M_0 move towards the xy-plane until the RF pulse is turned off. If M_0 is flipped exactly into the xy-plane, the flip angle amounts to 90° and we therefore speak of a 90° pulse. M0 then generates an oscillating magnetic field in the xy-plane that can be detected since it induces a voltage oscillating at Larmor frequency in a detector. After switching off the RF pulse, relaxation back to equilibrium state begins. On account of dephasing, there is a fast decay in the amplitude of the detected signal, which is called free induction decay (FID)[62].

There are two essential aspects of relaxation. On the one hand, the longitudinal magnetization is being recovered during the longitudinal relaxation time T1 due to thermal interactions with the ambient tissues (spin-lattice relaxation)[63]. On the other hand, the dephasing of the spins leads to a decline of transversal magnetization during the transversal relaxation time T2[63]. This

process is based on interactions between the spins (spin-spin relaxation)[64]. T1 and T2 have no relation and T2 is generally much shorter than T1[63]. T1 and T2 relaxation times vary for different tissues[62].

T1-weighted images accentuate the contrast between tissues of different T1 relaxation times, while the impact of T2 relaxation time is minimized[63]. Due to their good contrast, they are used for generating high-quality anatomical images[62]. T2-weighted images emphasize T2 contrasts and are very sensitive for differences in water content of the tissues[64]. Water has a long T1 and a long T2 relaxation time as well[63]. In T1 weighting, tissues with a short T1 are highlighted, which is why water appears black in a T1-weighted image[63]. T2-weighted images highlight tissues with long T2 relaxation times and therefore make water appear bright[63].

Additionally, the T2* relaxation time can be defined, which includes T2 and besides depends on inhomogeneities on account of the external field, tissue susceptibility as well as diffusion processes[62]. This quality has high relevance for its usage in fMRI, as described below[63].

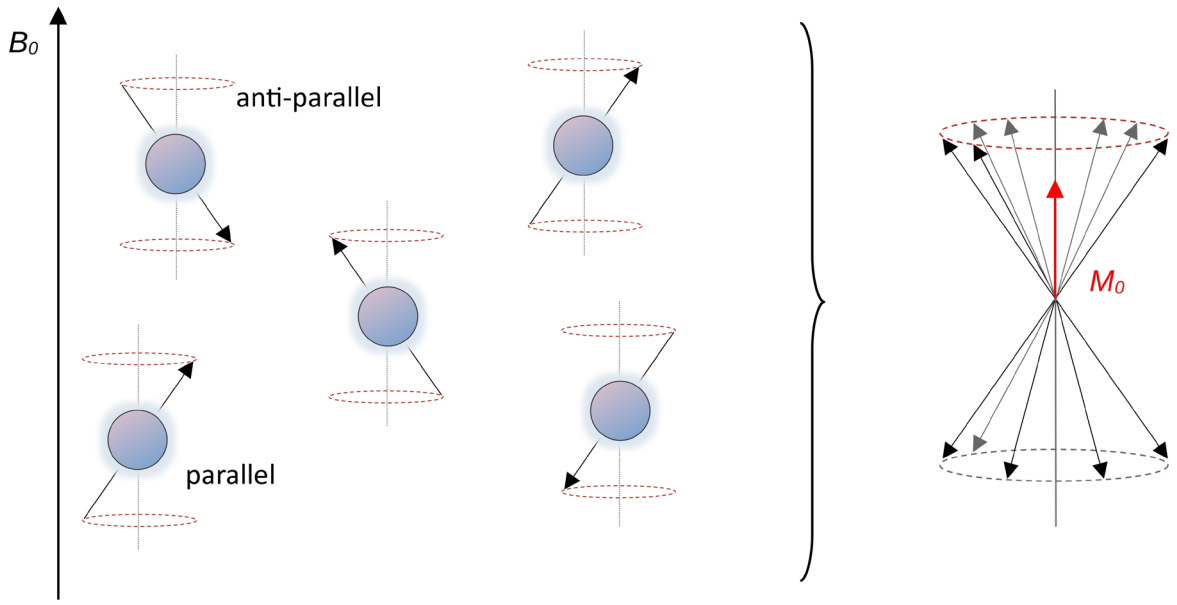

Figure 4: Orientation of the protons in the external magnetic field B_0 and resulting net magnetization M_0. In equilibrium, proton precession is out of phase. The orientation of the nuclei is either parallel or antiparallel to B_0, while the parallel orientation slightly overweights, producing M_0. Adapted from McRobbie et al. (2017)[62].

2.3.2. Physiology of BOLD-fMRI

Making processes of brain metabolism visible by means of MRI is not a trivial task. Since the concentration of hydrogen nuclei is predominant in tissue, common metabolic reactions do not cause a significant signal change[65].

A strategy of measuring brain activity indirectly was described by Ogawa and colleagues and is based on its correlation with oxygen supply and local blood flow[65,66]: The blood oxygen level can be reflected owing to the BOLD effect, which arises from the opposed magnetic properties of oxyhemoglobin and deoxyhemoglobin. Oxygenated hemoglobin is diamagnetic whereas deoxygenated hemoglobin is paramagnetic. An increasing concentration of paramagnetic deoxyhemoglobin in blood causes an alteration of the magnetic susceptibility between the vessel and the ambient tissue. Additionally, deoxyhemoglobin has an influence on the spin properties of hydrogen nuclei in nearby tissue regions, which intensifies the BOLD effect. When applying the gradient-echo imaging sequences, as described below, the resulting local field inhomogeneities lead to a loss of signal intensity of the respective region, which causes the BOLD contrast: regions of high deoxyhemoglobin concentration appear hypointense in the image[66].

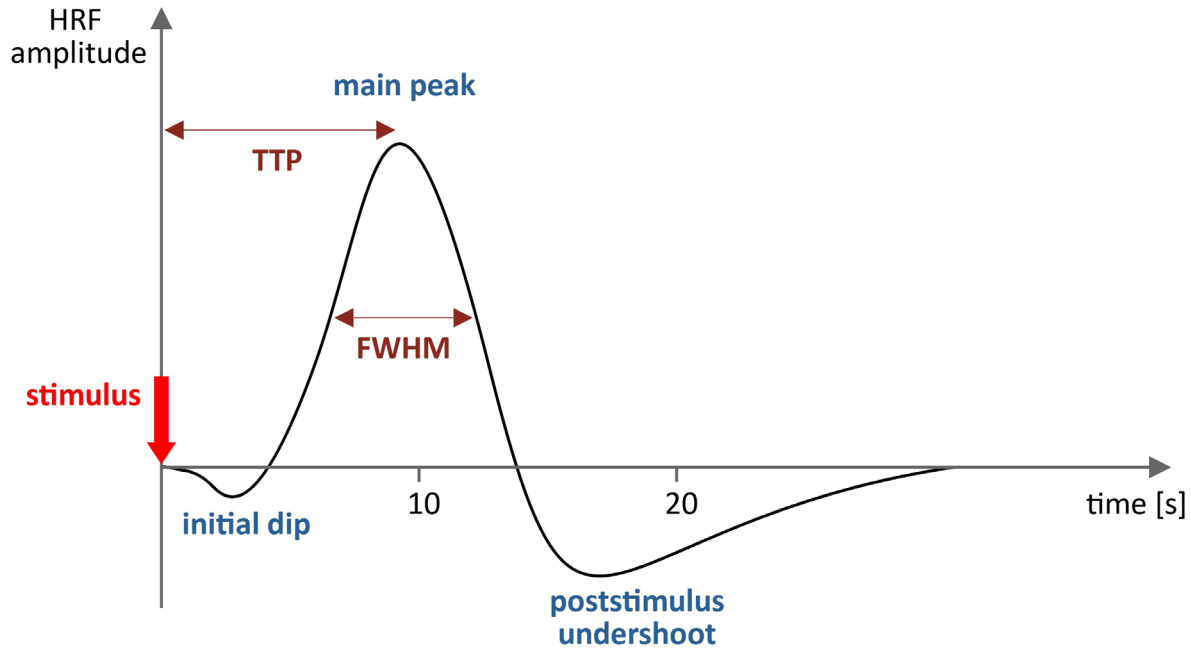

Figure 5: Hemodynamic response function. After a stimulus application, an initial dip of BOLD response can be recorded due to the enhanced local oxygen consumption during neural activity. The reactive vasodilatation leads to increased oxygen supply and is reflected in the main peak of the hemodynamic response function (HRF), followed by the poststimulus undershoot[67–69]. Abbreviations: FWHM (full width at half maximum), TTP (time-to-peak).

Practically speaking, the accelerated dephasing of nuclear spins due to the paramagnetic properties of deoxyhemoglobin leads to a decrease of the T2*-weighted signal[70]. When performing a cognitive task, the following can be observed: During activation of a brain region, local oxygen consumption rises up[70]. But simultaneously, vasodilatation leads to an increase of blood and oxygen supply, which is why the result is a reduced deoxyhemoglobin concentration and a consecutive overall rise in the T2*-weighted BOLD-Signal of the

respective brain area[70]. The BOLD-Signal plotted against time can be depicted in the hemodynamic response function (HRF)[71,72]. Particular parameters of the HRF like response amplitude, time-to-peak as well as full width at half maximum (FWHM) allow conclusions to be drawn about magnitude of response, latency and neural activity duration[73,74] (see Figure 5).

2.3.3. Gradient-Echo Echo-Planar Imaging

In functional imaging, fast image acquisition as well as a high sensitivity to local field inhomogeneities are needed. Basically, gradient-echo echo-planar-imaging (GE-EPI) meets these requirements. Echo-planar-imaging (EPI) was born of the research of Peter Mansfield[75]. Due to its structure, EPI is the fastest type of pulse sequence which enables slice acquisition within less than 100 ms, however, it suffers from limitations concerning image quality[62]. The concept of gradient echo (GE) is determined by applying a magnetic field gradient, which causes a linear alteration of the magnetic field and therefore a rapid dephasing of the transverse magnetization and loss of the signal[62]. In consequence, repetition time (TR) can be reduced, and accelerated data acquisition is possible[62]. GE-EPI is built up from a single RF pulse followed by a GE series[62]. Corresponding so-called "blips" ensuing every readout gradient reversal are used instead of a train of phase-encoding gradients and allow stepwise phase encoding, since each blip adds phase encoding to the preceding[62]. This results in a characteristic path through the k-space and contributes to fast data acquisition[62].

2.3.4. fMRI Designs: Strategies in Stimulus Presentation

Regarding the timing and coordination of stimulus presentation and fMRI sequence, block and event-related designs come into question as well as combinations of both[76]. All of these strategies meet different requirements and none of them are free of disadvantages[76,77]. The block design is characterized by so-called blocks consisting of sequences of either identical stimuli building a task condition or a combination of tasks[77,78]. Different task conditions can be alternated[76]. In further data processing, the hemodynamic response to condition-specific stimuli is averaged[77]. Advantages of the block design are robust results[79], adequate statistical power[80] as well as a high BOLD signal change in comparison to the baseline[81]. On top of that, block designs are useful for the detection of task-specific Regions of Interest (ROI)[82]. A disadvantageous aspect is, that priming effects and influence of intention due to stimulus repetition cannot be avoided[83]. Furthermore, block designs are not applicable for a detailed analysis of the response during a block, since subtle effects are averaged out[84], which makes them suitable for cortical response classi fication but inadequate for the analysis of single trials[83].

In an event-related design, stimuli are presented separately, which allows for an analysis of individual HRFs[76]. Stimulus prediction and associated biases can therefore be prevented by varying the interstimulus interval (ISI)[85]. Event-related designs can be time-consuming[86], have high trial-by-trial variation and low signal-to-noise ratio[83]. Despite these limitations, there are application examples where they have many advantages. For example, event-related designs can be used in language mapping, where they can produce particularly sensitive results[87].
Combinations of block design and event-related design try to unify advantages and to circumvent the downsides of both concepts[77]. In the end, the election of a suitable fMRI design depends on the individual research question.

2.4. Processes of Cortical Reorganization and Plasticity

Until the late 20th century, the concept of immutability of the mature nervous system was a prevailing basic assumption in neuroscience and medicine[88]. This idea was influenced by Santiago Ramón y Cajal (Nobel Prize 1906) who systematically exposed cells of the central and peripheral nervous system to different noxae[89]. He observed and described processes of growth but considered them as reactive aberrations of apoptotic events without a functional meaning[89]. Also, subsequent studies of David Hunter Hubel and Torsten Niels Wiesel (Nobel Prize 1981) who investigated information processing and plasticity of the visual system in cats[90–92] were based on the assumption that the fully developed cortex retains a static organization[93].
In the late 20th century, numerous trials on non-human primates[94–97] were able to disprove this. These trials followed the principle of modifying the sensory input of the experimental animals by means of radical interventions such as the dissection of a peripheral nerve[94], amputation of digits[98], the fusion of two fingers[99], or a skin island transfer[100]. Subsequently, an invasive cortical mapping was performed in order to analyze the cortical representations[95]. The researchers observed that changes of peripheral stimuli can lead to cortical reorganization[100] and that sensory cortical representations of skin areas can even enlarge as a consequence of tactile stimulation[101]. Their most essential finding was for sure, that neural plasticity is not an inert and static property, since it can be affected by experience[101].
This section provides a brief overview of the underlying cellular processes of functional adaptation in the nervous system. Since they are so complex, this summary cannot claim to be exhaustive, but it should at least clarify the core properties of cortical reorganization. In addition, recent advances in the understanding of the reorganization of the neocortex and aspects of cortical adaptation in DCM are summarized.

2.4.1. Properties of Cortical Reorganization at the Cellular Level

As described in subsection 3.2.2, cortical areas can be allocated to specific functions. Nevertheless, the cortex is capable of dynamic functional and structural adaptation, in response to changing demands and conditions of the environment or lesions of the nervous system[102]. In the case of the cortical representations of the skin surface in S1 this means, that in spite of somatotopic arrangement, an incessant modification in reaction to use, learning, development of skills and injury is performed[103]. This somatosensory reorganization is based on neural plasticity[11].

The concept of neural plasticity includes a variety of complex processes, which allow neurons to modify their activity[11]. E.g., on the level of synaptic transmission in the framework of short-term plasticity, amplitudes of postsynaptic potentials can either be increased or decreased in response to the frequency of action potentials of the presynaptic neuron[104]. On top of that, synaptic plasticity, which is often referred to in the context of learning and memory, is an aspect of neuroplasticity[105]. The idea of synaptic plasticity goes back to Donald Hebb, who was searching for the anatomical and physiological basis of learning and developed the thesis, that repetitive co-activation of a presynaptic and a postsynaptic neuron can strengthen their interconnection[106]. This concept of long-term potentiation could later be experimentally verified[107,108]. Several molecular mechanisms are assumed to contribute to this process, such as an increase of the presynaptic glutamate release, triggered by the positive feedback of molecular messengers, the genesis of new synapses and dendritic spines or the intensified expression of pos synaptic α-amino-3-hydroxy-5-methyl-4-isoxazolepropionic acid (AMPA) receptors[105]. The opposed process is called long-term depression and leads to a decrease in synaptic transmission as consequence of continued low-frequency stimulation[105,109]. Finally, even larger-scaled processes like neurogenesis, cell migration or collateral sprouting of axons are aspects of neural plasticity[11]. But in the mature nervous system, axon growth is limited to short distances and neurogenesis only occurs to a small extent, which is why the nervous system is not capable of full neural damage compensation[88].

2.4.2. Reorganization of Cortical Areas

When focusing on neural networks instead of individual neurons, certain patterns of functional organization become apparent. One of these patterns is modularity, the principle of separate organizational entities, each with a specific function[11]. If one of those modules fails, this can potentially be compensated by the others[11,110]. For instance, such modules can be found in the somatosensory cortex, which is organized in columns, that can be allocated to a particular sensory modality and region of the skin surface[44]. The principle of modularity is closely linked to redundancy, which implicates the co-existence of many identical modules with the same function, while degeneracy implicates, that also different modules are capable of fulfilling the

same function and are therefore replaceable to a certain extent[11]. These principles can contribute to a simplified concept of how cortical remodeling can occur. Such cortical reorganization has been described in a variety of different pathologies, so far. A comparatively well-researched example is the recovery after ischaemic stroke[111–115]. Diffuse connectivity between different brain areas and a redundancy of pathways might contribute to recovery[116]. Even ipsilateral pathways can be involved while the lateralization of sensory and motor cortex representations can be weakened[116–118]. Increased bihemispheric sensory processing in stroke is seen as a compensational mechanism which comes into play in more extensive lesions but correlates with weaker clinical outcome[112,116,119].

An example which does not involve a brain lesion, is cortical reorganization after limb amputation. Since it changes the sensory input as well as the behavior, this is a strong trigger factor of cortical remapping[120]. It could be shown, that after an arm amputation, the neighbored somatosensory representation area of the lower face can expand to the representation area of the missing arm, which is correlated with phantom pain[120–123]. Phantom pain as a consequence of cortical remapping is the basis of the maladaptive plasticity theory[121], which shows that cortical reorganization can also be dysfunctional.

2.4.3. Cortical Reorganization in Degenerative Cervical Myelopathy

Only a few studies investigated cortical adaptation processes in DCM so far[124]. Conventional magnetic resonance (MR)-morphological parameters like intramedullary signal changes are correlated with the clinical presentation only to a certain extent[125]. Particularly, these do not reliably predict the outcome of surgery[125,126]. Ambiguities in treatment decisions emerge from these circumstances, notably in mild cases[125]. Against this background, it seems plausible, that adaptation processes at the cortical and the spinal level may contribute to the clinical outcome. Previous studies, which investigated this subject, were commonly based on fMRI or navigated transcranial magnetic stimulation (nTMS). nTMS is a non-invasive neurophysiological method[127,128], which uses electromagnetic induction[129] causing a stimulation of superficial cortical layers[128,130]. It can be applied in functional cortical mapping and when used with higher stimulation frequencies, i.e., repetitive transcranial magnetic stimulation (rTMS), it has also neuromodulatory effects[129]. TMS is less suitable for mapping somatosensitive cortex functions. The procedure is cumbersome because no immediate and objectively measurable output can be evoked during stimulation of somatosensitive cortex areas[131]. Underlying principles of fMRI are described in further detail in section 3.3.

The arguably best explored aspect of cortical reorganization in DCM is the adaptation of the motor system, even if research in this thematic field is still expandable since results of the existing studies do not seem to be consistent. Zdundzyk and colleagues (2018) showed by means of nTMS, that patients suffering from DCM had a reduced corticospinal excitability

compared to healthy control subjects[14]. Further on, they detected a higher activation in non-primary motor areas in patients with mild symptoms, while severe impaired patients showed stronger cortical inhibition and a diminished motor area. The authors concluded that a recruitment of nonprimary motor areas had a compensatory effect[14].

Changes of the motor network after surgical decompression were investigated by Ryan et al. (2018) using fMRI[20]. They documented an increased percentage of BOLD signal in the motor network of both hemispheres after surgical decompression. Regarding the ipsilateral supplementary motor area (SMA), this was associated with functional recovery. The volume of activation (VOA) of the motor areas did not change significantly within the follow-up of six weeks[20]. In contrast, Bhagavatula et al. (2016) reported an increased recruitment of sensorimotor areas before surgery represented by the VOA, which was reduced after surgery, but still higher than in control subjects[19].

Concerning adaptation in the somatosensory system, there is even less literature available. Duggal et al. (2010) showed that preoperatively patients demonstrate a smaller VOA in the postcentral gyrus than healthy control subjects[18]. After decompression, VOA had almost the same size as in controls. Additionally, patients showed a slight improvement of clinical output, which was, however, not significant[18]. Owing the fact that these findings were based on a study design that portrayed activation in sensory areas as a side effect of a motor task, i.e., no specific task evoking sensory activation was used, further investigation of sensory reorganization processes in DCM is justified and appropriate. Within this framework, sensory function should be studied as isolated as possible.

There exists a variety of different factors influencing surgical outcome[13], which might be a reason, why relations between cortical representations and clinical status are not simple to draw. In surgical outcome prediction, involvement of different diagnostic modalities therefore gains in importance[13,26] and needs to be considered in any research approach on DCM as well.

2.4.4. The Role of Hemispheric Lateralization in Neural Network Adaptation

Hemispheric lateralization is caused by an asymmetry between the left and the right hemisphere regarding the representation of brain functions[132]. A classic example of human behavior, which is based on hemispheric asymmetries, is handedness[133]. In general, there is broad consensus, that the primary processing of somatosensory information is primarily localized on the hemisphere which is contralateral to the stimulated skin region[134,135]. Both hemispheres can perform the basic functions of somatosensory information processing[134]. But the hemispheres never perform separately: Subcortical pathways allow an involvement of both hemispheres in the processing of unilateral somatosensory stimuli[134], as demonstrated by investigations on split-brain patients[136,137]. The hemisphere ipsilaterally to the stimulated skin region may not merely be involved in somatosensory processing via higher-order connections

of association areas[134]. It can also be directly addressed by a unilateral stimulus. Thus, degrees of asymmetry in information processing can evolve: In healthy, right-handed people, stimulation of the preferred hand leads to a strongly lateralized cortical response, while the stimulation of the left, less-preferred hand leads to a bi-hemispheric, scarcely lateralized response[135].

The importance of hemispheric lateralization for compensatory effects in lesions of the nervous system is subject of recent research. For instance, cerebral stroke can cause adaptation processes in both hemispheres[138]. Depending on the location and size of the lesion as well as the stage after the incident, activation of contralesional areas can either contribute to recovery or indicate a weak clinical outcome[138–141]. E.g., it could be shown by means of fMRI, that a co-activation of contralesional cingulate regions can have positive effects on the motor recovery in stroke affecting the basal ganglia[140]. In contrast, another fMRI-based study demonstrated, that higher ipsilesional activation in the primary motor cortex (M1) was associated with a better treatment outcome[142]. Lateralization in somatosensory areas was analyzed using fMRI, e.g., in the pathology of cerebral palsy, whereby a negative correlation between two-point discrimination and functional lateralization in S2 was found[143]. In conclusion, lateralization of brain functions can be affected by cerebral lesions and has an influence on recovery[138].

Regarding hemispheric lateralization of somatosensory cortical areas in DCM, no data appears to exist to date according to extensive literature search. However, it seems plausible, that lesions, which do not involve the cerebrum itself, but the spinal cord, can lead to remodeling processes, inter alia, in somatosensory networks and consecutively to a change of functional lateralization in the cortex.

2.5. Hypotheses and Objectives

The main objective of the present thesis is a better understanding of reorganization processes of the somatosensory system in DCM. As described in subsection 3.4.3, previous studies draw an incomplete and partially incoherent picture of cortical adaptation processes in patients suffering from DCM. Their results suggest that at least adaptation in the motor system could have compensatory effects and potentially influences the clinical outcome in a positive way[14,19]. Concerning the somatosensory system, few empirical conclusions about adaptation processes in DCM were drawn so far. In particular, it is desirable to find out, whether DCM-related changes within the somatosensory system[18] have a compensatory, neutral or even maladaptive influence on the clinical symptomatology. To come closer to answering this basic question, the following research questions and corresponding hypotheses will be studied:

I. *Do patients suffering from DCM show altered patterns of BOLD response to somatosensory stimulation in comparison to healthy control subjects?*

DCM has previously been shown to have effects on the extent and intensity of motor cortex activity[14,19,20]. On this basis, the following hypothesis is made regarding the somatosensory system: DCM patients have different activation patterns in the primary and secondary somatosensory cortex (measured by fMRI) compared to healthy controls.

II. *Do DCM patients differ from healthy control subjects in the hemispheric lateralization of somatosensory information processing?*

Hemispheric lateralization of cortex functions may be altered in various lesions of the central nervous system[138–141,143]. This may have compensatory effects or be a purely degenerative correlate[138–141]. Based on these findings in literature on other pathologies, the hypothesis is that patients suffering from DCM show significantly different cortical lateralization of somatosensory function in contrast to healthy control subjects.

III. *Does a correlation between limb-specific somatosensory modalities and BOLD activation in the primary and secondary somatosensory cortex exist in DCM patients?*

In DCM, somatosensitive fiber tracts at the spinal cord level may be damaged, resulting in reduced vibration sensation and alteration of somatosensory evoked potentials (SSEPs) in terms of latency delay[12,144,145]. It seems plausible that this attenuated input is also associated with reduced cortical responses in fMRI. Thus, it is hypothesized that for the respective limb (e.g., the right hand), the BOLD activation of DCM patients is correlated with the vibration sensation and the latencies of the SSEPs.

IV. *Is there a correlation between established clinical outcome measures of DCM and BOLD response in somatosensory cortical regions to peripheral stimulation?*

Various scores and questionnaires can be used in the clinical assessment of DCM. Here, the Japanese Orthopaedic Association (JOA) score[38,146] (Japanese Orthopaedic Association, 1994), the Disabilities of the Arm, Shoulder and Hand (DASH)[147] and Short Form 12 (SF-12)[148] questionnaires are considered. These reflect somatosensory impairment to varying degrees. The JOA score, for example, includes somatosensory impairment in addition to motor impairment and autonomous dysfunction[38,149]. It is possible to consider the items of the JOA score that represent somatosensory function in isolation as "sensory JOA". In this context, it can be hypothesized that more pronounced clinical impairment, represented by

the JOA, DASH and SF-12, is correlated with lower BOLD responses in somatosensory cortical regions. In particular, this correlation is expected for the sensory JOA score.

3. Materials and Methods

The following chapter comprises a description of the methods applied in this research project. In this framework, the composition of the study population (section 4.1) as well as the methods used for the assessment of the clinical condition (section 4.2) are stated. Subsequently, sections 4.3 to 4.6 address the acquisition and analysis of fMRI data, whereas the clinical contextualization of fMRI data is subject of section 4.7.

3.1. Study Design and Participants

In total, 18 subjects were included in the study, consisting of nine right handed patients aged between 37 and 74 (56 ± 12 years [mean ± standard deviation (SD)], 7 male) and suffering from radiographically confirmed DCM and furthermore nine age- and gender-matched healthy control subjects (34 - 71 years, 57 ± 12 years, 7 male). Only patients which underwent an anterior surgical decompression of the cervical spine at the Department of Neurosurgery of the University Hospital Cologne irrespective of their study participation were recruited. The study measurements were performed in a time period of no more than 14 days prior to surgery.

All patients were screened for and included in the "Cerebral Reorganization in Cervical Myelopathy Measured by Navigated Transcranial Magnetic Stimulation" (CReMe) multicenter study (registered at clinicaltrials.gov, registration number: 898 30 535). The CReMe study is a prospective clinical study conducted at the Departments of Neurosurgery of the Charité Berlin, the University Hospital of Cologne, the University Hospital of the Technical University of Munich (TUM, Klinikum Rechts der Isar) and the University Hospital of Bern (Inselspital). The study is conducted in collaboration with the German Spine Society (Deutsche Wirbelsäulenstiftung). Aim of the CReMe multicenter study is an improved diagnostic power in DCM by means of nTMS, since radiological findings cannot sufficiently indicate disease progression or predict surgical outcome[14]. The CReMe multicenter study is nTMS-based and includes follow-up measurements in intervals of 9 and 24 months after surgical decompression. The present thesis is based on a preoperative cross section cohort measured at the University Hospital Cologne. In the context of this local spin-off project of the CReMe study, additional data were acquired (thus exceeding the general study protocol of the multicenter study), i.e., motor and somatosensory task-related fMRI measurements as well as additional behavioral and neurophysiological measures (see subsections 4.2.2 to 4.2.4) to analyze the research questions mentioned in section 3.5.

The requirements for the study participants, as outlined in Table 1 and Table 2, were reasoned, inter alia, by the exclusion criteria of nTMS and fMRI, by ethical considerations, by legal reasons as well as by potential confounders in data analysis. All participants gave their written informed consent after an individual explanatory conversation with a study physician and

sufficient time for contemplation. The research project adhered to the Declaration of Helsinki (version 2013) and was approved by the Ethics Commission of the Cologne University's Faculty of Medicine (application number 18-058, date of decision: 2018/03/08).

Table 1: Inclusion criteria.

Patients	Control subjects
• age > 18 • written informed consent after medical information of a study physician and adequate reflection period • full capacity of informed consent, contractual capacity • cervical spinal stenosis, confirmed by means of imaging modalities with or without myelopathy, middle- or high-grade signs of paralysis of one or more limbs • sufficient general state of health, evaluated by the study physician • clinical indication for decompressive surgery of the cervical spine due to DCM	• age > 18 • written informed consent after medical information of a study physician and adequate reflection period • full capacity of informed consent, contractual capacity • sufficient general state of health, evaluated by the study physician

Table 2: Exclusion criteria.

Patients	Control subjects
• symptomatic tinnitus • Ménière's (MD) • cardiac pacemaker, electrodes of deep brain stimulation • diagnosed epilepsy or increased risk of epilepsy • insufficiently treated diagnosed psychiatric disorder • pregnancy • major cognitive disorder • alcohol or drug dependency • consume of alcohol or mind-altering medicaments immediately prior to the date of measure, potentially causing deviating test results and attention deficits • severe migraine or cluster headache • placement in an institution mandated by public authorities • contraindications of MRI*, TMS	• symptomatic tinnitus • Ménière's (MD) • cardiac pacemaker, electrodes of deep brain stimulation • diagnosed epilepsy or increased risk of epilepsy • insufficiently treated diagnosed psychiatric disorder • pregnancy • major cognitive disorder • alcohol or drug dependency • consume of alcohol or mind-altering medicaments immediately prior to the date of measure, potentially causing deviating test results and attention deficits • severe migraine or cluster headache • placement in an institution mandated by public authorities • contraindications of MRI*, TMS • previous surgery involving the nervous system

*Particularly with regard to the MRI measurements, the following exclusion criteria were checked: cardiac pacemaker, cardiac valve replacement, cochlear implants, implanted medication pumps, vascular clips, MRI incompatible metal implants, intracranial metal splinters, intrauterine device, pregnancy, claustrophobia, psychiatric disorders

3.2. Clinical Assessment

The clinical assessment comprised a selection of questionnaires, clinical tests, a neurological examination as well as the assessment of somatosensory evoked potentials (SSEPs). In the sections below, these are described in more detail. Table 3 provides an overview about the different components of the clinical assessment. The primary objective was a global capture of the neurological state of health. By this context, a higher validity of individual outcome measures and a better interpretability of the data were aimed. Both, the patient, and the control group underwent the clinical tests and the neurological examination. Thereby, the physical health of the control subjects could be ascertained. The specific clinical questionnaires and SSEPs were only assessed in the patients' subgroup.

3.2.1. Clinical Questionnaires

In order to obtain a broad picture of the patients' general clinical status, three different questionnaires were used. Each of them has a distinct emphasis:

SF-12

First of all, the Short Form 12 (SF-12) questionnaire[148], a shortened version of the Short Form 36 (SF-36)[150,151], was acquired as a generic indicator of health-related quality of life[152]. On the one hand, it provides a physical score, representing self-perceived health, physical capacity and pain[153]. On the other hand, it provides a mental score, indicating mental well-being, negative affects and social capability[153]. The SF-12 has been scaled on the basis of a representative sample of the German population[153]. The scores range between 0 and 100, while higher values indicate higher life quality[152]. Concerning the standard population, physical and mental SF-12 scores were adjusted to have a mean of 50 and a standard deviation of 10[153].

DASH

Additionally, the Disabilities of the Arm, Shoulder and Hand (DASH) questionnaire[147] was applied. This measure has been developed for the purpose of a standardized evaluation of functionality and symptoms regarding specifically the upper extremity and is applicable in a wide array of musculoskeletal disorders[154]. The DASH questionnaire has been standardized and validated in German for patients suffering from different disorders of the upper extremity[155]. It consists of 30 items and provides a score ranging from 0 to 100[155]. The higher the DASH score, the stronger the impairment[155].

JOA

The JOA score (Japanese Orthopaedic Association, 1994) is a widely established measure in western countries for the assessment of clinical impairment due to DCM[38,146] and the primary outcome after surgical decompression[149]. The JOA score captures motor as well as somatosensory function of the upper and lower extremities and the bladder function[38,149]. It ranges from 0 (severe impairment) to 17 (full score)[38], while the different domains of the JOA score allow even a separate consideration of sub-scores representing the somatosensory, the motor and the autonomous impairment[17]. The JOA score allows an identification of the grade of impairment and distinguishes grade normal function (16 - 17), grade 1 (12 - 15), grade 2 (8 - 11) and grade 3 (0 - 7)[156].

Table 3: Clinical assessment.

Clinical questionnaires	• SF-12 (Short Form 12) • DASH (disabilities of the arm, shoulder and hand questionnaire) • JOA (Japanese Orthopaedic Association score)
Clinical tests	• NHPT (Nine Hole Peg Test) • FTT (Finger Tapping Test): visually paced* and without pacing • HHD (Hand-Held Dynamometry) • 6MWT (Six Minute Walk Test)*
Neurological examination	• testing of reflexes* • muscle power acquisition (MRC scale) • testing of clonus and muscle tone* • testing of Romberg sign* • Unterberger stepping test* • sensation of pain and temperature (anamnesis)* • testing of proprioception* • sensation of vibration (Rydel-Seiffer tuning fork test)*
Somatosensory evoked potentials (SSEPs)	

*Additionally acquired data exceeding the general study protocol of the Cerebral Reorganization in Cervical Myelopathy Measured by Navigated Transcranial Magnetic Stimulation (CReMe) multicenter study

3.2.2. Clinical Tests

Patients and control subjects underwent several clinical tests within the framework of the CReMe multicenter study. These were performed in order to acquire detailed information about motor and somatosensory function and to contextualize single findings within a broader clinical picture. Since not all of these tests are part of the main analysis in the present dissertation, they are only concisely mentioned at this point. The detailed results are itemized in the Appendix (see Tables 9 and 10).

In order to assess manual skills, the subjects conducted the Nine-Hole Peg Test (NHPT)[157], which is referred to as a gold standard measure for the determination of manual dexterity[158]. Here, the participants were asked to place nine pegs, one by one, in nine holes on a board as quickly as they could, while the time was stopped. This task was performed in four different trials: forward and backward, once with the left and once with the right hand. In addition, the interplay of somatosensory and motor function was tested using the Finger Tapping Test (FTT), a widely used neurophysiological tool for the assessment of hand coordination and fine motor skills[159,160]. Concretely, the FTT was performed using an in-house purpose-developed script on the basis of the PsychoPy software package[161] (https://www.psychopy.org/). The subjects' finger taps were recorded by pressing a key. The test was conducted once using the right and once using the left index finger, while the maximal number of finger taps, the subject could perform within one minute, was counted in the first pass. In a second pass (additionally to the standard CReMe regime), the subjects were told to perform the task synchronously to a visual stimulus: The finger taps were visually paced by a red circle on a screen, flashing with a frequency of 3 Hz. Also, the second pass took one minute.

By means of a Hand-Held Dynamometry (HHD)[162] using a bulb dynamometer, the maximum isometric grip strength of the subjects was obtained[163]. This method was initially developed in reaction to the polio epidemic at the beginning of the 20th century[164] and nowadays applies in several muscular, skeletal and neurological illnesses[163,165,166].

Moreover, the Six-Minute Walk Test (6MWT)[167] was applied. It indicates the total distance a subject can walk during a time period of six minutes[168]. The 6MWT is commonly applied in several different diseases for an approximate estimate of the general physical status[168].

3.2.3. Neurological Examination

The neurological examination focused on the somatosensory and motor function. Within this framework, the reflex status of the upper and lower extremities was acquired including the testing of physiologic (biceps tendon, triceps tendon, patellar and Achilles tendon reflex) and pathologic (Trömner and Babinski sign) reflexes. Muscle power was assessed using the Medical Research Council (MRC) scale (Medical Research Council: Nerve Injuries Committee 1943) as an ordinal measure in order to detect any loss of power or paresis. The grading according to MRC scale is the following: 0 = no contraction, 1 = flicker or trace of contraction, 2 = active movement, with gravity eliminated, 3 = active movement against gravity, 4 = active movement against gravity and resistance, 5 = normal power. Clonus and muscle tone with specific attention to spasticity, rigidity, paratonia and hypotonia were tested by flexing and extending the subject's limbs passively[169].

Another aspect of the examination was the assessment of stance and gait. For this purpose, inter alia, the Romberg sign was tested[170]. It was developed for the detection of sensory ataxia

due to spinal cord damage and can be considered as positive if patients show a postural instability or even tendency to fall when the eyes are closed[169]. In addition, the Unterberger stepping test was performed[171] in order to assess imbalance due to vestibular or cerebellar disorders as differential diagnostic causes[172]. Here, the patient's ocular fixation was also temporarily removed by closing the eyes, while the patient was marching at least 30 seconds in place with the arms extended forward. The test was considered as positive, if the patient tended to rotate more than 45° in the left or the right direction. To assess gait pattern, subjects were instructed to place one foot in front of the other on an imaginary line (one time with ocular fixation and one time without). Meanwhile, the study physician paid attention for any gait abnormities and postural instability. If it was limited, the accomplished walking distance was recorded.

Beyond that, data was collected about the different components of somatosensation. The key focus of the present study was, however, on the sensation of light touch, since epicritic stimuli could be realized in the fMRI experiment outlined in subsection 4.3.2 without inconveniences for the trial participants. Anomalies in the sensation of pain and temperature were not practically tested but identified anamnestically. For a qualitative impression, the sensation of touch of the upper and lower limb was manually tested by the study physician[169]. Patients were specifically asked about paresthesia and hypesthesia. Proprioception was clinically tested by slightly bending the thumbs and the big toes of the patients upwards and downwards, while patients were instructed to keep their eyes close and to report the direction of the joint motion[169]. This test was repeated five times while the number of wrong statements were counted. Moreover, sensation of vibration (i.e., pallesthesia) was assessed at both sides of the body once at the radial styloid process representative for the upper extremity and once at the medial malleolus for the lower extremity. The vibration testing was performed using a 128 Hz Rydel-Seiffer tuning fork for the detection of sensation loss[173,174]. The basis of the vibrating tuning fork was one after another placed on the bony structures mentioned above, while patients had to tell when they stopped perceiving the declining vibration. Sense of vibration was scored according to a numerical scale ranging from 0/8 (complete loss of the vibratory sense) to 8/8 (maximum vibratory sense)[173,175].

3.2.4. Somatosensory Evoked Potentials

SSEPs were evoked by stimulation of the posterior tibial nerve at the medial malleolus (pulse frequency 3.1 Hz, pulse duration 0.2 ms). Potential differences were recorded from the primary somatosensory cortex using a stainless-steel needle electrode positioned at Cz' according to the international ten-twenty system[176] (see Figure 6), 3 cm behind Cz, corresponding to the projection area of the lower limb in the primary somatosensory cortex[177]. The reference electrode was placed frontomedian at Fz.

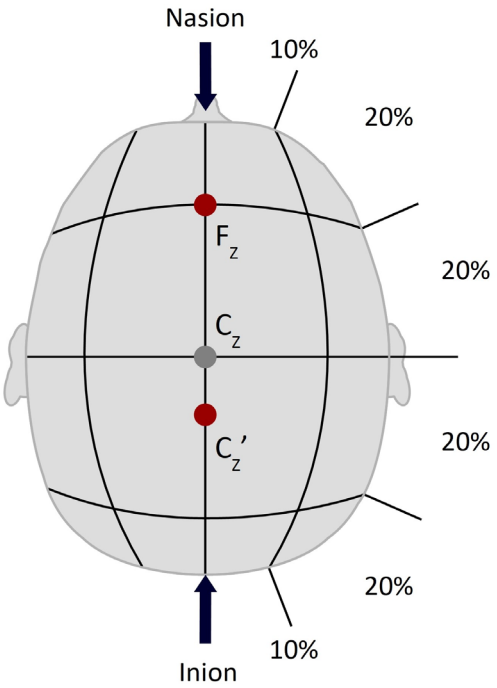

Figure 6: Positions of the needle electrodes according to the international ten-twenty system[176] during the measurement of tibial somatosensory evoked potentials. The measurement electrode is positioned at Cz' and the reference electrode at Fz. Adapted from Malmivuo and Plonsey, 1995[178].

The stimulation was performed at the lowest possible intensity evoking a motor response (usually about 10 - 20 mA), but never at a higher level than the individual threshold of discomfort. The signals were filtered and amplified (bandwidth 10 Hz - 250 Hz) and responses were averaged over 200 repetition cycles. During the SSEP acquisition, the software VikingQuest Master v11.0.0 (VIASYS™ NeuroCare, Madison, Wisconsin, USA) associated with the applied system for electromyography (EMG), nerve conduction studies (NCS) and evoked potentials (EPs) (VikingQuest™, VIASYS™ NeuroCare, Madison, Wisconsin, USA) was used. The software NicVue®, v2.9.1 (VIASYS™ NeuroCare, Madison, WI, USA) served for the measurements of latencies and amplitudes.

The latencies of distinct SSEP components (N33, P40, N0 and P60) and associated peak-to-peak amplitudes (N33/P40; P40/N50; N50/P60) were measured. The component N33 is assumed to be a reflection of thalamic or thalamocortical activity, while P40 represents the response in BA 3b in the primary somatosensory cortex[179]. P60 reflects the activity within parietal association areas, whereas the neurophysiological correlate of N50 remains unclear[179]. A typical stimulus response function of tibial SSEPs is demonstrated in Figure 7.

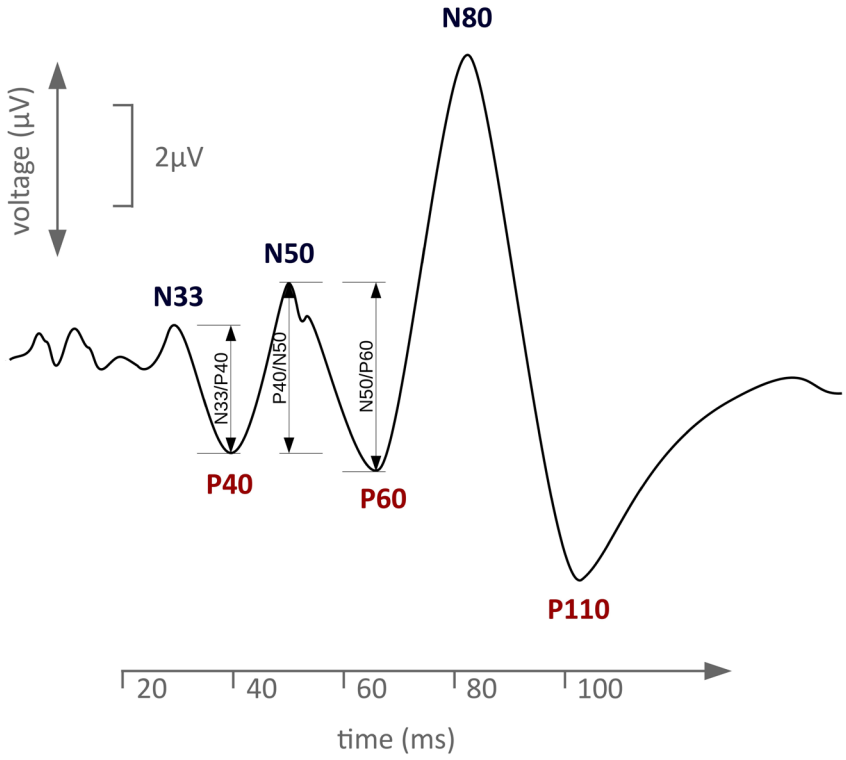

Figure 7: W-shaped stimulus response function of somatosensory evoked potentials. The stimulation was applied at the posterior tibial nerve and the potentials were recorded from the Scalp. Adapted from Stöhr 2005[177].

3.2.5. Statistical Interpretation of Clinical Outcome Measures

After confirmation for normal data distribution using the Shapiro Wilk test[180], the comparison of differences in clinical characteristics between the DCM group and the control group could be performed using an independent samples two-tailed t-test.

For the explorative purpose of detecting correlations between the clinical parameters in the patients' group, Spearman's rank-order correlation coefficient ρ was computed between any possible combination of respectively two clinical parameters. Here, a nonparametric measure of rank correlation was chosen since some of the variables were ordinally scaled. The demographic parameters "age" and "gender" were included as well, while the parameter "gender" was transformed in binomial scale artificially by assigning "male" and "female" the numbers 1 and 2. Furthermore, patient age, clinical scores, vibratory sensation, SSEP latencies, walking test, grip strength, finger tapping, and NHPT results were included in this analysis. The Spearman's correlations were considered significant if their p-values were below a significance threshold of $p \leq 0.05$.

The statistics and visualization of clinical outcome measures was realized using Python in a JupyterLab Environment[181] involving the packages NumPy[182], pandas[183], Matplotlib[184], SciPy[185], statsmodels[186], Pingouin[187] and seaborn[188].

3.3. BOLD fMRI Imaging Procedures and Data Acquisition

This section is concerned with the experimental setup and the imaging procedure as well as the ensuing preprocessing steps, which are necessary for the further statistical analysis of the data. The latter was performed at the single-subject level on the one hand, and at a group level on the other hand. Thereby, it was made sure, that individual effects, which are observed at the single-subject level, but averaged out in the group analysis, cannot be missed.

3.3.1. Scanner Data and Anatomical MRI

The entire imaging data of this clinical study was acquired by means of a 3 Tesla whole body MRI scanner (Ingenia, Phillips, Best, Netherlands) and a 32-channel head coil. Before acquiring the functional volumes, a T1 weighted high resoluted anatomical image was taken. Here, a T1 turbo field echo (T1FTE) sequence was used with 1 mm isotropic resolution and 180 sagittal slices, field of view (FoV) = 213 mm x 212 mm, flip angle = 8°, TR = 8.3 ms and echo time (TE) = 3.8 ms.

3.3.2. Task fMRI Session

Task-related fMRI volumes were acquired, using a GE-EPI sequence. The BOLD fMRI protocol consisted of repetitive sensory stimulation of the patient's backs of the hands and feet, corresponding to four different task conditions (sensory stimulation of the right hand, sensory stimulation of the left hand, sensory stimulation of the right foot, sensory stimulation of the left foot) (Figure 8). The latter was performed by means of a soft piece of felt, attached to an MR-compatible extension rod. During the measurements, a screen behind the MR scanner and a projection via a mirror under the head coil allowed the patient to respectively receive an announcement of the following task segment as well as the instruction, to close the eyes during the task. The synchronization of the display and the fMRI sequence was ensured by an in-house python-based script, developed using the PsychoPy software package[161] (https://www.psychopy.org/). The task fMRI was organized as a block design, consisting of 20 blocks with alternating epicritic stimulation of the extremities (Figure 8). One of these blocks had a duration of 32 sec including 14 sec task and 18 sec stimulus-free intertrial interval (ITI). The complete examination took almost 11 min and produced 320 NIfTI volumes in total, each containing for every single task segment 16 functional whole brain images with 35 slices of 3 mm thickness. Further imaging parameters of the fMRI session were: TR = 2000 ms, TE = 30

ms, voxel size = 3.0 mm × 3.0 mm × 3.0 mm and FoV = 230 mm × 230 mm. The flip angle of the RF pulse was 90°.

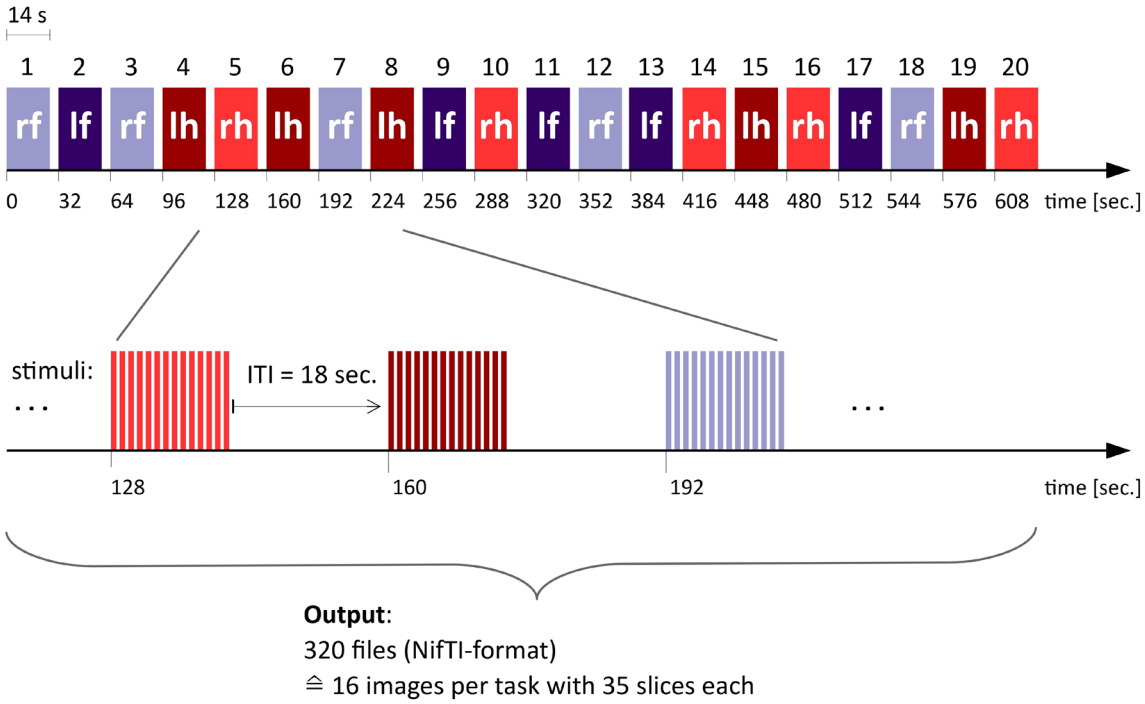

Figure 8: Task-based functional magnetic resonance imaging protocol. The data acquisition was organized as a block design consisting of 20 task segments in total. During the protocol, each of the four tasks was repeated five times in varying order. The stimulated extremity of the respective task condition can be identified with the following abbreviations: lh (left hand), rh (right hand), lf (left foot), rf (right foot).

3.4. Preprocessing of fMRI Data

Before a statistical analysis of cortical activation can be conducted, fMRI data needs to pass through a number of preprocessing steps[189]. The latter were performed using MATLAB® 2019a (MATLAB 2019) and the Statistical Parametric Mapping software package SPM12, revision 7487 (Wellcome Department of Imaging Neuroscience, London, UK; https://www.fil.ion.ucl.ac.uk/spm/)[190]. Figure 9 illustrates the sequence of preprocessing steps, which are outlined in the following.

BOLD signal changes due to head motion are a major confound in fMRI[191]. Regarding the fMRI session, we accepted a spatial deviation of about ± 1 mm in translation and ± 1° in rotation at maximum. Small movements, inter alia, caused by respiration, blood flow and pulse are physiological and inevitable[192], which is why a subsequent motion-correction, the realignment, is indispensable[189]. In the first preprocessing step, the functional EPI images of one fMRI

session were therefore realigned to an average of all volumes. This works with a rigid body transformation on the basis of three translational and three rotation parameters[193].

Then, a coregistration of the high-resolution T1 weighted anatomical image to the low-resolution EPI volumes of the respective subject was performed. After this form of adjustment, functional volumes match the anatomical image spatially[195]. Coregistration is necessary, since structural and functional data are not acquired simultaneously, and the exact spatial position of the test person may therefore deviate[195]. Furthermore, the T2* weighted EPI technique, which is applied in the functional sequences, causes intrinsically geometric distortion[195].

Coregistration therefore requires a rigid body affine transformation with three shear and three zoom parameters, additional to three translational and three rotational parameters[193].

Subsequently, the structural volumes were segmented into gray matter (GM), white matter (WM) and cerebrospinal fluid (CSF). This was performed by means of unified segmentation, a probabilistic method combining the approach of voxel-wise intensity-based tissue classification and the approach of standard brain template-based tissue identification[194]. The segmentation is necessary, since CSF and WM are frequently afflicted with artifacts, while GM is related to neural activation[196,197].

In preparation of any statistical analysis, involving more than one subject, the normalization into a standard space, by means of rigid body transformation with 12 parameters and a nonlinear transformation is necessary[193]. Here, the deformation field, provided by the segmentation step, was used for the normalization of the functional volumes into standard Montreal Neurological Institute (MNI) space.

For the purpose of noise reduction, spatial smoothing was finally performed by calculating a weighted average over the respectively adjacent voxels[197]. An isotropic Gaussian kernel of 6 mm FWHM was applied.

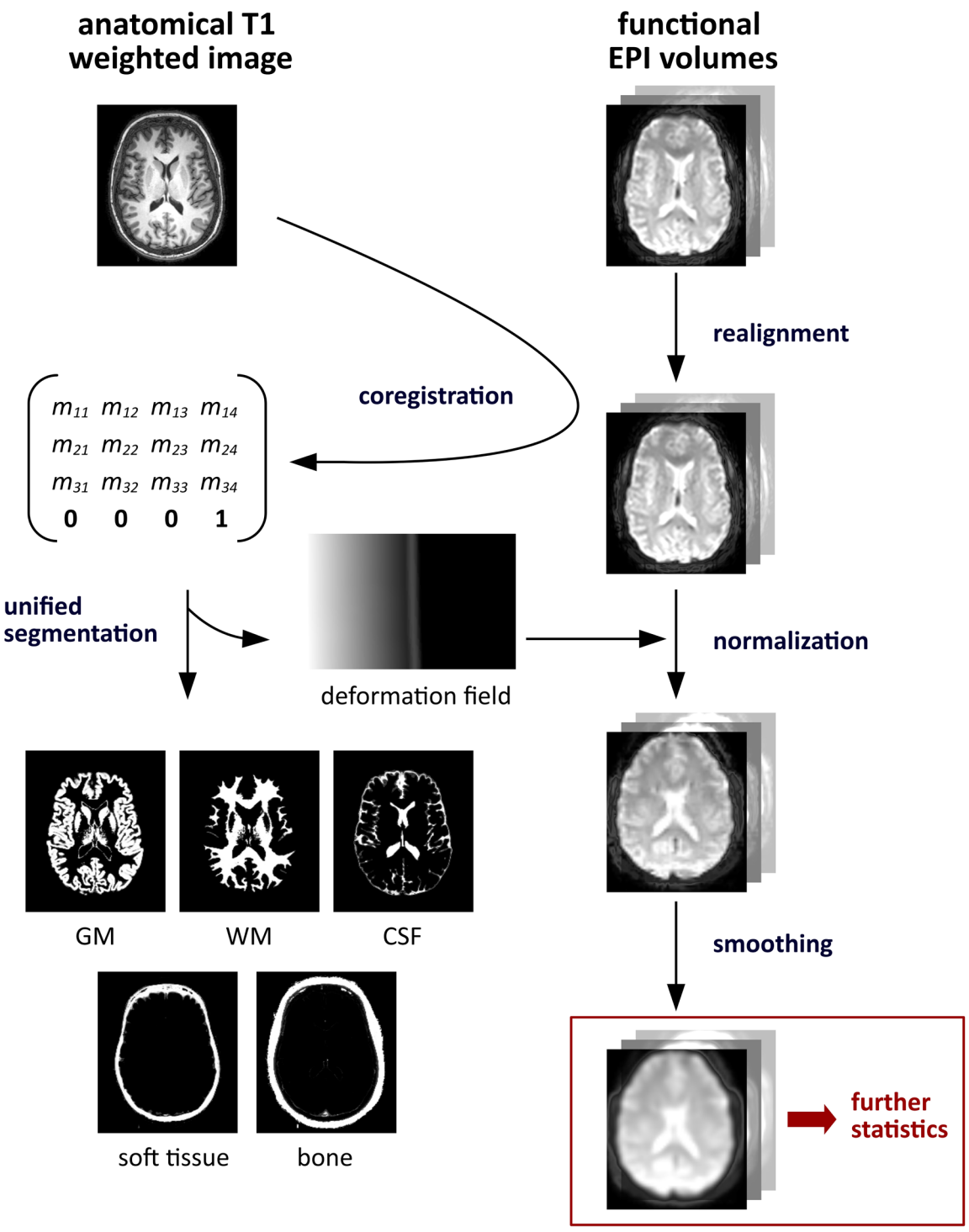

Figure 9: Preprocessing procedure. The flowchart visualizes the sequence of preprocessing steps applied to the data obtained from the functional magnetic imaging (fMRI) procedures at the single subject level[190,194]. Abbreviations: CSF (cerebrospinal fluid), EPI (echo-planar imaging), GM (grey matter), WM (white matter).

3.5. Statistical Analysis of BOLD Activation

The Analysis of BOLD activation was performed using SPM12, revision 7487 (Wellcome Department of Imaging Neuroscience, London, UK)[190]. The following section describes the methodological approach of the fMRI data analysis on both the single subject and the group level, including the main features of ROI definition.

3.5.1. Statistical Parametric Mapping

Single Subject Analysis

At the level of each single subject, a general linear model (GLM) analysis[198] was performed. GLM was used to voxel-wise approximate a HRF related to the respective stimulus[198]. Boxcar stimulus functions convolved with the canonical HRF[198,199] were used for modeling the four somatosensory task conditions. A high-pass filter of 1/128 Hz was applied on the time series of each voxel. The output of the 1st level analysis were three-dimensional data matrices, the statistical parametric map (SPM), for every single participant and every task condition. In each SPM, a specific t-value is assigned to every voxel[193]. Basic t-contrasts were applied for each subject in order to observe the primary effect of every stimulus type at the single subject level. Voxels were considered as significantly activated, if their t-values undercut a siginficance threshold of $p \leq 0.05$, family-wise error (FWE) corrected for multiple comparisons at the voxel level.

Group Analysis

Based on the task-specific contrast images provided by the single subject analysis, a secondlevel GLM analysis followed. The latter was the precondition for the comparison of parameter estimates for somatosensory task conditions between patients and controls at the group level. A three-way analysis of variance (ANOVA) was performed, including the factors “group” (patients/controls), “limb” (hand/foot) and “side” (right half of the body/left half of the body). The effect of each task condition on the BOLD activation was analyzed for both groups. Additionally, simple contrast images were generated indicating the effect, which the factor “group” had on the cortical response to each task condition. This involved both testing for a negative effect, i.e., a reduced BOLD activation in the patient group (contrast: “controls minus patients”) and for a positive effect, which would mean an increased BOLD activation in the patient group (contrast: “patients minus controls”). T-values passing a significance threshold of $p < 0.05$, FWE corrected were identified as significant. For the purpose of discussing smaller effects, which did not resist FWE correction, voxels, whose t-values passed a significance threshold of $p < 0.001$, uncorrected, were reported additionally. Significance levels are specified at the appropriate place. The visualization of cortical response at the group level was

performed using CAT12 (http://www.neuro.uni-jena.de/cat)[200] and MRIcroGL (https://www.mccauslandcenter.sc.edu/mricrogl/home)[201].

3.5.2. ROI Definition

In order to analyze the local functional somatosensory response under the four respective task conditions, six anatomical ROIs were defined, based on the MNI-space matching probabilistic cytoarchitectonic atlas of the SPM anatomy toolbox v3.0[202–204]. These included S1, consisting of BA 1[205,206], BA 2[207], BA 3a and BA 3b[205,206], as well as S2[208,209]. S2 is located in the parietal operculum[210] and corresponds partly to BA 40 and BA 43[208]. However, there is more recent histological evidence, suggesting this classification to be obsolete and indicating, that a differentiation of S2 in four distinct subordinate cytoarchitectonical areas does reflect reality much better[208]. This is why we choose to forgo a distinction of BAs in S2. In the following, we instead refer to S2 as a whole.

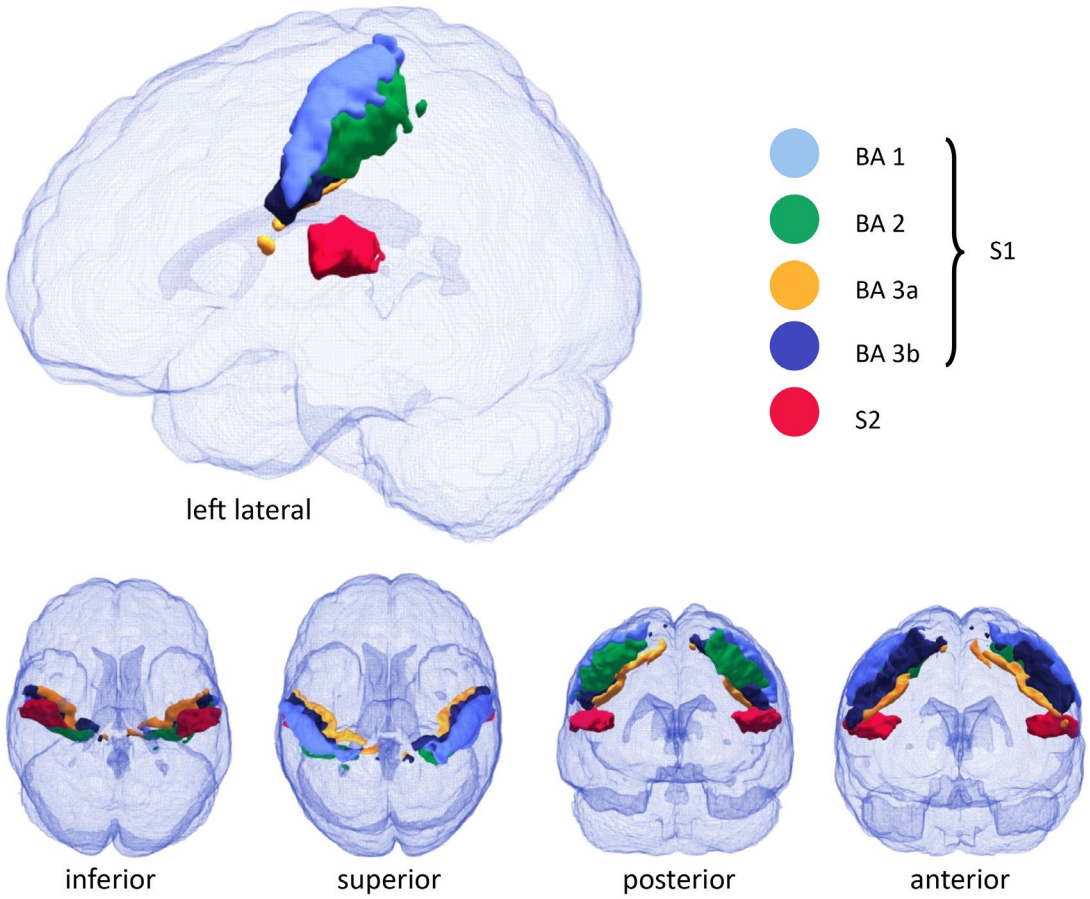

Figure 10: Regions of interest. Visualization of the primary (S1) and secondary (S2) somatosensory cortex according to the maximum probability maps (MPMs) provided by the statistical parametric mapping (SPM) anatomy toolbox v3.0[202–204].

The cytoarchitectonic probabilistic maps were developed on the basis of histological analysis of post-mortem brains and they allocate values to each individual voxel, which indicate the probability of belonging to specific brain areas[202]. The probabilistic maps of different ROI may overlap which would cause multiple entries of functional activation in the statistical analysis. This would have diluted the results. To prevent this problem, maximum probability map (MPM) were used. Here, each voxel is allocated to the ROI, it most likely belongs to[202]. A drawback of MPMs is, that ROI obtained in this way are quite strictly defined. Given the fact, that preceding studies proved, that the localization of cortical activation areas in patients with cervical spondylotic myelopathy may differ from conditions in healthy subjects[14,18], it cannot be precluded, that the ROI might slightly miss the exact localization of functional areas in individual cases.

Using MATLAB® 2019a (MATLAB 2019) and the SPM12 (Wellcome Department of Imaging Neuroscience, London, UK; https://www.fil.ion.ucl.ac.uk/spm/)[190], function ImCalc, all the positive values in the MPM of the specific ROI were allocated to the value 1. The result of this segmentation was a binary mask for each ROI, which could then be applied to the functional data in order to identify the relation of activated clusters to anatomy and to analyze activation of each single ROI separately. For the purpose of visualization (see Figure 10), the individual segmented binary masks of the elected ROIs as well as of the complete brain were rendered using ITK-SNAP v3.8.0[211] and were assembled by means of ParaView[212,213].

3.6. Analysis of Hemispheric Lateralization

Hereinafter, the calculation of lateralization indices (LIs) as well as their statistical evaluation should be outlined.

3.6.1. Calculation of Lateralization Indices (LI)

With a view to the cortical representation of somatosensory stimuli, the existence of a clear hemispheric dominance was investigated. In other words, it was analyzed if the cortical representation of the left extremities was localized primarily on the right hemisphere and vice versa. An adequate and established instrument herefore is the LI. With regard to a task condition, it indicates the hemispheric dominance and quantifies the degree of lateralization[214–216]. This measure is primarily applied in the assessment of language lateralization[217], but it can as well be used in the investigation of other brain functions like memory[218] or the processing of audition[219], vision[220] and sensorimotor information[143,221]. The task-related activation maps (i.e., SPMs) obtained from the fMRI data serve as the data basis for the computation of the LI[222]. Various approaches for evaluating hemispheric lateralization are available, providing different degrees of robustness and reproducibility[216].

Classical LI

The classical approach of LI calculation is based on the following formula[214,215,217,223]:

$$LI = f \cdot \frac{Q_{LH} - Q_{RH}}{Q_{LH} + Q_{RH}} \quad (1)$$

Q_{LH} and Q_{RH} result from the fMRI measurements and refer to the left and the right hemisphere[217]. The variable f is an optional scaling factor, which determines the range of possible LI values[217]. Here, f was defined as 1. Hence, LI values range from -1 to +1, while positive values indicate a dominance of the left hemisphere and negative a dominance of the right hemisphere[224–226]. Q_{LH} and Q_{RH} can be determined in accordance to varied standards. For instance, Q_{LH} and Q_{RH} can result from the sum of activated voxels in a respective ROI above a previously defined fixed intensity threshold, or from the signal change amplitude[217]. The classical threshold-based approach is problematic, since the resulting LI depends strongly on the arbitrarily determined threshold[225–227]. This is why a threshold-independent approach is the method of choice for a robust analysis of lateralization[222,226].

Average LI

A more sophisticated method for the assessment of cortical lateralization has been presented by Kayako Matsuo and colleagues[228]. The so-called AveLI can be computed as follows:

$$sub\text{-}LI = f \cdot \frac{Q_{LH} - Q_{RH}}{Q_{LH} + Q_{RH}} \quad (2)$$

$$AveLI = \frac{\sum sub\text{-}LI}{VN} \quad (3)$$

Here, a separate, so-called subordinate LI (sub-LI) is calculated for every positive t-value existing in a ROI, while the respective t-value serves as the threshold[228]. Subsequently, the overall AveLI is computed as the mean of all sub-LIs, while the number of sub-LIs equals the total count of voxels with positive t-values VN in a bihemispheric ROI[228]. Main advantages of the AveLI approach are its resistance to outliers and its high reproducibility[222,228]. Each positive t-value contributes to the AveLI, while higher t-values are given more weight for the purpose of noise reduction at the lower t-values[222,228].

The concrete approach used in this thesis is the following: The previously created binary masks (see subsection 4.5.2), based on the tissue probability maps, were separately applied on the activation maps (SPMs) of the study participants provided by the single subject analysis step. This was the precondition for calculating individual AveLIs for each ROI. The computation of

the AveLIs was conducted by means of MATLAB® 2019a (MATLAB 2019) in accordance to the approach provided by Matsuo and colleagues[228]. The output was an AveLI for each ROI of a subject and for each of the four task conditions. In one exceptional case, in which one of the patients did not show any BOLD activation in the respective BA, AveLI was set to the value 0, which expresses absent hemispheric lateralization. AveLIs were calculated at the single subject level since it could be assumed, that the AveLIs of the unequally impaired patients might show a high scattering.

3.6.2. Statistical Analysis of Hemispheric Lateralization

First of all, the AveLIs calculated for a specific ROI and task condition were respectively tested for normal distribution using the Shapiro Wilk test[180]. If the obtained p-Value was larger than 0.05, a normal distribution was assumed. This was the necessary precondition for applying a two-sided t-test for independent samples, to analyze the AveLIs for significant differences between patients and control subjects on the one hand and between the ROIs on the other hand. A false discovery rate (FDR) correction for multiple comparisons[229] was performed (alpha level = 0.05).

The visualization, the plotting and the statistical analysis of hemispheric lateralization was performed by means of Python using a JupyterLab Environment[181]. The applied packages and libraries were namely: NumPy[182], pandas[183], Matplotlib[184], SciPy[185], statsmodels[186] and seaborn[188].

3.7. fMRI in the Context of Clinical Symptoms

Correlation analyses between tactile stimulation-associated BOLD response and clinical parameters were performed for the patients' group. Here, contrast images associated with tactile stimulation of the respective extremity and side of the body were selected and entered into an SPM multiple regression analysis with the specific clinical parameter as covariate. Hereby, relationships between clinical scores (JOA, sensory JOA, DASH, physical SF-12) and BOLD response following the tactile stimulation of each extremity were investigated. Likewise, pallesthesia of each extremity was correlated with BOLD response to somatosensory stimulation of the same extremity (e.g., pallesthesia of the left hand and tactile stimulation of the left hand). Finally, left and right tibialis SSEP latencies (N33 and P40) were used as covariates for regression analyses of BOLD response to stimulation of the upper and lower extremity of the respective side of the body. Correlations were reported, if the respective t-values passed a significance threshold of $p < 0.001$, uncorrected.

4. Results

The results of this thesis are presented later in this chapter. More detailed, results of the clinical assessment are outlined at the very beginning (section 5.1). Next, sections 5.2 and 5.3 focus on the findings of the BOLD fMRI data while section 5.4 tries to contextualize the BOLD fMRI data against the background of the clinical findings.

4.1. Results of the Clinical Assessment

The following section addresses the clinical results according to the following structure: First, the reasons for the patients' surgical indications are stated briefly (subsection 5.1.1). Second, the physical state of the participants is evaluated in general and more particularly with regard to DCM by means of the pertinent clinical questionnaires (subsection 5.1.2). And third, subsections 5.1.3 to 5.1.4 outline the results of the measurement variables which involve both motor and sensory function and of the electrophysiological examination. Subsection 5.1.5 pictures associations between the different parameters in a correlation matrix and serves the gain of an overall impression of the clinical data.

4.1.1. Preconditions of the Surgical Intervention

The DCM patients showed different phenotypes of the pathology, like the level and the extent of their lesion, which was planned to be treated by means of a ventral surgical decompression. Five of the nine patients suffered from a stenosis between two cervical spinal segments (CV 3/4, CV 5/6 or CV 6/7). Two patients showed a spinal narrowing involving three segments (CV 4/5 and CV 5/6 or CV 5/6 and CV 6/7) and two further patients showed an involvement of four segments (CV 4/5, CV 5/6 and CV 6/7). The surgery indication was justified individually in each case. Besides the severity of symptoms and the dynamics of the pathology, the patients' personal demands on the functionality were considered. The spectrum of patients ranged from a musician impeded in his professional practice by mild somatosensory deficits up to patients suffering from DCM for many years until the surgical intervention became essential because of a pronounced deterioration of symptoms culminating in autonomous dysfunction. The period of time from the first beginning of symptoms until surgical treatment relevantly differed between the patients (47 ± 66 months [5;216 months]). An important reason for late treatment was delayed diagnostic identification of DCM and referral to a neurosurgical clinic.

Table 4: Demographic data and clinical state.

	DCM patients	Control subjects	P-value	Max. Range
n	9	9	-	-
Age	56 ± 12	57 ± 12	0.864	-
Gender (male/female)	7/2	7/2	1.000	-
Handedness (right/left)	9/0	9/0	1.000	-
Extent of stenosis (number of segments)	3 ± 1	-	-	-
Approx. symptomatic time period (months)	47 ± 66	-	-	-
JOA scores	13.3 ± 2.3	-	-	0 – 17
Motor upper	2.9 ± 1.1	-	-	0 – 4
Motor lower	3.4 ± 0.6	-	-	0 – 4
Sensory deficit	4.4 ± 1.0	-	-	0 – 6
Bladder dysfunction	6.7 ± 0.5	-	-	0 – 3
DASH score	33.78 ± 28.77	-	-	0 – 100
SF-12 physical	39.15 ± 10.41	-	-	0 – 100
SF-12 mental	54.13 ± 9.46	-	-	0 – 100
6MWT (meters)	490 ± 111	609 ± 101	0.029	-

4.1.2. Preoperative Clinical Situation

Patients showed different qualities and intensities of impairment. For an overview of the preoperative clinical situation, this subsection outlines the physical condition of the subjects in general and, in particular, the impairment of somatosensory functionality. The SF-12 questionnaire[148,153] was used to obtain a general impression of the patients' health-related quality of life (Figure 11).

The physical SF-12 score indicated, that patients mostly were below the average of a representative sample of the German population. However, only two patients had a physical score lower than two standard deviations below the mean of the standard population, i.e., they were in poorer physical condition than 97 % of the standard population. The mental SF-12 scores of the DCM patients did not relevantly differ from the standard population. On average, patients had even a slightly higher mental condition than the standard population. Coinciding with the physical SF-12, the results of the 6MWT[167] spoke for a reduced physical state of the patients' group, whose walking distance was significantly reduced in comparison with the control group ($p = 0.029$). The patients' disability involving the upper extremities, measured by means of the DASH questionnaire[147,154], varied widely (33.78 ± 28.77).

Interindividual differences regarding the JOA score (Japanese Orthopaedic Association, 1994) were relatively small (13.3 ± 2.3). In more detail, two DCM patients showed functional deficits corresponding to grade 2 (JOA score 8 - 11). Five patients were mildly impaired (grade 1, JOA score 12 - 15) and two further patients showed normal function according to their JOA score (JOA score ≥ 16). None of the patients achieved the full score regarding the somatosensory function. Table 4 gives an overview about the demographic and clinical properties of the DCM

patients and the healthy control group. Detailed clinical data at the single subject level is provided in the Appendix (see Table 9 and 10).

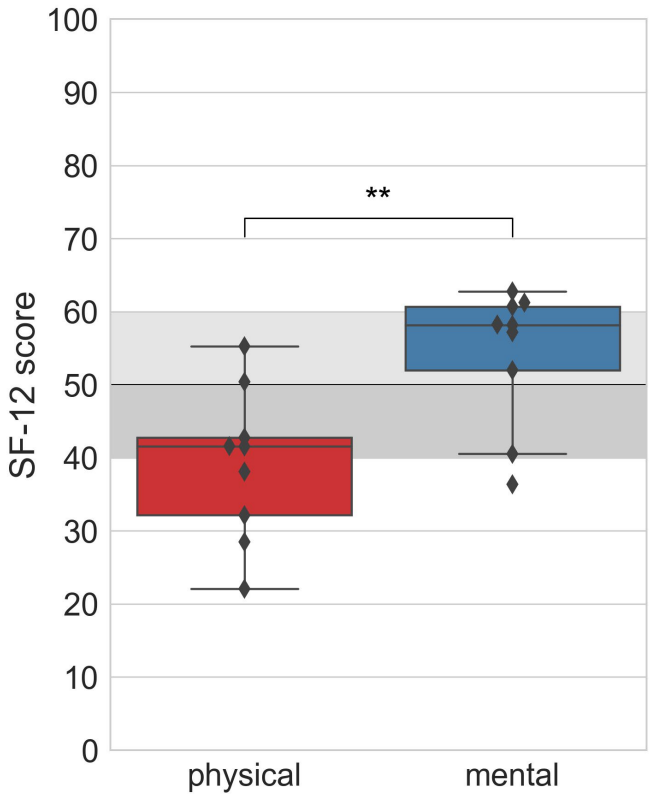

Figure 11: Physical and mental Short Form 12 scores of the patients in comparison with German standard population. The boxes extend from the upper to the lower quartile. A black line within each box indicates the median. The whiskers each extend to the furthest data point within 1.5 times the interquartile range. On average, the patients' physical Short Form 12 (SF-12) score was approximately one standard deviation (SD) lower than the score of the standard population (mean 50 ± 10), whereas the patients' mental score was not inferior compared to the standard. Degenerative cervical myelopathy (DCM) patients had significantly lower physical SF-12 scores than mental SF-12 scores (*p ≤ 0.05, **p ≤ 0.01, ***p ≤ 0.001).

4.1.3. Sensorimotor Skills

In human activity, sensory and motor function are inseparably linked. This is why besides somatosensory function, motor skills are outlined briefly, even though they are not the main topic of this thesis (see Table 5).

All nine patients showed paresthesia to different extends and six of nine patients reported manifest hypesthesia involving at least one limb. Four patients stated a pathological sensation of temperature. Two patients were suffering from allodynia of one upper limb and two other patients showed mildly reduced proprioceptive function of the lower extremity. Within the control group, no such deficits or symptoms could be detected. In the testing of the vibratory

sense, patients performed worse than control subjects. This applied for every limb, but the difference was solely significant for the left upper extremity (p = 0.030). For the right upper extremity, at least a statistical trend towards inferiority of the patient group (p = 0.085) can be described. Regarding the status of reflexes, in seven of the patients anomalies could be found: Four of them showed increased reflexes, whereas the other three featured reduced reflex response in distinct muscles. Pathological reflexes (Trömner, Babinski) could not be detected. Muscle tone was increased in three patients and reduced in another patient. Paresis of different muscle groups were present in six patients. Closely linked to the assessment of muscle power was the testing of grip force applying HHD. Here, patients were characterized by insignificantly weaker performance than control subjects: With their dominant (right) hand, patients achieved 73 ± 24 kPA and controls reached 79 ± 24 kPA. The left hand generated 68 ± 24 kPa in the patient group and 79 ± 20 kPa in the control group. The findings of the control subjects were physiologically.

Table 5: Clinical examination: sensorimotor skills.

	DCM patients	Control subjects	P-value	Max. Range
Paresthesia	9/9	0/9	-	-
Hypoesthesia	6/9	0/9	-	-
Pathological Sensation of temperature	4/9	0/9	-	-
Allodynia	2/9	0/9	-	-
Vibratory sense				
Right upper extremity	5.8/8 ± 2.5/8	7.3/8 ± 0.5/8	0.085	0/8 – 8/8
Left upper extremity	6.7/8 ± 1.4/8	7.1/8 ± 0.8/8	0.465	0/8 – 8/8
Right lower extremity	5.4/8 ± 2.5/8	6.9/8 ± 1.4/8	0.148	0/8 – 8/8
Left lower extremity	4.8/8 ± 2.3/8	6.9/8 ± 1.2/8	0.025	0/8 – 8/8
Increased reflexes	4/9	0/9	-	-
Reduced reflexes	3/9	0/9	-	-
Pathological reflexes (Trömner, Babinski)	0/9	0/9	-	-
Increased muscle tone	3/9	0/9	-	-
Reduced muscle tone	1/9	0/9	-	-
Grip force right hand, HHD (kPa)	73 ± 24	79 ± 24	0.563	-
Grip force left hand, HHD (kPa)	68 ± 24	79 ± 20	0.290	-
Positive Romberg sign	1/9	0/9	-	-
Positive Unterberger stepping test	1/9	0/9	-	-

One of the patients showed a positive Romberg sign as an indicator of spinal ataxia. Three patients featured atypical findings in the performance of the Unterberger stepping test. More precisely, two of them could not perform this test adequately due to their tendency to fall and in one case, Unterberger's test was de facto positive (60° rotation to the right direction), which would speak for an additional vestibular disorder.

Two parameters which cover the sensorimotor interplay are the NHPT and the FTT. On average, patients needed more time than control subjects for the performance of the NHPT (see Table 6). This applied for each trial type, i.e., for the forward and backward performance and for both hands. However, this difference between both groups was not significant.

Table 6: Nine-Hole Peg Test results. This table shows the time (sec), patients and controls needed to complete the test (mean ± SD).

		DCM patients	**Control subjects**	**P-value**
Left hand	Forwards	18.4 ± 6.8	14.4 ± 2.8	0.121
	Backwards	6.7 ± 1.0	5.9 ± 1.1	0.128
Right hand	Forwards	23.6 ± 19.8	15.6 ± 2.4	0.245
	Backwards	7.8 ± 4.7	6.0 ± 1.2	0.284

For both groups (patients and control subjects), the visually paced FTT trial revealed mean intertap intervals (mITIs) matching the given pacing interval (⅓ sec) quite well (see Table 11, Appendix). The coefficient of variation (CoV), which was calculated over the mITIs and indicates the dispersion, did not relevantly vary between both groups. The FTT trial at maximum speed, which was performed without a pacing stimulus, presented a different picture. Here, patients showed on average a slower tapping frequency, i.e., a shorter mITI and a larger associated CoV compared to control subjects even though both deviations were not statistically significant. The results of both FTT trials are visualized in Figure 12.

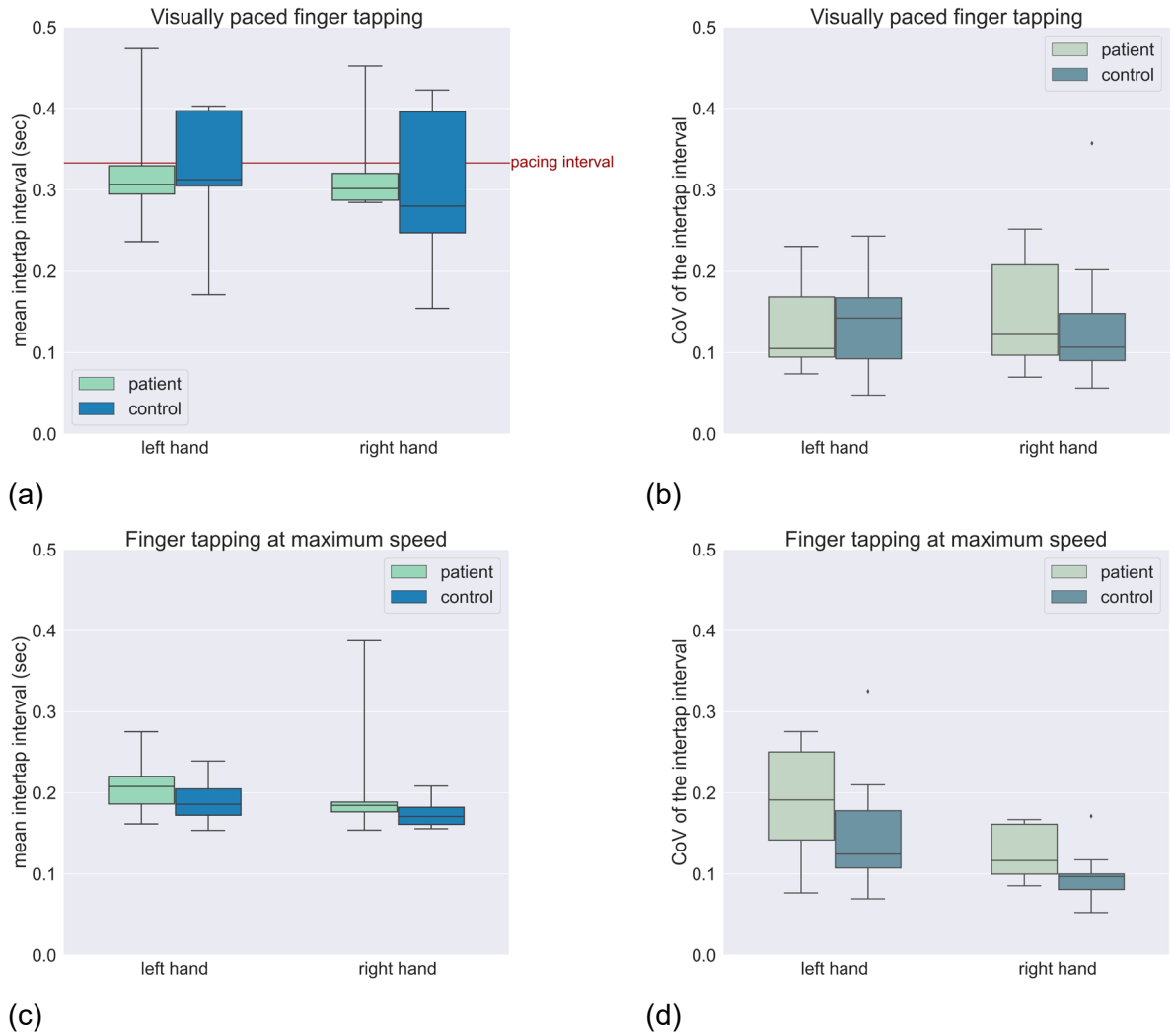

Figure 12: Behavioral finger tapping results. Results of visually paced finger tapping are shown above (a, b). Below, the results of the finger tapping session at maximum speed (unpaced) are visualized (b, c). The mean intertap intervals (mITIs) are displayed on the left side (a, c) and the coefficients of variation (CoV) at the right side (b, d). Patient data are shown in green and control data are shown in blue. The boxes extend from the upper to the lower quartile. A black line within each box indicates the median. The whiskers each extend to the furthest data point within 1.5 times the interquartile range. Differences between patients and controls were not significant but pointed toward reduced frequencies and higher CoVs in patients for FTT at maximum speed. (*p ≤ 0.05, **p ≤ 0.01, ***p ≤ 0.001).

4.1.4. Electrophysiological Findings

Due to the limited diagnostic validity of the late SSEP components such as N50 and P60, which can primarily be interpreted as certainly pathologic if they are absent[179], focus regarding the evaluation of latencies and associated side differences is instead set on N33 and P40 (see Table 7 and Table 8). Three patients featured pathologically prolonged latencies on both sides

as well as pathological side differences (higher than the upper standard limits proposed by Stöhr, 2005). Three further patients showed pathological side differences and normal latencies. In two of the patients, no pathological alteration of latencies or side differences could be detected. One of the patients did not show any responses to peripheral stimulation of the posterior tibial nerve at all. This subject was not taken into account in the calculation of average latencies. Amplitudes were interpreted as 0 in this case. Tibial SSEP latencies are visualized in Figure 13.

The peak-to-peak amplitudes (N33/P40) amounted 0.80 ± 0.55 regarding stimulation of the left and 1.23 ± 0.80 regarding stimulation of the right tibial nerve. Hence, they were lower than the reference range proposed by Stöhr, 2005 (2.8 ± 1.41)[177]. In contrast, the respective side differences of the peak-to-peak amplitudes (N33/P40) (0.59 ± 0.50) did not relevantly differ from the reference range (0.67 ± 0.78)[177].

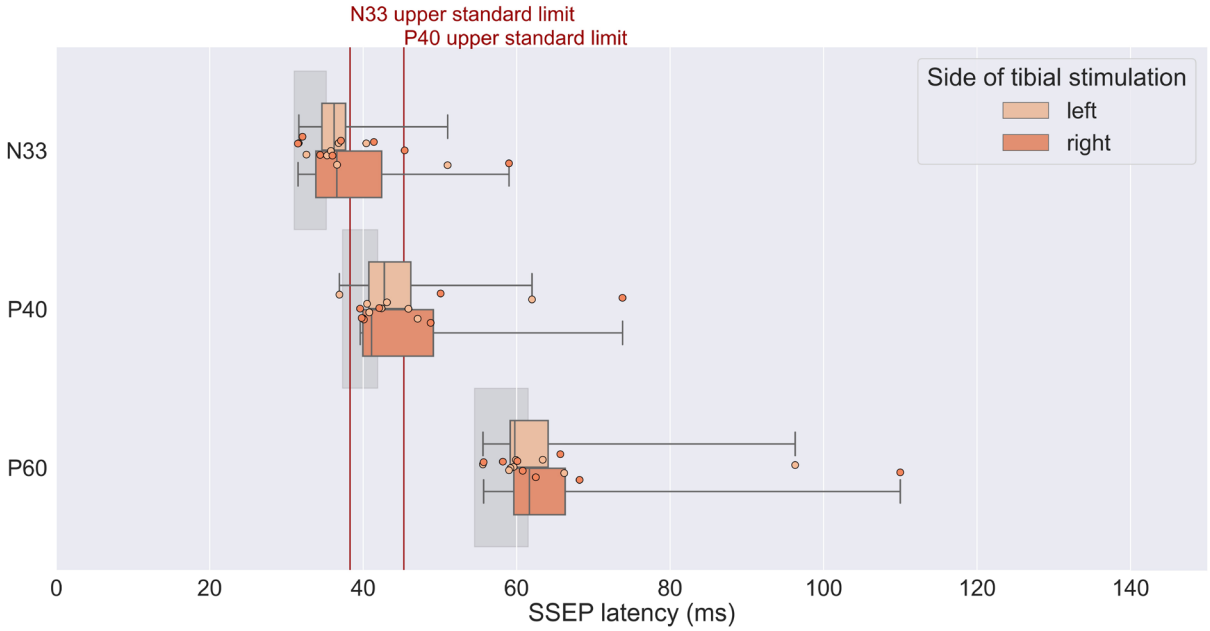

Figure 13: Latencies of the tibial somatosensory evoked potentials in the patients' group. The boxes extend from the upper to the lower quartile of the somatosensory evoked potential (SSEP) latencies. A black line within each box indicates the median. The whiskers each extend to the furthest data point within 1.5 times the interquartile range. Normal ranges and upper standard limits proposed by Stöhr (2005) are shown in grey shading and red lines. Three of the patients showed pathologically prolonged latencies on both sides.

Table 7: Tibialis somatosensory evoked potential latencies. The latencies (ms) of the degenerative cervical myelopathy (DCM) patients' group (mean ± SD) are listed with accompanying standard values and upper standard limits from reference works.

	DCM patients		**Standard values**	**Upper standard limits**
	left	right	Stöhr, 2005	Stöhr, 2005
Latency of N33 (ms)	37.5 ± 6.1	39.61 ± 9.1	33.1 ± 2.1	38.3
Latency of P40 (ms)	44.8 ± 7.6	46.79 ± 11.7	39.6 ± 2.3	45.3
Latency of P60 (ms)	64.9 ± 13.1	67.65 ± 17.6	58.0 ± 3.5	

Table 8: Side differences of the tibialis somatosensory evoked potential latencies. Standard values from reference works (ms) are listed next to the degenerative cervical myelopathy (DCM) patients' side differences (mean ± SD).

	DCM patients	**Standard values**	**Upper standard limits**
		Stöhr, 2005	Stöhr, 2005
Side difference of N33 latency (ms)	4.1 ± 2.4		2.5
Side difference of P40 latency (ms)	3.3 ± 3.7	0.89 ± 0.68	2.6
Side difference of P60 latency (ms)	4.8 ± 4.6		

4.1.5. Association of Clinical Parameters

Figure 14 shows the results of pair-wise Spearman's correlation regarding the clinical and demographic parameters. It is important to note, that this approach is not hypothesis-driven but merely explorative. Therefore, the interpretability is quite limited, and any results can at most be a starting point for subsequent investigations with a larger sample size. The primary aim of this correlation analysis is a better overview of the huge amount of qualitatively different parameters. Therefore, only a few noticeable individual aspects are pointed out.

For instance, a significant negative correlation between the DASH score and the physical SF-12 can be found. This means, that an underlying clinical impairment may be reflected both in a higher DASH score and a reduced SF-12 score. Moreover, negative correlations between the sensory JOA and the respective SSEP latencies can be deduced from the correlation matrix, indicating that a lower (weaker) sensory JOA score is associated with prolonged SSEP latencies. The association between the (overall) JOA score and the SSEP latencies is less pronounced. No significant correlation between the sensory JOA and sensation of vibration can be found. However, the (overall) JOA seems to be correlated positively with the vibratory sensation of the right upper and lower extremity.

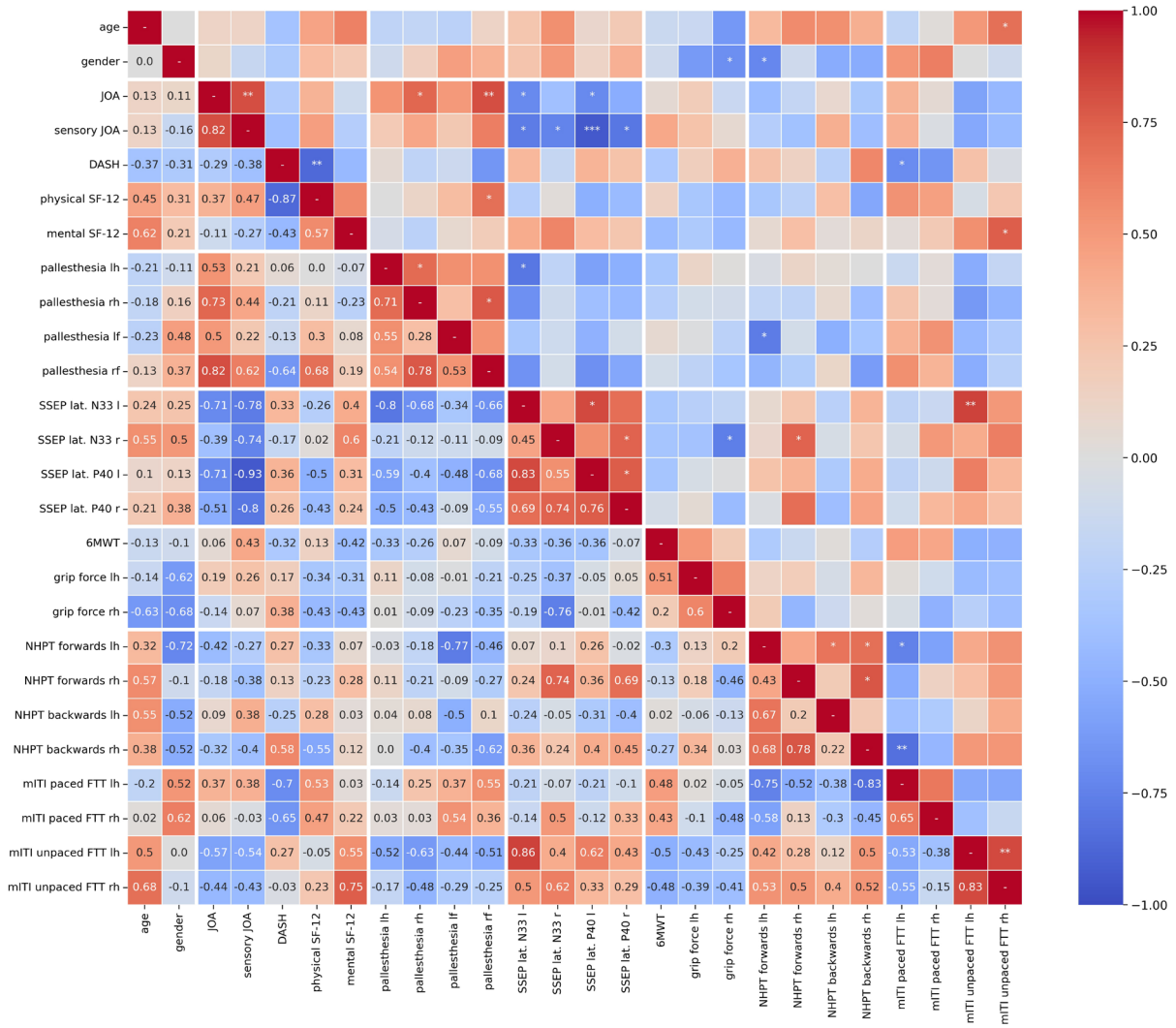

Figure 14: Correlation of clinical and demographic parameters. Spearman correlation was calculated pairwise between the parameters acquired from the patients. The spearman correlation coefficients for each pair of parameters are given in the lower triangle of the correlation matrix. In the upper triangle, significant correlations are labeled as follows: *p ≤ 0.05, **p ≤ 0.01, ***p ≤ 0.001. For better clarity, the P60 SSEP latencies as well as the side differences of the SSEP latencies have been omitted in this presentation. A complete representation can be found in the Appendix (see Figure 21). Abbreviations: 6MWT (Six-Minute Walk Test), DASH (Disabilities of the Arm, Shoulder and Hand questionnaire), FTT (Finger Tapping Test), JOA (Japanese Orthopaedic Association score), lat. (latency), lf (left foot), lh (left hand), mITI (mean intertap interval), NHPT (Nine-Hole Peg Test), rh (right hand), rf (right foot), SF-12 (Short Form 12 score).

4.2. Analysis of Task-related Response

The following section focuses on the BOLD activation measured within the framework of fMRI acquisition. Here, BOLD response of the single subjects is briefly described at first, in order to

outline the data, on which the group analysis was based on. Second, the group analysis is presented, in which the effect of DCM on BOLD response was tested by means of an ANOVA.

4.2.1. Single Subject Analysis

Movement effects of the single subjects during the fMRI procedure did not exceed ± 1 mm in translation and ± 1° in rotation.

Eight of nine DCM patients and eight of nine control subjects showed significant ($p \leq 0.05$, FWE corrected) BOLD activation within the somatosensory cortex in response to somatosensory stimulation of the right (dominant) hand (see Table 12, Appendix). In six of the patients just as in six of the control subjects, significant activation in the somatosensory cortex could be identified under every single one of the four task conditions. One patient did not show any significant BOLD activation, neither in response to stimulation of the upper nor the lower extremities. Two further patients showed cortical response solely to stimulation of the dominant hand. With regard to the control subjects, every one of them did show significant BOLD activation under at least one of the task conditions (see Table 13, Appendix).

4.2.2. Group Analysis

Task-related BOLD activation at the group level

In general, control subjects showed a larger recruitment of cortical regions than DCM patients (see Figure 22, Appendix). This finding applied for all task conditions, but particularly for the tactile stimulation of the right (dominant) hand.

To better identify activation specifically in the somatosensory cortex, Figures 15 and 16 visualize exclusively BOLD activation in S1 and S2 using a transparent MNI template. Both patients and controls showed a pronounced left hemispheric cortical response in S1 and S2 ($p \leq 0.05$, FWE corrected) to right (dominant) hand stimulation (Table 15, Appendix and Figure 15). Beyond that, the control group showed a slight ipsilateral coactivation in S2 ($p \leq 0.001$, uncorrected), which was absent in the patient group. Referring to S1 in greater detail, the following could be observed: In the patients' group, the left BA 2 was significantly ($p \leq 0.05$, FWE corrected) involved in the processing of stimuli affecting the right hand, whereas activation in BA 1, BA 3a and BA 3b, which could be observed without applying a correction for multiple comparisons ($p \leq 0.001$), did not survive FWE correction. The control group showed significant activation in BA 1, BA 2 and BA 3b ($p \leq 0.05$, FWE corrected). Here, solely activation in BA 3a did not survive the FWE correction.

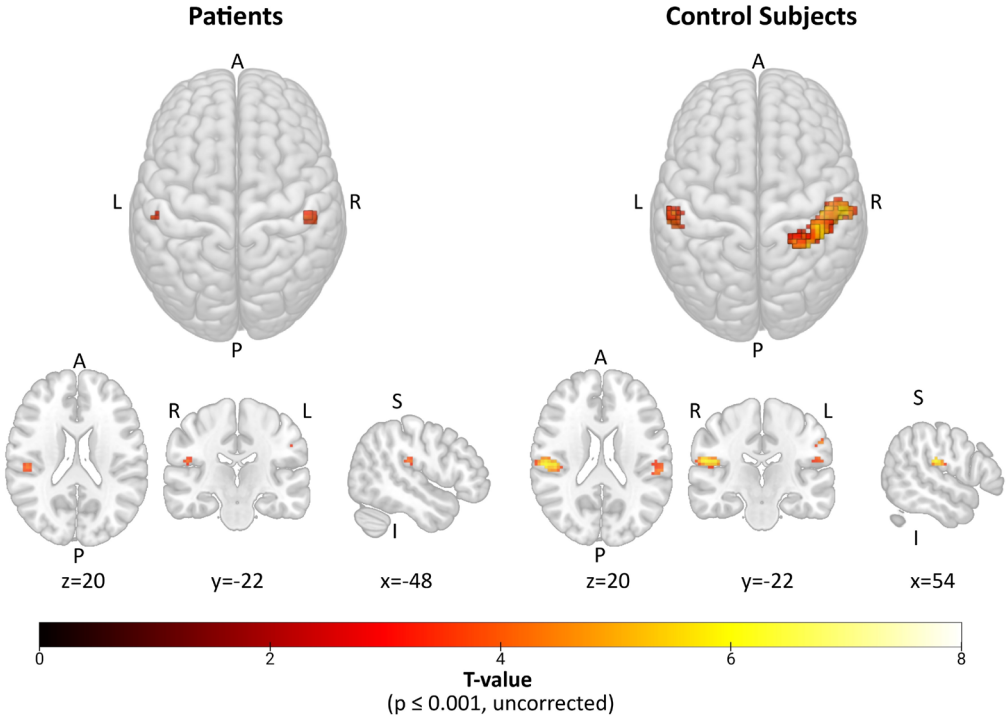

(a) Somatosensory stimulation of the left hand.

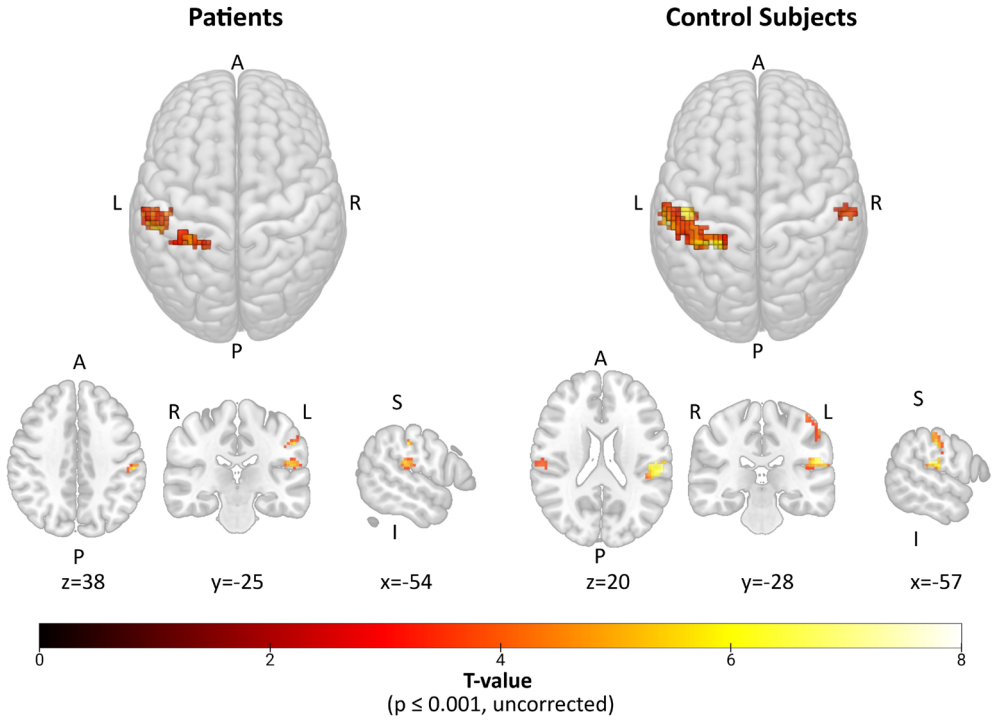

(b) Somatosensory stimulation of the right hand.

Figure 15: Cortical activation within the somatosensory cortex in response to somatosensory stimulation of the upper extremities. Blood oxygenation level dependent (BOLD) response ($p \leq 0.001$) in the primary (S1) and secondary (S2) somatosensory cortex to stimuli affecting the left hand (a) and the right hand (b) is demonstrated. The slices at the bottom show the local maximum with the highest T-value for the patients (left) and for the control subjects (right). The statistical parametric maps were masked for bihemispheric S1 and S2. DCM patients showed a reduced recruitment of cortical regions and a much scarcer involvement of ipsilateral S2 than control subjects.

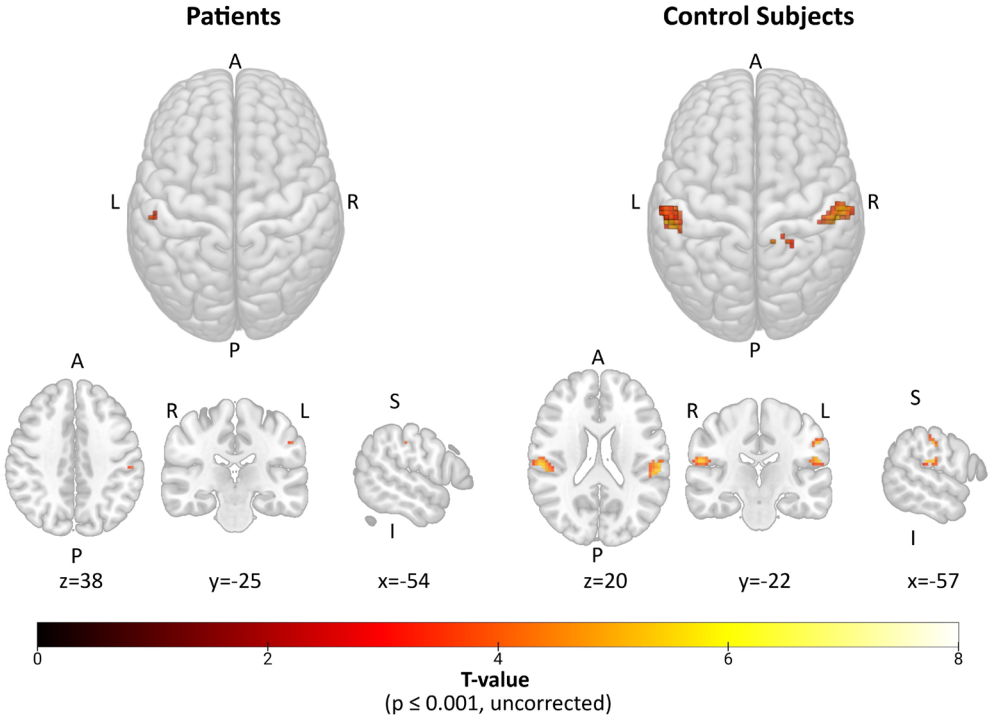

(a) Somatosensory stimulation of the left foot.

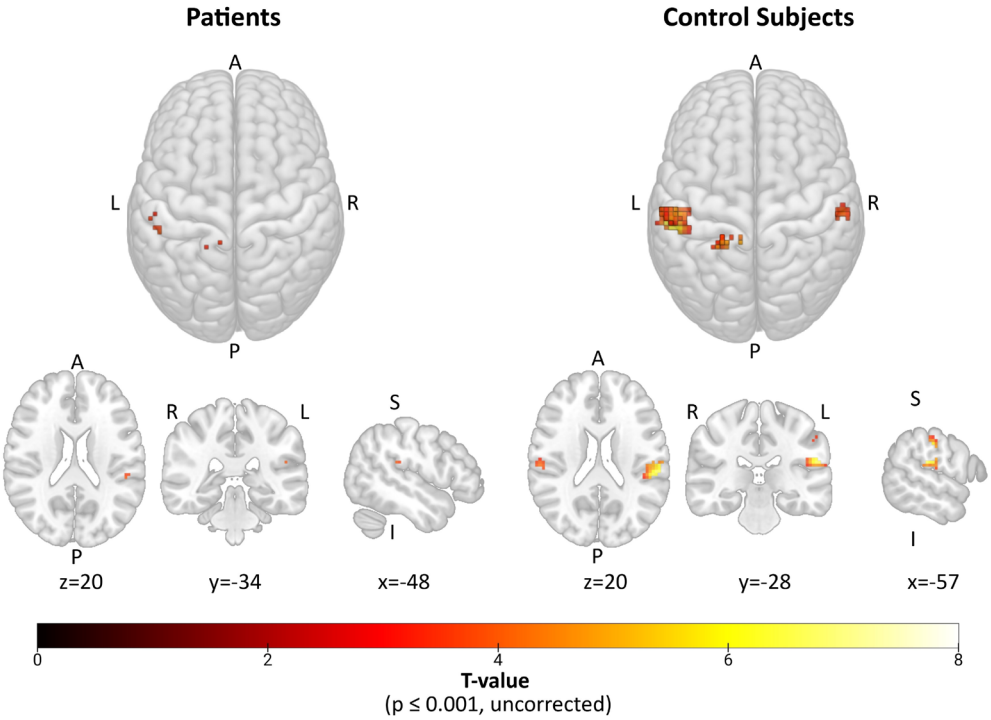

(b) Somatosensory stimulation of the right foot.

Figure 16: Cortical activation within the somatosensory cortex in response to somatosensory stimulation of the lower extremities. Blood oxygenation level dependent (BOLD) response ($p \leq 0.001$) in the primary (S1) and secondary (S2) somatosensory cortex to stimuli affecting the left foot (a) and the right foot (b) is demonstrated. The slices at the bottom show the local maximum with the highest T-value for the patients (left) and for the control subjects (right). The statistical parametric maps were masked for bihemispheric S1 and S2. DCM patients showed a reduced recruitment of cortical regions and a much scarcer involvement of ipsilateral S2 than control subjects.

Regarding the other task conditions (somatosensory stimulation of the left hand, the right foot and the left foot), controls respectively featured significant responses within the somatosensory cortex ($p \leq 0.05$, FWE corrected), including a consistent activation within the ipsilateral S2 ($p \leq 0.001$, uncorrected). In contrast, patients showed only poor activation in S1 ($p \leq 0.001$, uncorrected) and a much scarcer involvement of ipsilateral areas. Remarkably, BOLD activation of the patients' group in response to epicritic stimulation of every limb expect the right, preferred hand did not survive FWE correction.

Local maxima of the delineate ROI under the respective task conditions are outlined in Tables 14 to 17 (Appendix). If significant ($p \leq 0.001$, uncorrected) BOLD activation can be observed for both patients and control subjects in the respective ROI, the right column displays the Euclidean distance (ED). FWE corrected p-values ≤ 0.05 were marked with an asterisk in the tables. Activated clusters ($p \leq 0.001$, uncorrected) within S1 and S1 (masked SPMs) are three-dimensionally (3D) visualized in Figure 15 and 16.

Effects of DCM on Cortical Response

Within the framework of between-subject ANOVA, contrast images showing the effect of DCM on the cortical response were generated. The ANOVA results demonstrate for every task condition that patients did not show significantly more activation than controls in any voxel. Conversely, there were clusters in which BOLD activation was higher in healthy control subjects than in patients ($p \leq 0.001$, uncorrected). Hence, a negative effect of DCM on the cortical responsiveness to somatosensory stimuli could be identified. However, this effect manifested itself most clearly under the task condition of somatosensory stimulation of the right (preferred) hand. Under the other task conditions, areas of significantly higher ($p \leq 0.001$, uncorrected) activation within the control group compared to the patients involved evidently fewer voxels. Figures 17 and 18 show the voxels of significantly ($p \leq 0.001$, uncorrected) higher BOLD-activation, that controls showed in comparison to the DCM patients.

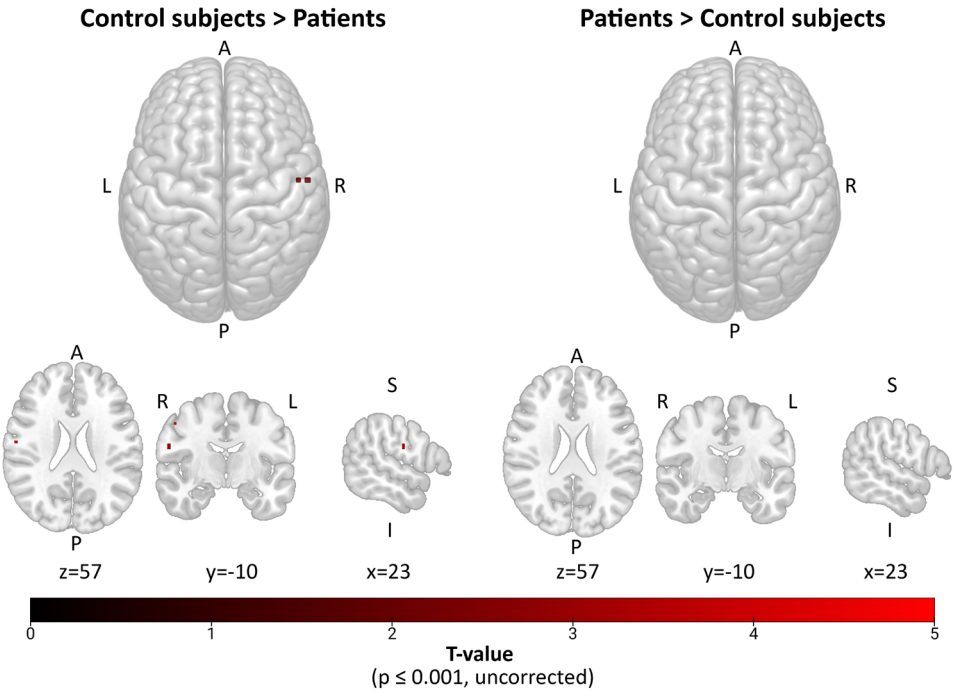

(c) Somatosensory stimulation of the left hand.

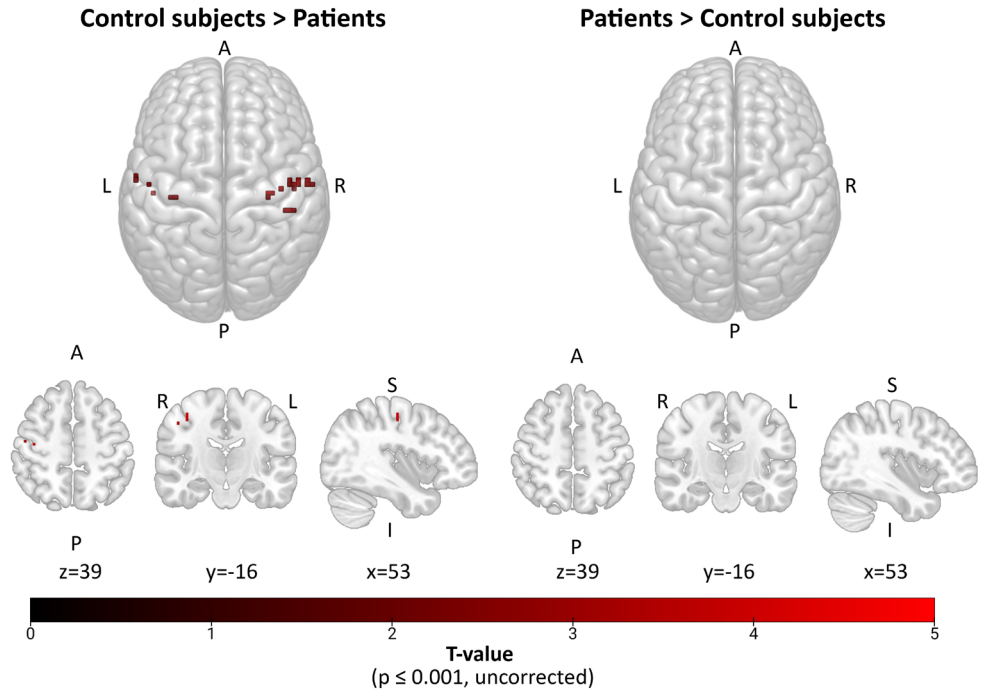

(d) Somatosensory stimulation of the right hand.

Figure 17: Contrast images provided by the Analysis of variance for tasks involving the upper extremities. Blood oxygenation level dependent (BOLD) responses in the primary (S1) and secondary (S2) somatosensory cortex are compared between patients and control subjects showing significantly higher BOLD activation in controls ($p \leq 0.001$). Results are demonstrated for somatosensory stimulation of the left (a) and right (b) upper extremity. The statistical parametric maps were masked for bihemispheric S1 and S2. BOLD response was reduced in DCM patients compared to control subjects.

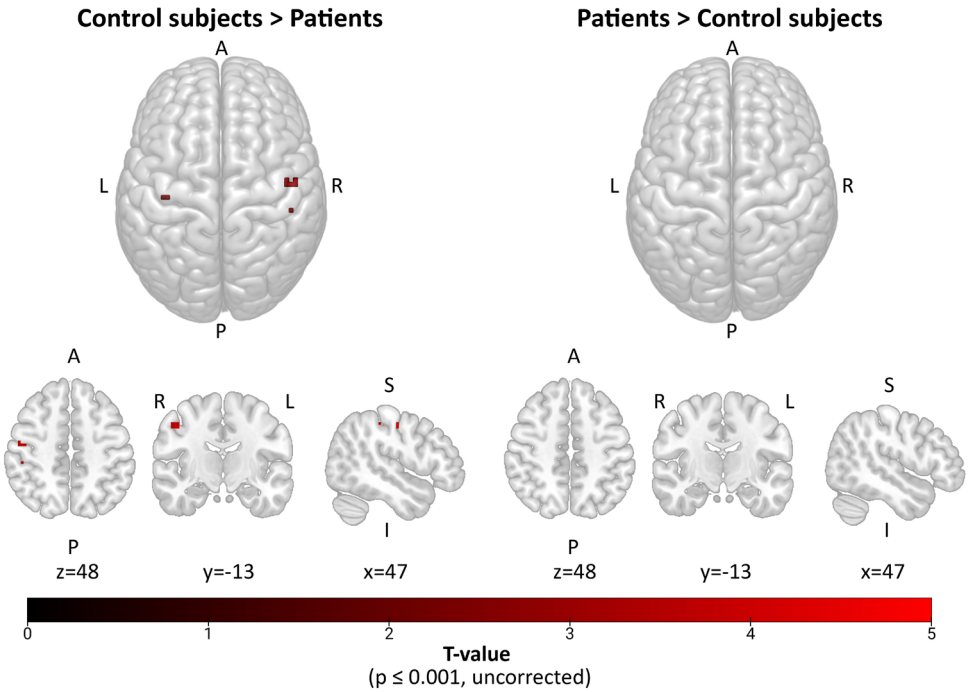

(a) Somatosensory stimulation of the left foot.

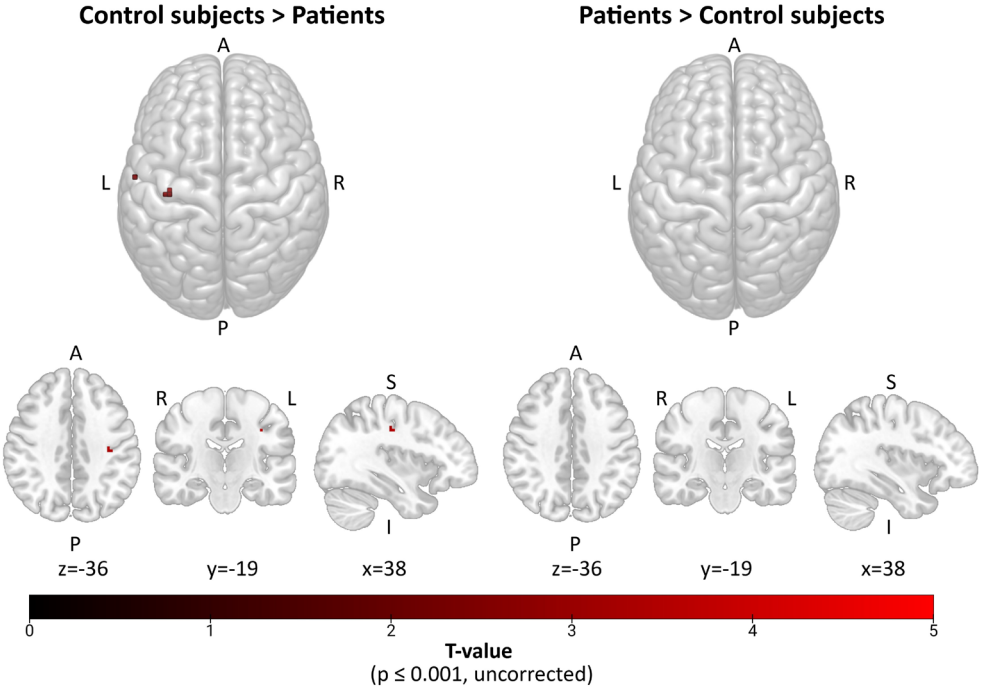

(b) Somatosensory stimulation of the right foot.

Figure 18: Contrast images provided by the Analysis of variance for tasks involving the lower extremities. Blood oxygenation level dependent (BOLD) responses in the primary (S1) and secondary (S2) somatosensory cortex are compared between patients and control subjects showing significantly higher BOLD activation in controls ($p \leq 0.001$). Results are demonstrated for somatosensory stimulation of the left (a) and right (b) lower extremity. The statistical parametric maps were masked for bihemispheric S1 and S2. BOLD response was reduced in DCM patients compared to control subjects.

4.3. Hemispheric Lateralization

AveLIs were calculated for each subject, task condition and ROI, respectively. If no BOLD activation was measured, the AveLI was set to 0 (equivalent to no hemispheric lateralization), which applied to BA 2 in one of the patients regarding “somatosensory stimulation of the left foot”.

The processing of stimuli involving the right extremities showed in both, the patient, and the control group a clear hemispheric lateralization in favor of the left cortical hemisphere (See Figure 19). Thereby, the control groups’ AveLIs of the ROI S1 and S2 differentiated significantly from the AveLI computed for the hemispheres involving the BOLD-activation of the whole brain. This could be shown for cortical response to somatosensory stimuli affecting the right hand ($p \leq 0.001$, FDR corrected) as well as the right foot ($p \leq 0.0001$, FDR corrected). Also in the patients’ group, AveLIs of cortical response to somatosensory stimulation of the right hand differed in S1 and S2 significantly from the AveLI of the hemispheres ($p \leq 0.0001$, FDR corrected). Regarding the task condition "somatosensory stimulation of the right foot", this effect was not significant DCM patients.

In contrast, cortical response to somatosensory stimulation of the left extremities was not generally lateralized to one hemisphere. Notably, the statistical scattering due to interindividual differences was higher, too. This could be observed even more clearly in the patient group than in the control group and becomes apparent in the standard deviations, stated in Table 18 (Appendix).

With a view on the BAs representing S1, significant differences of these ROI can only be observed in the control group (See Figure 23, Appendix). In this regard, somatosensory stimulation of the left lower extremity is associated with significant differences between the AveLIs of BA 1 in contrast to BA 3a and BA 3b ($p \leq 0.01$). Here, BOLD activation tends to be lateralized to the right hemisphere in BA 1 and to the left hemisphere in BA 3a and BA 3b. Somatosensory stimulation of the right lower extremity led to significantly more pronounced lateralization of functional brain activity to the left hemisphere in BA 2 ($p \leq 0.01$) and BA 3a ($p \leq 0.001$) in comparison to BA 1. Differences between both groups did not survive FDR correction for multiple comparisons. However, statistical trends ($p \leq 0.1$, uncorrected) towards a more pronounced lateralization of the processing of stimuli affecting the right upper extremity to the left hemisphere can be described for S1 ($p = 0.0591$, uncorrected) and BA 3a ($p = 0.0538$, uncorrected) in the patient group.

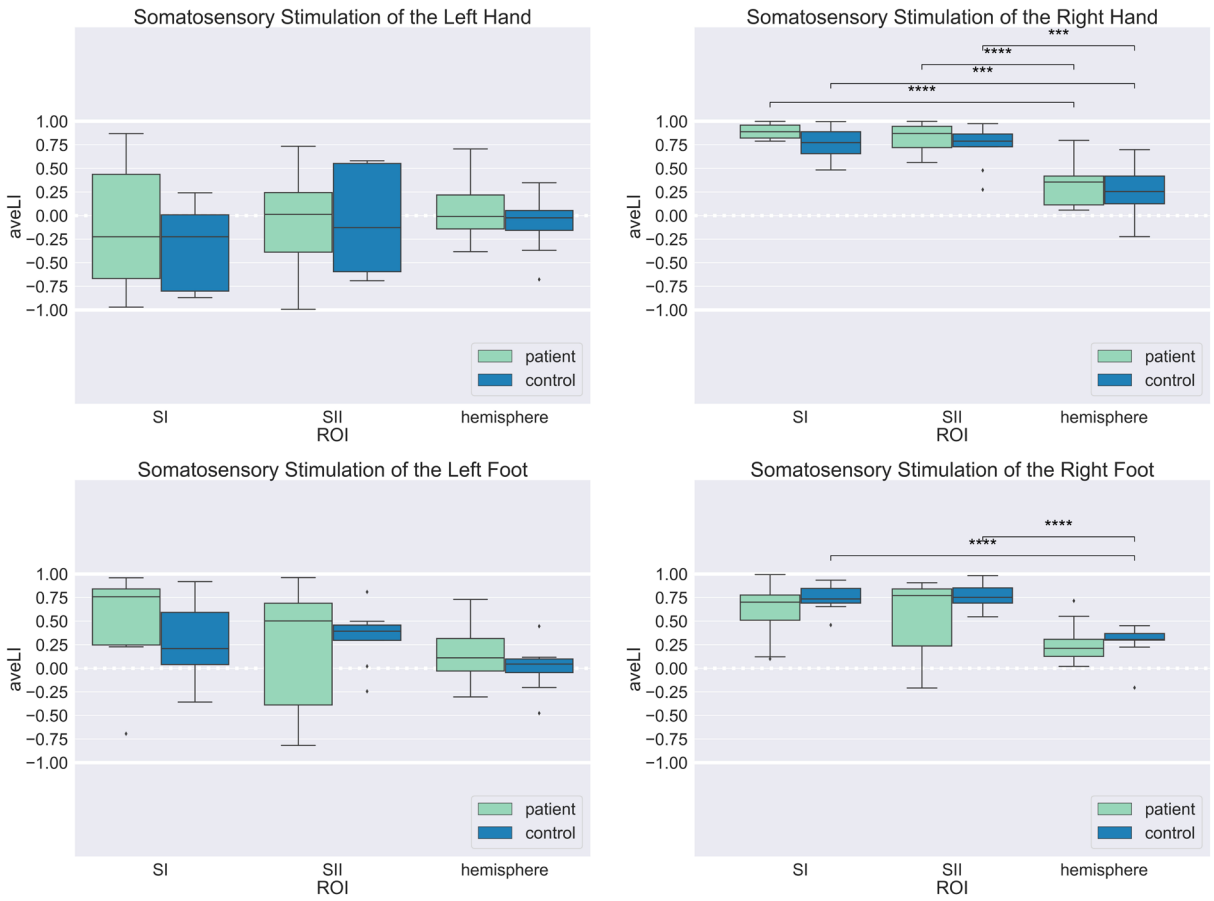

Figure 19: Hemispheric lateralization in the primary and secondary somatosensory cortex. Average lateralization indices (AveLIs) are demonstrated for every group (patients: green, controls: blue), task condition and region of interest (ROI), respectively. Positive values indicate a lateralization of blood oxygenation level dependent (BOLD) activity to the left hemisphere while negative values indicate a right hemispheric lateralization (*p ≤ 0.05, **p ≤ 0.01, ***p ≤ 0.001).

4.4. fMRI Data in the Context of Clinical Symptoms

For the purpose of a better understanding of the interplay between clinical symptoms and BOLD response, SPM multiple regression analyses were performed as described in section 4.7. The latter did occasionally indicate correlations between covariates and BOLD activation in S1 and S2 associated with specific tasks. None of the observed interrelations did survive FWE correction; nevertheless, the significant correlations ($p \leq 0.001$, uncorrected) are briefly summarized in the following.

4.4.1. Clinical Questionnaires

Regarding stimulation of the right foot, a positive correlation was found between sensory JOA and BOLD response in a cluster of voxels in left S2 (local maximum at MNI coordinates (x, y,

z): -48, -19, 11; T = 5.39, p = 0.001, uncorrected). This indicates a more pronounced BOLD activation in patients with higher sensory JOA and thus fewer somatosensory deficits. Concomitantly, a negative correlation was found in a cluster in the right (ipsilateral) S1 (local maximum: 54, -22, 50; T = 5.05; p = 0.001, uncorrected). There was no correlation found between the overall JOA score and BOLD response to any of the tasks in S1 and S2.

A few hints for a negative interrelation between the DASH score and BOLD activation could be observed. A negative correlation could be reported for the task “stimulation of the left foot”, which involves a cluster in right S1 (local maximum: 60, -4, 17; T = 7.72; p ≤ 0.001, uncorrected) and left S2 (local maximum: -57, -25, 17; T = 7.33; p ≤ 0.001, uncorrected). Likewise, a negative correlation was observed for the task “stimulation of the right hand” in a cluster in right S1 (local maximum: 45, -13, 47; T = 6.34; p ≤ 0.001, uncorrected). This speaks for reduced BOLD response in patients with higher DASH score and hence higher clinical impairment. In line with this, physical SF-12 was positively correlated with BOLD response to somatosensory stimulation of the right hand involving a cluster in right S1 (local maximum: 15, -43, 65; T = 6.94; p ≤ 0.001, uncorrected).

4.4.2. Sensation of Vibration

The vibratory sense of the left upper extremity showed a positive correlation with BOLD response to somatosensory stimulation of the left hand. This involved a cluster of voxels in right S1 (local maximum: 39, -31, 59; T = 5.85; p ≤ 0.001, uncorrected) and would imply higher BOLD response in patients with superior sensation of vibration. Regarding the other task conditions, no correlation with the vibratory sense of the respective extremity was found.

4.4.3. Electrophysiological Latencies

SPM multiple regression analyses involving SSEP latencies as covariates could only be computed for eight of the nine patients, since one of them did not show any SSEP responses. There could be found a negative correlation between BOLD response to somatosensory stimulation of the left hand and the latency of N33 in right S1 (local maximum: 24, -37, 62; T = 5.22; p ≤ 0.001, uncorrected). The same was found for P40 (local maximum: 24, -37, 62; T = 6.09; p ≤ 0.001, uncorrected). Additionally, BOLD response to somatosensory stimulation of the right foot was negatively correlated with N33 in left S2 (local maximum: -45, -19, 14; T = 6.01; p ≤ 0.001, uncorrected). This finding applied for P40 as well (local maximum: -45, -19, 14; T = 14.63; p ≤ 0.001, uncorrected). Figure 20 exemplarily shows the BOLD response to somatosensory stimulation of the right foot that was negatively correlated with the P40 SSEP latency of the right tibial nerve. All in all, these observations provide preliminary evidence for a

negative interrelation between prolonged SSEP latencies and BOLD response in contralateral somatosensory regions (the longer the latencies, the lower the BOLD response).

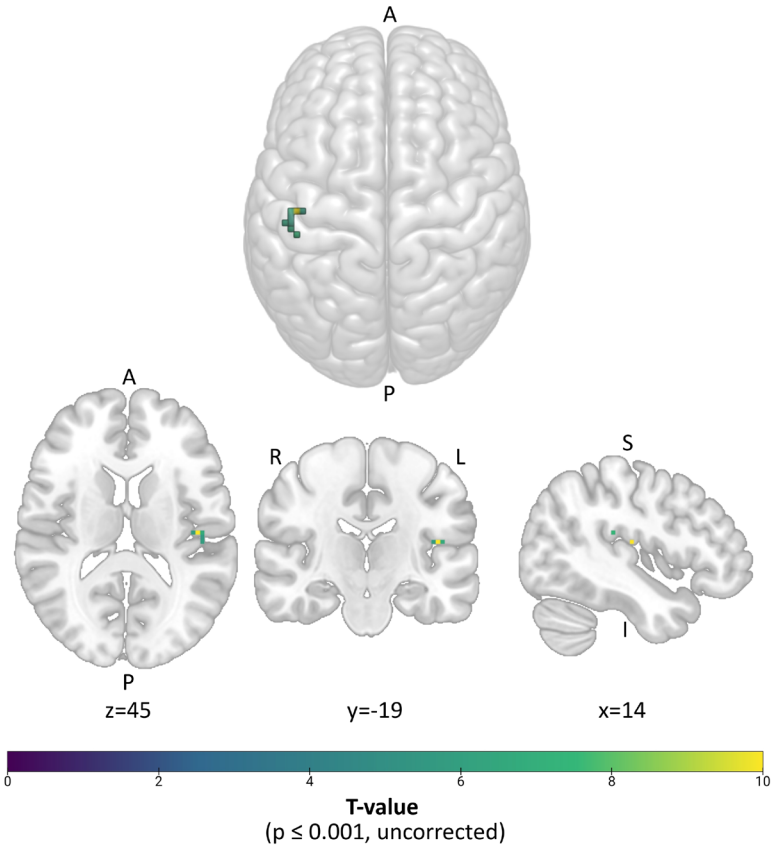

Figure 20: Exemplary statistical parametric mapping regression analysis. Cluster of neural activation in response to somatosensory stimulation of the right foot in left secondary somatosensory cortex (S2) negatively correlated with P40 somatosensory evoked potential (SSEP) latency of the right tibial nerve ($p \leq 0.001$, uncorrected). The statistical parametric map (SPM) was masked for S1 and S2.

5. Discussion

The main objective of this thesis was to investigate the cortical adaptation behavior within the somatosensory system in DCM. This issue was examined with BOLD fMRI, flanked by a clinical assessment which involved not only clinical questionnaires and tests but also a comprehensive neurological examination as well as the assessment of SSEPs. In the sections below, the main findings will be discussed. At the beginning, the underlying clinical aspects will be briefly addressed (section 6.1). Subsequently, BOLD fMRI findings including hemispheric lateralization (sections 6.2 and 6.3) will be discussed. Special attention will be paid to differences between the dominant and non-dominant limb representations as well as to the background of adaptation processes in the motor network which have been reported already in the scientific literature. Finally, associations between clinical properties and fMRI findings will be discussed (section 6.4).

5.1. Clinical Aspects

The clinical evaluation of the study participants provided a large number of different parameters. One important reason for the acquisition of many different clinical attributes is that at present no representative, conclusive and common diagnostic criteria are established for DCM[230,231]. These individual aspects were essential for a contextualization of the BOLD fMRI data and for comparisons with preceding studies, in which, e.g., cortical adaptation processes were described for specific clinical sub-groups of DCM patients[14,15]. In the following, clinical aspects of the underlying study population are discussed.

5.1.1. Preconditions of the Surgical Intervention

With regard to the patient collective, its heterogeneity is particularly noteworthy. The latter applied not only to the localization of the spinal lesion, but also to the surgical indication, which was based on the individual degree of suffering. Another important observation is that delayed diagnosis was apparently frequent in the sample examined. Late diagnosis of DCM in primary care tends to be the rule rather than the exception and can involve several years of repeated medical consultations and wrong diagnoses[231–234]. Those aspects of heterogeneity within the patient collective and delayed diagnosis may be possible further confounding factors in data analysis.

5.1.2. Preoperative Clinical Situation and Sensorimotor Skills

SF-12 and DASH scores as well as the achieved walking distances during the 6MWT revealed a reduced physical constitution of the patient collective in comparison to healthy people.

However, no severely impaired participants were among the patients, as indicated by the JOA scores. None of the patients reached the full sensory JOA score, which indicates that all patients had somatosensory deficits (see also Table 9, Appendix). In particular, all patients showed paresthesia involving at least one limb. This may be considered characteristic of DCM, since paresthesia is known to be present in almost every case of the disease[235]. Certainly, patients showed some interindividual variation regarding the localization of paresthesia and the impairment of other somatosensory modalities, such as proprioception, sensation of pain and temperature. Pallesthesia was reduced in patients on average. Manifest motor deficits (paresis) were present in six of nine patients. In the FTT and the NHPT, patients showed weaker performance than control subjects. However, the difference was not significant. This might most likely be attributed to the fact, that most of the patients were only mildly impaired according to their JOA score.

In future studies, it would be interesting to investigate a larger sample size for specific patterns of clinical impairment. This would potentially allow a further classification in clinical sub-groups, which could be investigated regarding their specific behavior of cortical adaptation. Furthermore, the clinical presentation and the type of the spinal lesion might be correlated more precisely. For instance, one could assume, that a rather left lateralized spinal lesion would be correlated with somatosensory deficits accentuated to the left side of the body.

5.1.3. Electrophysiological Findings

Seven out of nine patients showed pathological electrophysiological findings, which involved absent or delayed SSEP responses as well as pathological side differences regarding the SSEP latencies. This means noninvasive, objective and quantitative evidence of a lesion involving the somatosensory neural pathway[177] and substantiates the sensory deficits patients perceived subjectively.

5.1.4. Association of Clinical Parameters

The correlation analysis described in subsection 5.1.5 provided the indication of a negative correlation between the DASH score and the physical SF-12 score in the patient collective. This is not surprising, since both scores measure the physical state of the patients, even though the DASH score is more specific for impairment of the upper extremity. Stronger physical impairment is reflected in higher DASH and lower SF-12 scores.

An interesting aspect is the detected negative correlation between the sensory JOA and the SSEP latencies. It leads to the assumption, that the sensory JOA might be particularly sensitive to neural damage along the somatosensory pathway, for which prolonged SSEP latencies are an indicator[236]. In contrast, no significant correlation between the sensory JOA and the

sensation of vibration could be found. This might be owing to the fact, that sensation of vibration measured by a tuning fork is a rather rough, semiquantitative measure[237].
Regarding all these considerations, it should be stressed, that the underlying explorative findings need to be verified on the basis of a larger sample size and applying an FDR correction for multiple comparisons.

5.2. BOLD Activation within the Somatosensory System in DCM

As outlined in the introductory subsection 3.4.3, the cortical adaptation of somatosensory areas in DCM has hardly ever before been investigated specifically, to the best of our knowledge. In the following, BOLD fMRI findings are discussed.

5.2.1. Reduction of Cortical Responsiveness in DCM

The analysis of BOLD activation at the group level revealed a reduced cortical responsiveness to peripheral somatosensory stimuli in patients suffering from DCM. The latter was a global observation, applying for all four limbs, which could be shown by the contrast images (see Figures 17 and 18). This might provide evidence of functional degeneration and would match preceding fMRI findings showing reduced VOA in S1 in DCM patients[18,20], albeit the motor task-based study designs of Duggal et al. (2010) and Ryan et al. (2018) were not tailored to adaptation processes in the somatosensory system. Likewise, recent morphological analyses substantiate the aspect of degeneration: GM atrophy assessed by anatomical MRI was shown in DCM patients affecting both motor and somatosensory cortical areas[238]. These GM volume reductions were present in moderate clinical stages already and even more pronounced in severe stages[238].
Functional correlates of degeneration, which could be observed by means of fMRI in the present study, seem plausible given the several known pathophysiological mechanisms causing neural damage in DCM – even though their precise interplay has not been unscrambled, so far[239]. Naturally, the primary neural injury at the level of the stenosis plays an important role in the pathophysiology of DCM[240]. Damage mechanisms like ischemia, hypoxia and inflammation lead to structural and cellular changes such as interstitial edema, demyelination, axon degeneration and neuron loss[239,240]. Since neural fiber tracts can partly be harmed, it might be expected, that afferent signals transmitting tactile information and subsequently cortical BOLD response can be attenuated[20,241].
This thesis focused on adaptation in DCM at the cortical level. However, the primary lesion at the spinal level was not assessed. In future studies, it would be important to quantify the spinal lesion by imaging methods and to analyze its relations to cortical alterations. The latter could not be performed within the framework of the present study, since it would have required even

more time resources in terms of scanning time (thus representing a considerable burden for the participants). Matters are complicated by the fact that so far there is no well-established, standardized and sufficiently conclusive imaging approach to quantify the severity of spinal cord compression[242,243]. Instead, different measures have been reported in scientific literature. For instance, these involved the measurement of the spinal cord volume based on anatomical MRI[15], the T1 relaxation times[243] or T2-weighted signal intensity[244] at the level of the stenosis, or even spinal diffusion tensor imaging (DTI)[245–247]. Such additional imaging tools may be needed, since conventional MR findings sometimes cannot explain the patients' clinical state sufficiently[125,245]. Some of these imaging modalities might perspectively help to differentiate the impact of higher-order compensatory processes that have been described in the scientific literature[14,15] from local alterations at the spinal level. At least they could close some gaps in diagnostic investigation. Spinal DTI, e.g., might be used as an indicator of disease progression during the conservative management of mild DCM[245]. At present, it is no common method, inter alia, due to the lack of standardized image acquisition sequences and data processing workflows[245].

5.2.2. Dominant versus Non-dominant Hand Representation

Remarkably, the cortical somatosensory representation of the right (preferred) hand seemed to be more robust to deviations due to DCM than the representations of the other tested limbs. In comparison to the other tasks, BOLD activation in DCM patients following stimulation of the right hand survived FWE correction most reliably (see subsection 5.2.2), though it was clearly less pronounced than in the control group as displayed by the contrast images (see Figure 17 and 18). A similar performance of the dominant hand's sensorimotor system has previously been reported in other pathologies. For instance, it makes a difference whether stroke affects the dominant or the non-dominant hemisphere[248,249]. It has been shown, that patients in which the dominant hand was affected by stroke were clinically less impaired than patients featuring symptoms involving the non-dominant hand[248]. Certainly, it would be interesting to investigate this accidentally discovered phenomenon in DCM in more detail. A larger sample size would allow a comparison of subgroups with a rather left or right lateralized lesion identified by means of clinical or MR morphological criteria. Thereby, it could be ascertained whether a right lateralized spinal cord lesion in right-handed patients had indeed less impact on the clinical presentation than a left lateralized lesion, or not.

There is strong evidence, that the sensorimotor network shows hemispheric differences regarding structure and function[250–252]. For instance, it was shown, that performing a motor task with the non-dominant hand in the same quality as with the dominant hand involves more effective connectivity measured by means of task-based fMRI in the cortico-cerebellar somatosensory network[252]. Consequently, using the non-dominant hand would require more

network resources and would therefore be less efficient. The review article of Andersen and Siebner (2018) collated underpinnings revealing that not only hand preference, but also manual skills are related to the microstructure of the central nervous system[253]. These findings were based on fractional anisotropy (FA), a surrogate parameter acquired by diffusion tensor imaging (DTI) which is derived from the directionality of water diffusion and allows conclusions on the orientation and integrity of neural fiber tracts[254].

In right-handed people, dexterity is correlated with right-left asymmetry regarding the integrity of the contralateral corticospinal tract (CST), expressed by the FA value[253,255–258]. A larger dexterity advantage for the right (preferred) hand was associated with higher mean FA of the left in contrast to the right CST[253,258]. This relationship was investigated in several studies, whereby dexterity was defined by varying features such as painting skills[258], ability to play a selected musical instrument[257] or the attribute of congenital one-handedness[255,256]. Beyond this, it was observed that immobilization of the upper extremity was associated with a reduction of FA in the contralateral CST[259]. Against this background, it might in a future perspective be worth analyzing cerebral diffusion weighted imaging (DWI) data in DCM patients. Especially, microstructural alterations of the CST in DCM before and after surgical decompression might be addressed. Moreover, it could be evaluated, if pronounced dexterity has a protective impact on the clinical presentation.

Another finding of the present thesis was that healthy control subjects featured a consistent co-activation (under all task conditions) in ipsilateral S2, which was much less involved in the patients' group (see subsection 5.2.2). Indeed, an involvement of ipsilateral S1 and S2 cortices in the processing of unilateral stimuli is physiologic in healthy people, though usually less pronounced than the contralateral BOLD response[260,261]. Especially the consistent presence of bilateral S2 activation following tactile stimulation of the right hand is well supported by scientific evidence[262]. Bilateral BOLD response in both S1 and S2 following stimulation of the right or left hand led to the assumption, that these areas were both involved in the integration of unilateral afferent somatosensory signals[263]. Remarkably, the bilateral activation in S2 declines with age, which was assumed to be an expression of degeneration processes in the ageing brain[264]. Since the control subjects of this thesis were age-matched, the partially absent BOLD activation in DCM patients cannot exclusively be attributed to age. Most likely, absent co-activation of ipsilateral S2 might be interpreted as a correlate of reduced somatosensory input and declined capability of integrating afferent signals in DCM.

5.2.3. Motor versus Sensory Adaptation in DCM

Regarding adaptation processes within the motor system, more differentiated analyses were already published by a few authors[14,15,20]. However, those partly contradict each other: Both Zdunczyk et al. (2018) and Cronin et al. (2021) reported a compensatory increased recruitment

of motor cortical areas in subgroups of DCM patients depending on the clinical severity. Zdunczyk et al. who investigated cortical reorganization by means of nTMS in a cohort of 18 DCM patients, found an increased activation in non-primary motor areas in mildly impaired patients (JOA > 12). In patients with severe symptoms (defined as JOA ≤ 12), the motor cortical area was reduced and cortical inhibition increased[14]. In contrast, the fMRI-based study of Cronin et al. involving 23 DCM patients showed that increased motor activation in contralateral M1 during a finger tapping task was correlated with clinical severity indicated by the mJOA[15]. I.e., a stronger clinical impairment was associated with a larger signal change. Additionally, they observed a positive correlation between the neuromorphometric parameter of spinal compression volume and the recruitment of larger motor cortical regions[15]. Hence, it does not seem to be clarified, whether a compensatory recruitment of cortical areas takes effect particularly in mild or severe stages of the disease. The diverging results might, inter alia, be attributed to the different methods applied. Results of nTMS and fMRI are not expected to be identical and a spatial mismatch of the measured cortical response is evidenced[265]. Using resting state fMRI, Wang and colleagues (2022) have shown that extensive interruptions between the thalamus and sensorimotor tracts occur in DCM even at asymptomatic stages[266]. However, they also demonstrated the formation of new connections, for example, between the brainstem and subcortical areas as well as visuospatial regions and the cerebellum, and suggested an efficacy on the maintenance of motor and postural control[266].

Correlates of compensation in DCM, as they were described with respect to the motor network[14,15,266], cannot be derived from the present results of this thesis. It therefore needs to be assumed that processes of degeneration prevail in the somatosensory network. This would agree with clinical observations in scientific literature, which evidence that somatosensory function can be impaired at an early stage in the natural history of DCM[21] and that paresthesia is not likely to recover after surgical decompression[235].

The question arises why indications of compensation processes were reported regarding the motor system but could not be observed within the somatosensory system in the results of this thesis (see section 5.2). In order to discuss this question, it might be useful to take a glance at earlier lesion studies in non-human primates again, as addressed before in section 3.4. In owl monkeys, cutting the dorsal column at a high cervical level instantaneously leads to a complete deactivation of the forelimb representations in S1, except parts that are innervated by afferents that were not affected by the lesion since they enter the spinal cord more cranially[267,268]. Over the following months, reactivation of these cortical forelimb representations occurs by preserved somatosensory inputs from other body regions, e.g., the lower face[267–269]. However, this does not imply recovery of perceptive function[268]. It rather seems to imply that the compensatory potential of adaptation processes following lesions affecting somatosensory pathways is quite limited. In incomplete lesions of the dorsal column, a few remaining afferents

can expand their representative areas in the somatosensory cortex and to an extend assure functional preservation[267,268]. For sure, it must be recognized that the spinal lesions of DCM patients are only comparable with the precisely defined lesions of these animal studies within certain limits. E.g., the factor time needs to be kept in mind, since some of the patients were exposed to the damaging factor of their CSS over years. Consequently, it seems to be necessary to assume that damaging and reorganizing aspects took effect simultaneously. Dhillon et al. (2016) did consider this aspect by emulating the pathophysiological conditions of DCM in an animal model. They artificially induced CSS causing spinal cord compression in rats by the implantation of a water-absorbing expandable polymer in the dorsal epidural space at the cervical level[270]. The compression led to physical decay, indicated by neurobehavioral performance and SSEP amplitudes, which was partially reversible after surgical decompression[270]. It may be noted here that functional and neural degeneration due to the damaging effect of CSS seems plausible and can be observed clinically. Evidencing the existence of compensatory processes, whose effect may be clinically inapparent, is much more challenging. However, quite a few studies evidence adaptation processes regarding the structural and functional network connectivity in DCM which suggest a compensatory effect in the motor network. For instance, an enhanced integration of visual information in cerebellar motor control may have a compensatory effect in DCM[271]. Likewise, increased functional connectivity at the brainstem level seems to be associated with better functional maintenance[265].

Ultimately, it needs to be considered that somatosensation (input) and motor function (output) are inseparably linked according to neural physiology[272]. The interplay with somatosensory input allows for precise motor function and can be evidenced electrophysiologically. E.g., a peripheral deafferentation leads to increased MEP amplitudes induced by TMS due to disinhibition[273]. Clinically, reduced motor function can be observed if the proprioceptive and exteroceptive feedback conveyed by somatosensory afferent fibers is lacking. For instance, this phenomenon can be observed in sensory ataxia, where gait is abnormal due to the missing somatosensory input[274]. Somatosensory feedback is so crucial for adequate motor control that even efforts are made to artificially create sensory input in limb prostheses aiming improved performance[275,276].

Potential reciprocal impacts like lacking inhibition at the motor cortical level due to a damage of somatosensory afferents[273] need to be considered when correlates of cortical activity in fMRI or nTMS are interpreted. Presuming that somatosensory fibers might be more vulnerable than the strongly myelinated fibers of α-motoneurons[277], spinal cord injury caused by CSS would lead to a more pronounced loss of somatosensory fibers and consequently reduced somatosensory input. This could explain the reduced cortical BOLD response to peripheral somatosensory stimuli. The resulting reduction of inhibition could potentially explain the

positive correlation between spine compression and BOLD activation in M1 during finger tapping that was reported by Cronin et al. (2021)[15]. Against this background, a more pronounced motor cortical activation in DCM patients can be compatible with reduced responses in the somatosensory cortex. A functionally relevant compensatory effect cannot certainly be evidenced solely on the basis of these findings.

5.3. Hemispheric Lateralization in DCM

Both, patients and controls showed a strongly left-lateralized somatosensory representation of their right (dominant) extremities. In contrast, the somatosensory representation of the left extremities featured a less pronounced hemispheric lateralization. These observations are consistent with another recent publication, in which functional hemispheric asymmetry in healthy right-handed subjects was investigated based on functional near-infrared spectroscopy (fNIRS) and vibrotactile stimulation of the hands[135].

The behavior of hemispheric lateralization was not relevantly altered in DCM patients compared to control subjects, except for the processing of somatosensory stimuli affecting the right (dominant) hand. Here, DCM patients showed at least a statistical trend towards stronger lateralization to the left hemisphere in S1 and BA 3a. It can therefore be stated that the reduced ipsilateral co-activation within S2 in DCM patients, which emerged in the analysis of BOLD activation (see subsection 5.2.2), had hardly any impact on the AveLI.

5.4. Clinical Context of BOLD fMRI Findings

The regression analysis provided several correlations between the clinical parameters and BOLD response (see section 5.4). In the vast majority they indicated a statistical trend towards weaker BOLD response in stronger clinically impaired patients. Thus, clinical symptomatology was correlated with BOLD responses in the somatosensory cortex, and consequently, larger lesions can be expected to be associated with more pronounced somatosensory deficits as well as poorer functional measurement results. This supports the hypothesis described above (subsection 6.2.3) that the functional compensation potential in the somatosensory system is limited under present spinal cord compression. However, this does not provide any information about the regeneration potential after surgical decompression, which remains to be investigated.

5.5. Limitations

This study has a few general limitations, which must be clarified. The plausibly most crucial ones are the small sample size and the imbalanced gender relation of the study population.

The control subjects matched precisely the patients' age and gender, which enhanced the comparability between both groups. Unfortunately, much fewer female than male subjects could be included to the study. Gender as a possible confounder could, therefore, not be taken into account sufficiently. Moreover, it must be kept in mind that in particular the replicability of the results might be limited due to the small sample size[278]. A current trend in functional brain imaging leads towards ever larger sample sizes of several thousand subjects aiming to detect coherences of interindividual differences in functional and structural brain organization and to decode such complex processes as human cognition[279]. However, small-sample studies also remain relevant, since they are indispensable for the investigation of rarer clinical situations and usually allow adequate statements about main effects[279]. Especially studies addressing induced effects such as lesions[280] or tasks[281] mostly offer distinct reliability and effect sizes[279]. Nevertheless, investigations of a larger sample should be aimed in order to verify the observations outlined above. Moreover, they would allow the differentiation of clinical subgroups on the basis of clinical severity or the application of more complex statistical methods than the GLM. Data driven approaches, machine learning and statistical model selection provide larger sample sizes but could perspectively help to achieve a better understanding of the relationship and dynamics between degenerative processes in the somatosensory network and clinical stages of DCM.

Other limitations are closely linked to the method of fMRI and the pathology itself. These are outlined below.

5.5.1. Methodological Limitations of fMRI

BOLD fMRI (see subsection 3.3.2) has several inherent inaccuracies limiting the spatial and temporal resolution[282]. First, some physiological aspects can distort the correlation between neural activity and local blood flow. Apart from neural activation, vascular parameters like cerebral blood volume and oxygenation influence the fMRI signal[283]. In addition, motion and fluctuating vessel flow caused by the cardiac and respiratory cycle can lead to signal changes[284]. It is important to consider, that blood flow response happens on much larger timescales than neural activity and peaks with a delay of a few seconds after the actual event, wherefore finely scaled patterns reflecting local neural activity can hardly be measured[282].

Second, MR physical aspects such as the magnetic field strength, TE (echo time) and the applied MRI sequence affect the measurable fMRI signal[283], which is why the results of different fMRI studies are not necessarily comparable with each other.

And third, individual aspects of the subjects like age, sex, head motion[285] and neuropsychological factors such as visually and auditory induced signal and emotional state[286] can act as confounders. In order to protect against noise and visual stimuli, subjects of the

presented study were equipped with ear plugs and ear defenders, and they were instructed to keep their eyes closed during the fMRI task conditions.

In addition to the primary fMRI data acquisition, the subsequent data processing and analysis is associated with several limitations. For instance, it was shown that different coexisting preprocessing pipelines and thresholding can lead to variability in hypothesis outcome despite rather consistent unthresholded SPMs and significant consensus for activated regions[287].

An important pitfall of brain imaging studies addressing specifically the somatosensory cortex is the accuracy of the available topographic maps, since they are not as precise as the ones that exist, e.g., for the visual cortex[288]. Maps representing the body surface in S1 are relatively compact and anatomically localized on the postcentral gyrus, where partial volume effects can impede a differentiation between somatosensory responses and motor activity in the directly adjacent precentral gyrus[288,289]. Imaging at ultra-high magnetic fields (≥ 7 T) could perspectively help to achieve more detailed and accurate cortical somatotopic maps at a higher spatial resolution[288]. In the study presented in this thesis, it was attempted to minimize subject movement during the data acquisition. Additionally, beyond a distinction of larger ROIs provided by the SPM anatomy toolbox v3.0[202–204], no fine-structured somatotopic categorization was applied to the SPMs.

5.5.2. Obstacles in Researching DCM

Some inevitable limitations are closely linked to the pathology of DCM itself and are outlined as follows. A bias emerges from the fact, that only patients with elective surgical interventions could be included to the study due to organizational aspects (quite demanding study protocol requiring additional appointments for the fMRI and nTMS examination). Hence, very acute courses of the disease could not be considered. Since DCM is a pathology of the higher age, its incidence is associated with an increased probability of comorbidities[290], which are potential confounders in the data analysis. It was tried to preempt these confounders by applying detailed exclusion criteria and by performing a comprehensive clinical examination, but particularly pathologies, which had not been diagnosed so far, could not be excluded with absolute certainty. Patients, that were included in the study, displayed differences in the localization and expansion of their spinal lesion and thus showed an inhomogeneous clinical impairment. In the majority of the cases, it was hardly possible to find out, how long the spinal canal stenosis persisted before it was noticed by symptoms and detected by means of imaging procedures. Of course, even the symptomatic time period was quite individual. Concerning the spinal lesion and its effect on the clinical presentation, identifying an explicit and conclusive grade of severity in CSS is naturally a major problem. A standardized index does not exist[32]. Closely linked to this fact is the observation, that radiographic parameters such as intramedullary signal changes measured by MRI are not necessarily correlated with the

patients' clinical picture or the surgical outcome[125]. An explanation for this paradox behavior might be compensation by neural adaptation. The clinical picture, which was multimodally acquired in the present study might be the result of spinal impairment and mechanisms of compensation. This aspect complicates causal attributions between initial spinal lesion, clinical status and cortical responsiveness.

5.6. Conclusion

The present thesis aimed at a better understanding of the adaptive behavior of the somatosensory system in DCM. One of the key findings was that DCM patients featured a reduced cortical responsiveness to peripheral somatosensory stimuli. In particular, co-activation in S2 ipsilateral to the stimulated side was consistently present in the healthy control group but was found to be reduced or absent in the patients. Remarkably, the cortical somatosensory representation of the right (preferred) hand appeared to be more robust to deviations due to DCM compared to the representations of the other tested limbs. Hemispheric lateralization regarding the processing of somatosensory stimuli demonstrated no relevant differences between DCM patients and healthy control subjects. The multiple regression analysis of clinical parameters and BOLD activation provided preliminary evidence of poorer response in the somatosensory cortex in stronger clinically impaired patients.

In conclusion, degenerative processes seem to predominate in the studied collective of DCM patients. This contrasts with previously reported evidence for compensatory mechanisms within the motor system[14,15] and fills an important gap in clinical research on cortical adaptations in DCM.

5.7. Outlook

The fundamental goal of research on cortex reorganization in DCM is to improve clinical care. A concrete effort is to identify predictors of surgical outcome based on imaging enabling better treatment decisions. The functional imaging changes outlined above need to be studied longitudinally to determine whether preoperative changes regress after surgical decompression in specific patient groups and whether they have predictive power for functional recovery. Based on such findings, patients may potentially be better selected for surgical therapy. Similarly, the influence of clinical factors, such as severity and duration of symptoms, on functional regeneration should be examined. These aspects will be investigated after completion of data acquisitions based on follow-up examinations after three, nine, and twenty-four months, which were part of the local study protocol but not subject of this thesis. In this framework, a multimodal approach will be used, combining the task fMRI data with resting state fMRI, DTI, nTMS, and electrophysiological findings. Applying different diagnostic

methods might facilitate surgical outcome prediction[291], albeit that available resources in clinical practice need to be considered.

Finally, as also exemplified in the patient population studied, DCM is often diagnosed with delay. Therefore, the improvement of diagnostic standards should be a short-term goal in patient care to enable timely treatment. This should include increased awareness of somatosensory deficits as an early symptom of DCM.

6. Bibliography

1 Bazzari AH, Parri HR. Neuromodulators and Long-Term Synaptic Plasticity in Learning and Memory: A Steered-Glutamatergic Perspective. *Brain Sci* 2019; **9**: 300.

2 Fiebig F, Herman P, Lansner A. An Indexing Theory for Working Memory Based on Fast Hebbian Plasticity. *eNeuro* 2020; **7**. DOI:10.1523/ENEURO.0374-19.2020.

3 Diniz CRAF, Crestani AP. The times they are a-changin': a proposal on how brain flexibility goes beyond the obvious to include the concepts of "upward" and "downward" to neuroplasticity. *Mol Psychiatry* 2023; **28**: 977–92.

4 Kato K, Sawada M, Nishimura Y. Bypassing stroke-damaged neural pathways via a neural interface induces targeted cortical adaptation. *Nat Commun* 2019; **10**: 4699.

5 Stefaniak JD, Halai AD, Lambon Ralph MA. The neural and neurocomputational bases of recovery from post-stroke aphasia. *Nat Rev Neurol* 2020; **16**: 43–55.

6 Wang H, Xiong X, Zhang K, *et al.* Motor network reorganization after motor imagery training in stroke patients with moderate to severe upper limb impairment. *CNS Neurosci Ther* 2023; **29**: 619–32.

7 Cocks G, Carta MG, Arias-Carrión O, Nardi AE. Neural Plasticity and Neurogenesis in Mental Disorders. *Neural Plast* 2016; **2016**: 3738015.

8 Pan S, Feng W, Li Y, *et al.* The microRNA-195 - BDNF pathway and cognitive deficits in schizophrenia patients with minimal antipsychotic medication exposure. *Transl Psychiatry* 2021; **11**: 117.

9 Hübener M, Bonhoeffer T. Neuronal Plasticity: Beyond the Critical Period. *Cell* 2014; **159**: 727–37.

10 Shaffer J. Neuroplasticity and Clinical Practice: Building Brain Power for Health. *Front Psychol* 2016; **7**. DOI:10.3389/fpsyg.2016.01118.

11 von Bernhardi R, Eugenín-von Bernhardi L, Eugenín J. What Is Neural Plasticity? In: von Bernhardi R, Eugenín J, Muller KJ, eds. The Plastic Brain. Cham: Springer International Publishing, 2017: 1–15.

12 Gibson J, Nouri A, Krueger B, *et al.* Degenerative Cervical Myelopathy: A Clinical Review. *Yale J Biol Med* 2018; **91**: 43–8.

13 Nouri A, Cheng JS, Davies B, Kotter M, Schaller K, Tessitore E. Degenerative Cervical Myelopathy: A Brief Review of Past Perspectives, Present Developments, and Future Directions. *J Clin Med* 2020; **9**: 535.

14 Zdunczyk A, Schwarzer V, Mikhailov M, *et al.* The Corticospinal Reserve Capacity: Reorganization of Motor Area and Excitability As a Novel Pathophysiological Concept in Cervical Myelopathy. *Neurosurgery* 2018; **83**: 810–8.

15 Cronin AE, Detombe SA, Duggal CA, Duggal N, Bartha R. Spinal cord compression is associated with brain plasticity in degenerative cervical myelopathy. *Brain Commun* 2021; **3**: fcab131.

16 Rahyussalim AJ, Saleh I, Wijaya MT, Kurniawati T. Cervical canal stenosis due to cervical spondylotic myelopathy C4-C5: A case report. *Int J Surg Case Rep* 2019; **60**: 82–6.

17 Zhou FQ, Tan YM, Wu L, Zhuang Y, He LC, Gong HH. Intrinsic Functional Plasticity of the Sensory-Motor Network in Patients with Cervical Spondylotic Myelopathy. *Sci Rep* 2015; **5**: 9975.

18 Duggal N, Rabin D, Bartha R, *et al.* Brain reorganization in patients with spinal cord compression evaluated using fMRI. *Neurology* 2010; **74**: 1048.

19 Bhagavatula ID, Shukla D, Sadashiva N, Saligoudar P, Prasad C, Bhat DI. Functional cortical reorganization in cases of cervical spondylotic myelopathy and changes associated with surgery. *Neurosurg Focus* 2016; **40**: E2.

20 Ryan K, Goncalves S, Bartha R, Duggal N. Motor network recovery in patients with chronic spinal cord compression: a longitudinal study following decompression surgery. *J Neurosurg Spine* 2018; **28**: 379–88.

21 Milligan J, Ryan K, Fehlings M, Bauman C. Degenerative cervical myelopathy: Diagnosis and management in primary care. *Can Fam Physician* 2019; **65**: 619–24.

22 de Oliveira Vilaça C, Orsini M, Leite MAA, *et al.* Cervical spondylotic myelopathy: what the neurologist should know. *Neurol Int* 2016; **8**: 69–73.

23 Meyer F, Börm W, Thomé C. Die degenerative zervikale Spinalkanalstenose. Aktuelle Strategien in Diagnostik und Therapie. *Dtsch Ärztebl* 2008; **105**: 366–72.

24 Law MD, Bernhardt M, White AA. Cervical spondylotic myelopathy: a review of surgical indications and decision making. *Yale J Biol Med* 1993; **66**: 165–77.

25 Nouri A, Tetreault L, Singh A, Karadimas SK, Fehlings MG. Degenerative Cervical Myelopathy: Epidemiology, Genetics, and Pathogenesis. *Spine* 2015; **40**: E675–93.

26 Severino R, Nouri A, Tessitore E. Degenerative Cervical Myelopathy: How to Identify the Best Responders to Surgery? *J Clin Med* 2020; **9**: 759.

27 Baptiste DC, Fehlings MG. Pathophysiology of cervical myelopathy. *Spine J* 2006; **6**: 190–7.

28 Lebl DR, Hughes A, Cammisa FP, O'Leary PF. Cervical Spondylotic Myelopathy: Pathophysiology, Clinical Presentation, and Treatment. *HSS J* 2011; **7**: 170–8.

29 Hueper K, Gutberlet M, Bräsen JH, *et al.* Multiparametric Functional MRI: Non-Invasive Imaging of Inflammation and Edema Formation after Kidney Transplantation in Mice. *PLOS ONE* 2016; **11**: e0162705.

30 Davies BM, Mowforth OD, Smith EK, Kotter MR. Degenerative cervical myelopathy. *BMJ* 2018; **360**: k186.

31 Kato S, Fehlings M. Degenerative cervical myelopathy. *Curr Rev Musculoskelet Med* 2016; **9**: 263–71.

32 Kalsi-Ryan S, Karadimas SK, Fehlings MG. Cervical Spondylotic Myelopathy: The Clinical Phenomenon and the Current Pathobiology of an Increasingly Prevalent and Devastating Disorder. *The Neuroscientist* 2013; **19**: 409–21.

33 Fehlings MG, Tetreault LA, Riew KD, *et al.* A Clinical Practice Guideline for the Management of Patients With Degenerative Cervical Myelopathy: Recommendations for

Patients With Mild, Moderate, and Severe Disease and Nonmyelopathic Patients With Evidence of Cord Compression. *Glob Spine J* 2017; **7**: 70S-83S.

34 McCartney S, Baskerville R, Blagg S, McCartney D. Cervical radiculopathy and cervical myelopathy: diagnosis and management in primary care. *Br J Gen Pract* 2018; **68**: 44–6.

35 Ludolph AC. Zervikale spondylotische Myelopathie. Dtsch. Ges. Für Neurol. Leitlinien Für Diagn. Ther. Neurol. 2017. www.dgn.org/leitlinien (accessed Aug 27, 2020).

36 Kadaňka Z, Bednařík J, Voháňka S, *et al.* Conservative treatment versus surgery in spondylotic cervical myelopathy: a prospective randomised study. *Eur Spine J* 2000; **9**: 538–44.

37 Kadaňka Z, Mares M, Bednaník J, *et al.* Approaches to spondylotic cervical myelopathy: conservative versus surgical results in a 3-year follow-up study. *Spine* 2002; **27**: 2205–10; discussion 2210-2211.

38 Kato S, Oshima Y, Oka H, *et al.* Comparison of the Japanese Orthopaedic Association (JOA) Score and Modified JOA (mJOA) Score for the Assessment of Cervical Myelopathy: A Multicenter Observational Study. *PLOS ONE* 2015; **10**: e0123022.

39 Tetreault L, Kopjar B, Côté P, Arnold P, Fehlings MG. A Clinical Prediction Rule for Functional Outcomes in Patients Undergoing Surgery for Degenerative Cervical Myelopathy: Analysis of an International Prospective Multicenter Data Set of 757 Subjects. *JBJS* 2015; **97**: 2038–46.

40 Frings S. Sensory cells and sensory organs. In: Barth FG, Giampieri-Deutsch P, Klein H-D, eds. Sensory Perception: Mind and Matter. Vienna: Springer, 2012: 5–21.

41 Barth FG. Sensory perception: Adaptation to lifestyle and habitat. In: Barth FG, Giampieri-Deutsch P, Klein H-D, eds. Sensory Perception: Mind and Matter. Vienna: Springer, 2012: 89–107.

42 Yohe LR, Brand P. Evolutionary ecology of chemosensation and its role in sensory drive. *Curr Zool* 2018; **64**: 525–33.

43 Trepel M. Neuroanatomie. München: Elsevier, Urban & Fischer, 2012.

44 Carpenter R, Reddi B. Neurophysiology: A Conceptual Approach, Fifth Edition. CRC Press, 2012.

45 Gescheider GA, Wright JH, Verrillo RT. Information processing channels in the tactile sensory system. New York: Psychology Press, 2009.

46 Postle BR. Essentials of cognitive neuroscience. Chichester, West Sussex: John Wiley & Sons, 2015.

47 Erlanger J, Gasser HS. Electrical signs of nervous activity. Oxford, England: Univ. Penn. Press, 1937.

48 Lloyd DPC. Neuron patterns controlling transmission of ipsilateral hind limb reflexes in cat. *J Neurophysiol* 1943; **6**: 293–315.

49 Hunt CC. Relation of Function to Diameter in Afferent Fibers of Muscle Nerves. *J Gen Physiol* 1954; **38**: 117–31.

50 Schalow G, Zäch GA, Warzok R. Classification of human peripheral nerve fibre groups by conduction velocity and nerve fibre diameter is preserved following spinal cord lesion. *J Auton Nerv Syst* 1995; **52**: 125–50.

51 Purves D, Augustine GJ, Fitzpatrick D, *et al.*, editors. Neuroscience, Sixth international edition. New York, Oxford: Sinauer Associates, imprint of Oxford University Press, 2018.

52 Penfield W, Boldrey E. Somatic Motor and Sensory Representation in the Cerebral Cortex of Man as Studied by Electrical Stimulation. *Brain* 1937; **60**: 389–443.

53 Penfield W, Rasmussen T. The Cerebral Cortex of Man: A Clinical Study of Localization of Function. Oxford, England: Macmillan, 1950.

54 Brodmann K. Vergleichende Lokalisationslehre der Grosshirnrinde in ihren Prinzipien dargestellt auf Grund des Zellenbaues. Leipzig: Barth, 1909.

55 Villringer A. fMRI of the Sensorimotor System. In: fMRI: From Nuclear Spins to Brain Functions. Springer, 2015: 509–21.

56 Rabi II. A New Method of Measuring Nuclear Magnetic Moment. *Phys Rev* 1938; **53**: 318.

57 Bloch F. Nuclear Induction. *Phys Rev* 1946; **70**: 460–74.

58 Bloch F, Hansen WW, Packard M. The Nuclear Induction Experiment. *Phys Rev* 1946; **70**: 474–85.

59 Purcell EM, Torrey HC, Pound RV. Resonance Absorption by Nuclear Magnetic Moments in a Solid. *Phys Rev* 1946; **69**: 37–8.

60 Bloembergen N, Purcell EM, Pound RV. Relaxation Effects in Nuclear Magnetic Resonance Absorption. *Phys Rev* 1948; **73**: 679–712.

61 Lauterbur PC. Image Formation by Induced Local Interactions: Examples Employing Nuclear Magnetic Resonance. *Nature* 1973; **242**: 190–1.

62 McRobbie DW, Moore EA, Graves M. MRI from picture to proton, Third Edition. Cambridge: Cambridge University Press, 2017.

63 Zabel H. Medical physics / Volume 1 : Physical aspects of organs and imaging. De Gruyter, 2017.

64 Brown RW, Cheng Y-CN, Haacke EM, Thompson MR, Venkatesan R. Magnetic Resonance Imaging: Physical Principles and Sequence Design. John Wiley & Sons, 2014.

65 Ogawa S, Lee T-M, Nayak AS, Glynn P. Oxygenation-sensitive contrast in magnetic resonance image of rodent brain at high magnetic fields. *Magn Reson Med* 1990; **14**: 68–78.

66 Ogawa S, Lee TM, Kay AR, Tank DW. Brain magnetic resonance imaging with contrast dependent on blood oxygenation. *Proc Natl Acad Sci U S A* 1990; **87**: 9868–72.

67 Cinciute S. Translating the hemodynamic response: why focused interdisciplinary integration should matter for the future of functional neuroimaging. *PeerJ* 2019; **7**: e6621.

68 Rangaprakash D, Tadayonnejad R, Deshpande G, O'Neill J, Feusner JD. FMRI hemodynamic response function (HRF) as a novel marker of brain function: applications

for understanding obsessive-compulsive disorder pathology and treatment response. *Brain Imaging Behav* 2021; **15**: 1622–40.

69 Schilling KG, Li M, Rheault F, *et al.* Anomalous and heterogeneous characteristics of the BOLD hemodynamic response function in white matter. *Cereb Cortex Commun* 2022; **3**: tgac035.

70 Gauthier CJ, Fan AP. Functional and Metabolic MRI. In: Cercignani M, Dowell NG, Tofts PS, eds. Quantitative MRI of the Brain. Principles of Physical Measurement, 2nd edn. Boca Raton: CRC Press, Taylor & Francis Group, 2018: 269–81.

71 Hirano Y, Stefanovic B, Silva AC. Spatiotemporal Evolution of the Functional Magnetic Resonance Imaging Response to Ultrashort Stimuli. *J Neurosci* 2011; **31**: 1440–7.

72 Martindale J, Mayhew J, Berwick J, *et al.* The Hemodynamic Impulse Response to a Single Neural Event. *J Cereb Blood Flow Metab* 2003; **23**: 546–55.

73 Lindquist MA, Meng Loh J, Atlas LY, Wager TD. Modeling the hemodynamic response function in fMRI: Efficiency, bias and mis-modeling. *NeuroImage* 2009; **45**: S187–98.

74 West KL, Zuppichini MD, Turner MP, *et al.* BOLD Hemodynamic Response Function Changes Significantly with Healthy Aging. *NeuroImage* 2019; **188**: 198–207.

75 Mansfield P. Multi-planar image formation using NMR spin echoes. *J Phys C Solid State Phys* 1977; **10**: L55–8.

76 Amaro E, Barker GJ. Study design in fMRI: Basic principles. *Brain Cogn* 2006; **60**: 220–32.

77 Petersen SE, Dubis JW. The mixed block/event-related design. *Neuroimage* 2012; **62**: 1177–84.

78 Dale AM, Buckner RL. Selective averaging of rapidly presented individual trials using fMRI. *Hum Brain Mapp* 1997; **5**: 329–40.

79 Loubinoux I, Carel C, Alary F, *et al.* Within-Session and Between-Session Reproducibility of Cerebral Sensorimotor Activation: A Test–Retest Effect Evidenced with Functional Magnetic Resonance Imaging: *J Cereb Blood Flow Metab* 2001; **21**: 592–607.

80 Friston KJ, Zarahn E, Josephs O, Henson RNA, Dale AM. Stochastic Designs in Event-Related fMRI. *NeuroImage* 1999; **10**: 607–19.

81 Buxton RB, Wong EC, Frank LR. Dynamics of blood flow and oxygenation changes during brain activation: The balloon model. *Magn Reson Med* 1998; **39**: 855–64.

82 Donaldson DI. Parsing brain activity with fMRI and mixed designs: what kind of a state is neuroimaging in? *Trends Neurosci* 2004; **27**: 442–4.

83 Lee D, Yun S, Jang C, Park H-J. Multivariate Bayesian decoding of single-trial event-related fMRI responses for memory retrieval of voluntary actions. *PLOS ONE* 2017; **12**: e0182657.

84 Meltzer JA, Negishi M, Constable RT. Biphasic hemodynamic responses influence deactivation and may mask activation in block-design fMRI paradigms. *Hum Brain Mapp* 2008; **29**: 385–99.

85 D'Esposito M, Zarahn E, Aguirre GK. Event-related functional MRI: Implications for cognitive psychology. *Psychol Bull* 1999; **125**: 155–64.

86 Bandettini PA, Cox RW. Event-related fMRI contrast when using constant interstimulus interval: Theory and experiment. *Magn Reson Med* 2000; **43**: 540–8.

87 Tie Y, Suarez RO, Whalen S, Radmanesh A, Norton IH, Golby AJ. Comparison of blocked and event-related fMRI designs for pre-surgical language mapping. *NeuroImage* 2009; **47 Suppl 2**: T107-115.

88 Steward O. Degenerative changes and reactive growth responses of neurons following denervation and axotomy: historical concepts and their modern embodiments. In: Kwakkel G, Cohen L, Selzer M, Miller R, Clarke S, eds. Textbook of Neural Repair and Rehabilitation: Volume 1: Neural Repair and Plasticity, 2nd edn. Cambridge: Cambridge University Press, 2014: 1–21.

89 Ramón y Cajal S. Estudios sobre la degeneración y regeneración del Sistema nervioso. Madrid: Moya, 1914.

90 Hubel DH, Wiesel TN. Receptive fields, binocular interaction and functional architecture in the cat's visual cortex. *J Physiol* 1962; **160**: 106–54.

91 Hubel DH, Wiesel TN. Receptive fields of single neurones in the cat's striate cortex. *J Physiol* 1959; **148**: 574–91.

92 Hubel DH, Wiesel TN. Receptive fields of cells in striate cortex of very young, visually inexperienced kittens. *J Neurophysiol* 1963; **26**: 994–1002.

93 Wiesel TN. Early explorations of the development and plasticity of the visual cortex: A personal view. *J Neurobiol* 1999; **41**: 7–9.

94 Merzenich MM, Kaas JH, Wall JT, Sur M, Nelson RJ, Felleman DJ. Progression of change following median nerve section in the cortical representation of the hand in areas 3b and 1 in adult owl and squirrel monkeys. *Neuroscience* 1983; **10**: 639–65.

95 Wall JT, Kaas JH, Sur M, Nelson RJ, Felleman DJ, Merzenich MM. Functional Reorganization in Somatosensory Cortical Areas 3b and 1 of Adult Monkeys After Median Nerve Repair: Possible Relationships to Sensory Recovery in Humans. *J Neurosci* 1986; **6**: 218–33.

96 Kaas JH, Krubitzer LA, Chino YM, Langston AL, Polley EH, Blair N. Reorganization of retinotopic cortical maps in adult mammals after lesions of the retina. *Science* 1990; **248**: 229–31.

97 Wang X, Merzenich MM, Sameshima K, Jenkins WM. Remodelling of hand representation in adult cortex determined by timing of tactile stimulation. *Nature* 1995; **378**: 71–5.

98 Merzenich MM, Nelson RJ, Stryker MP, Cynader MS, Schoppmann A, Zook JM. Somatosensory cortical map changes following digit amputation in adult monkeys. *J Comp Neurol* 1984; **224**: 591–605.

99 Clark SA, Allard T, Jenkins WM, Merzenich MM. Receptive fields in the body-surface map in adult cortex defined by temporally correlated inputs. *Nature* 1988; **332**: 444–5.

100 Merzenich MM, Jenkins WM. Reorganization of Cortical Representations of the Hand Following Alterations of Skin Inputs Induced by Nerve Injury, Skin Island Transfers, and Experience. *J Hand Ther* 1993; **6**: 89–104.

101 Jenkins WM, Merzenich MM, Ochs MT, Allard T, Guic-Robles E. Functional reorganization of primary somatosensory cortex in adult owl monkeys after behaviorally controlled tactile stimulation. *J Neurophysiol* 1990; **63**: 82–104.

102 Moucha R, Kilgard MP. Cortical plasticity and rehabilitation. In: Møller AR, ed. Progress in Brain Research. Elsevier, 2006: 111–389.

103 Godde B. Somatosensory Reorganization. In: Binder MD, Hirokawa N, Windhorst U, eds. Encyclopedia of Neuroscience. Berlin, Heidelberg: Springer, 2009: 3784–7.

104 David G, Barrett E. Short-term Plasticity: Facilitation, Augmentation, Potentiation, and depression. In: Selzer ME, Clarke S, Cohen LG, Kwakkel G, Miller RH, eds. Textbook of Neural Repair and Rehabilitation. Volume I - Neural Repair and Plasticity, 2nd edn. Cambridge: Cambridge University Press, 2014: 36–49.

105 Thomas G, Huganir RL. Long-term potentiation and long-term depression. In: Kwakkel G, Cohen L, Selzer M, Miller R, Clarke S, eds. Textbook of Neural Repair and Rehabilitation: Volume 1: Neural Repair and Plasticity, 2nd edn. Cambridge: Cambridge University Press, 2014: 1–21.

106 Hebb DO. The organization of behavior. New York: Wiley, 1949.

107 Bliss TVP, Lømo T. Long-lasting potentiation of synaptic transmission in the dentate area of the anaesthetized rabbit following stimulation of the perforant path. *J Physiol* 1973; **232**: 331–56.

108 Bliss TVP, Gardner-Medwin AR. Long-lasting potentiation of synaptic transmission in the dentate area of the unanaesthetized rabbit following stimulation of the perforant path. *J Physiol* 1973; **232**: 357–74.

109 Ito M, Sakurai M, Tongroach P. Climbing fibre induced depression of both mossy fibre responsiveness and glutamate sensitivity of cerebellar Purkinje cells. *J Physiol* 1982; **324**: 113–34.

110 Gershenson C. Guiding the self-organization of random Boolean networks. *Theory Biosci* 2012; **131**: 181–91.

111 Cramer Steven C., Nelles Gereon, Benson Randall R., *et al.* A Functional MRI Study of Subjects Recovered From Hemiparetic Stroke. *Stroke* 1997; **28**: 2518–27.

112 Ward NS, Brown MM, Thompson AJ, Frackowiak RSJ. Neural correlates of motor recovery after stroke: a longitudinal fMRI study. *Brain* 2003; **126**: 2476–96.

113 Biernaskie J, Szymanska A, Windle V, Corbett D. Bi-hemispheric contribution to functional motor recovery of the affected forelimb following focal ischemic brain injury in rats. *Eur J Neurosci* 2005; **21**: 989–99.

114 Hsu JE, Jones TA. Contralesional neural plasticity and functional changes in the less-affected forelimb after large and small cortical infarcts in rats. *Exp Neurol* 2006; **201**: 479–94.

115 Stinear CM, Barber PA, Smale PR, Coxon JP, Fleming MK, Byblow WD. Functional potential in chronic stroke patients depends on corticospinal tract integrity. *Brain* 2007; **130**: 170–80.

116 Murphy TH, Corbett D. Plasticity during stroke recovery: from synapse to behaviour. *Nat Rev Neurosci* 2009; **10**: 861–72.

117 Gonzalez CLR, Gharbawie OA, Williams PT, Kleim JA, Kolb B, Whishaw IQ. Evidence for bilateral control of skilled movements: ipsilateral skilled forelimb reaching deficits and functional recovery in rats follow motor cortex and lateral frontal cortex lesions. *Eur J Neurosci* 2004; **20**: 3442–52.

118 Brus-Ramer M, Carmel JB, Martin JH. Motor Cortex Bilateral Motor Representation Depends on Subcortical and Interhemispheric Interactions. *J Neurosci* 2009; **29**: 6196–206.

119 Cramer SC. Repairing the human brain after stroke: I. Mechanisms of spontaneous recovery. *Ann Neurol* 2008; **63**: 272–87.

120 Makin TR, Scholz J, Henderson Slater D, Johansen-Berg H, Tracey I. Reassessing cortical reorganization in the primary sensorimotor cortex following arm amputation. *Brain* 2015; **138**: 2140–6.

121 Flor H, Nikolajsen L, Jensen TS. Phantom limb pain: a case of maladaptive CNS plasticity? *Nat Rev Neurosci* 2006; **7**: 873–81.

122 Foell J, Bekrater-Bodmann R, Diers M, Flor H. Mirror therapy for phantom limb pain: Brain changes and the role of body representation. *Eur J Pain* 2014; **18**: 729–39.

123 Lotze M, Flor H, Grodd W, Larbig W, Birbaumer N. Phantom movements and pain An fMRI study in upper limb amputees. *Brain* 2001; **124**: 2268–77.

124 Sangondimath G, Mallepally AR, Marathe N, Mak K-C, Salimath S. Degenerative cervical myelopathy: Recent updates and future directions. *J Clin Orthop Trauma* 2020; **11**: 822–9.

125 Witiw CD, Mathieu F, Nouri A, Fehlings MG. Clinico-Radiographic Discordance: An Evidence-Based Commentary on the Management of Degenerative Cervical Spinal Cord Compression in the Absence of Symptoms or With Only Mild Symptoms of Myelopathy: *Glob Spine J* 2017; **8**: 527–34.

126 Shimomura T, Sumi M, Nishida K, *et al.* Prognostic Factors for Deterioration of Patients With Cervical Spondylotic Myelopathy After Nonsurgical Treatment. *Spine* 2007; **32**: 2474–9.

127 Barker AT, Jalinous R, Freeston IL. Non-invasive magnetic stimulation of human motor cortex. *Lancet Lond Engl* 1985; **1**: 1106–7.

128 Chail A, Saini RK, Bhat PS, Srivastava K, Chauhan V. Transcranial magnetic stimulation: A review of its evolution and current applications. *Ind Psychiatry J* 2018; **27**: 172–80.

129 Burke MJ, Fried PJ, Pascual-Leone A. Chapter 5 - Transcranial magnetic stimulation: Neurophysiological and clinical applications. In: D'Esposito M, Grafman JH, eds. Handbook of Clinical Neurology. Elsevier, 2019: 73–92.

130 Horvath JC, Perez JM, Forrow L, Fregni F, Pascual-Leone A. Transcranial magnetic stimulation: a historical evaluation and future prognosis of therapeutically relevant ethical concerns. *J Med Ethics* 2011; **37**: 137–43.

131 Holmes NP, Tamè L. Locating primary somatosensory cortex in human brain stimulation studies: systematic review and meta-analytic evidence. *J Neurophysiol* 2019; **121**: 152–62.

132 Noggle CA, Hall JJ. Hemispheres of the Brain, Lateralization of. Encycl. Child Behav. Dev. 2011.

133 Ocklenburg S, Güntürkün O. The lateralized brain. London: Academic Press, 2018.

134 Coghill RC, Gilron I, Iadarola MJ. Hemispheric Lateralization of Somatosensory Processing. *J Neurophysiol* 2001; **85**: 2602–12.

135 Jin SH, Lee SH, Yang ST, An J. Hemispheric asymmetry in hand preference of right-handers for passive vibrotactile perception: an fNIRS study. *Sci Rep* 2020; **10**: 13423.

136 Stein BE, Price DD, Gazzaniga MS. Pain perception in a man with total corpus callosum transection. *Pain* 1989; **38**: 51–6.

137 Lepore F, Lassonde M, Veillette N, Guillemot J-P. Unilateral and bilateral temperature comparisons in acallosal and split-brain subjects. *Neuropsychologia* 1997; **35**: 1225–31.

138 Dodd KC, Nair VA, Prabhakaran V. Role of the Contralesional vs. Ipsilesional Hemisphere in Stroke Recovery. *Front Hum Neurosci* 2017; **11**: 469.

139 Fregni Felipe, Boggio Paulo S., Valle Angela C., *et al.* A Sham-Controlled Trial of a 5-Day Course of Repetitive Transcranial Magnetic Stimulation of the Unaffected Hemisphere in Stroke Patients. *Stroke* 2006; **37**: 2115–22.

140 Li Y, Chen Z, Su X, *et al.* Functional lateralization in cingulate cortex predicts motor recovery after basal ganglia stroke. *Neurosci Lett* 2016; **613**: 6–12.

141 Touvykine B, Mansoori BK, Jean-Charles L, Deffeyes J, Quessy S, Dancause N. The Effect of Lesion Size on the Organization of the Ipsilesional and Contralesional Motor Cortex. *Neurorehabil Neural Repair* 2016; **30**: 280–92.

142 Quinlan EB, Dodakian L, See J, *et al.* Neural function, injury, and stroke subtype predict treatment gains after stroke. *Ann Neurol* 2015; **77**: 132–45.

143 Lemée J-M, Chinier E, Ali P, Labriffe M, Ter Minassian A, Dinomais M. (Re)organisation of the somatosensory system after early brain lesion: A lateralization index fMRI study. *Ann Phys Rehabil Med* 2019; **63**: 416–21.

144 Morishita Y, Hida S, Naito M, Matsushima U. Evaluation of cervical spondylotic myelopathy using somatosensory-evoked potentials. *Int Orthop* 2005; **29**: 343–6.

145 Nardone R, Höller Y, Brigo F, *et al.* The contribution of neurophysiology in the diagnosis and management of cervical spondylotic myelopathy: a review. *Spinal Cord* 2016; **54**: 756–66.

146 Srinivas R, Uppal S, Chandan YS, Rajmane P. Clinical outcome of cervical spondylosis myelopathy in preoperative and postoperative period. *Interdiscip Neurosurg* 2019; **18**: 100528.

147 Kennedy CA, Beaton DE, Solway S, McConnell S, Bombardier C. Disabilities of the arm, shoulder and hand (DASH). *DASH QuickDASH Outcome Meas User's Man Third Ed Tor Ont Inst Work Health* 2011.

148 Ware J, Kosinski M, Keller S. A 12-Item Short-Form Health Survey: Construction of Scales and Preliminary Tests of Reliability and Validity. *Med Care* 1996; **34**: 220–33.

149 Kato S, Oshima Y, Matsubayashi Y, Taniguchi Y, Tanaka S, Takeshita K. Minimum Clinically Important Difference and Patient Acceptable Symptom State of Japanese Orthopaedic Association Score in Degenerative Cervical Myelopathy Patients. *Spine* 2019; **44**: 691–7.

150 Ware JE jr, Snow KK, Kosinski M, Gandek B, New England Medical Center, The Health Institute. SF-36 Health Survey: Manual and interpretation guide. Boston, Mass.: The Health Institute, New England Medical Center, 1997.

151 Ware JE, Kosinski M. SF-36 Physical & Mental Health Summary Scales: A Manual for Users of Version 1. QualityMetric, 2001.

152 Wirtz MA, Morfeld M, Glaesmer H, Brähler E. Konfirmatorische Prüfung der Skalenstruktur des SF-12 Version 2.0 in einer deutschen bevölkerungs-repräsentativen Stichprobe. *Diagnostica* 2017; **64**: 84–96.

153 Wirtz MA, Morfeld M, Glaesmer H, Brähler E. Normierung des SF-12 Version 2.0 zur Messung der gesundheitsbezogenen Lebensqualität in einer deutschen bevölkerungsrepräsentativen Stichprobe. *Diagnostica* 2018; **64**: 215–26.

154 Hudak PL, Amadio PC, Bombardier C. Development of an upper extremity outcome measure: the DASH (disabilities of the arm, shoulder and hand) [corrected]. The Upper Extremity Collaborative Group (UECG). *Am J Ind Med* 1996; **29**: 602–8.

155 Germann G, Harth A, Wind G, Demir E. Standardisierung und Validierung der deutschen Version 2.0 des "Disability of Arm, Shoulder, Hand" (DASH)-Fragebogens zur Outcome-Messung an der oberen Extremität. *Unfallchirurg* 2003; **106**: 13–9.

156 Vitzthum H-E, Dalitz K. Analysis of five specific scores for cervical spondylogenic myelopathy. *Eur Spine J* 2007; **16**: 2096–103.

157 Mathiowetz V, Weber K, Kashman N, Volland G. Adult Norms for the Nine Hole Peg Test of Finger Dexterity. *Occup Ther J Res* 1985; **5**: 24–38.

158 Feys P, Lamers I, Francis G, *et al.* The Nine-Hole Peg Test as a manual dexterity performance measure for multiple sclerosis. *Mult Scler Houndmills Basingstoke Engl* 2017; **23**: 711–20.

159 Schmitt L. Finger-Tapping Test. In: Volkmar FR, ed. Encyclopedia of Autism Spectrum Disorders. New York, NY: Springer, 2013: 1296–1296.

160 Shirani A, Newton BD, Okuda DT. Finger tapping impairments are highly sensitive for evaluating upper motor neuron lesions. *BMC Neurol* 2017; **17**: 55.

161 Peirce J, Gray JR, Simpson S, *et al.* PsychoPy2: Experiments in behavior made easy. *Behav Res Methods* 2019; **51**: 195–203.

162 Lovett RW, Martin EG. Certain Aspects of Infantile Paralysis and a Description of a Method of Muscle Testing. *J Am Med Assoc* 1916; **LXVI**: 729–33.

163 Porto JM, Nakaishi APM, Cangussu-Oliveira LM, Freire Júnior RC, Spilla SB, Abreu DCC de. Relationship between grip strength and global muscle strength in community-dwelling older people. *Arch Gerontol Geriatr* 2019; **82**: 273–8.

164 Fisher MI, Harrington SE. Research Round-up. *Rehabil Oncol* 2015; **33**: 51.

165 Samuel D, Rowe P. An investigation of the association between grip strength and hip and knee joint moments in older adults. *Arch Gerontol Geriatr* 2012; **54**: 357–60.

166 Karthikbabu S, Chakrapani M. Hand-Held Dynamometer is a Reliable Tool to Measure Trunk Muscle Strength in Chronic Stroke. *J Clin Diagn Res JCDR* 2017; **11**: YC09-YC12.

167 Butland RJ, Pang J, Gross ER, Woodcock AA, Geddes DM. Two-, six-, and 12-minute walking tests in respiratory disease. *Br Med J Clin Res Ed* 1982; **284**: 1607–8.

168 Enright PL. The Six-Minute Walk Test. *Respir Care* 2003; **48**: 783–5.

169 McGee S. Chapter 61 - Examination of the Motor System: Approach to Weakness. In: McGee S, ed. Evidence-Based Physical Diagnosis (Fourth Edition). Philadelphia: Elsevier, 2018: 551-568.e2.

170 Romberg MH. Lehrbuch der Nervenkrankheiten des Menschen. Berlin: Duncker, 1846.

171 Unterberger S. Neue objektiv registrierbare Vestibularis-Körperdrehreaktion, erhalten durch Treten auf der Stelle. Der „Tretversuch". *Arch Für Ohren- Nasen- Kehlkopfheilkd* 1938; **145**: 478–92.

172 Hacke W. Neurologie. Berlin, Heidelberg: Springer-Verlag Berlin Heidelberg, 2010.

173 Rydel A, Seiffer W. Untersuchungen über das Vibrationsgefühl oder die sog. „Knochensensibilität" (Pallästhesie). *Arch Für Psychiatr Nervenkrankh* 1903; **37**: 488–536.

174 Liniger C, Albeanu A, Bloise D, Assal JP. The Tuning Fork Revisited. *Diabet Med* 1990; **7**: 859–64.

175 Xirou S, Kokotis P, Zambelis T, Anagnostou E. Vibratory testing with the 64 Hz Rydel-Seiffer tuning fork and its relation to the sural nerve action potential. *J Peripher Nerv Syst* 2020; **25**: 395–400.

176 Klem GH, Lüders HO, Jasper HH, Elger C. The ten-twenty electrode system of the International Federation. The International Federation of Clinical Neurophysiology. *Electroencephalogr Clin Neurophysiol Suppl* 1999; **52**: 3–6.

177 Stöhr M. Somatosensible Reizantworten von Nerven, Rückenmark und Gehirn (SEP). In: Stöhr M, Dichgans J, Buettner UW, Hess CW, eds. Evozierte Potenziale: SEP — VEP — AEP — EKP — MEP, 4. Auflage. Berlin, Heidelberg: Springer, 2005: 21–252.

178 Malmivuo J. Bioelectromagnetism. New York: Oxford University Press, 1995.

179 Maurer K, Lang N, Eckert J. Praxis der evozierten Potentiale: SEP, AEP, MEP, VEP, 2nd edn. Steinkopff-Verlag Heidelberg, 2005.

180 Shapiro SS, Wilk MB. An Analysis of Variance Test for Normality (Complete Samples). *Biometrika* 1965; **52**: 591–611.

181 Kluyver T, Ragan-Kelley B, Perez F, *et al.* Jupyter Notebooks – a publishing format for reproducible computational workflows. 2016.

182 Harris CR, Millman KJ, van der Walt SJ, *et al.* Array programming with NumPy. *Nature* 2020; **585**: 357–62.

183 McKinney W. Data Structures for Statistical Computing in Python. *Proc 9th Python Sci Conf* 2010; **445**: 51–6.

184 Hunter JD. Matplotlib: A 2D Graphics Environment. *Comput Sci Eng* 2007; **9**: 90–5.

185 Virtanen P, Gommers R, Oliphant TE, *et al.* SciPy 1.0: fundamental algorithms for scientific computing in Python. *Nat Methods* 2020; **17**: 261–72.

186 Seabold S, Perktold J. Statsmodels: Econometric and Statistical Modeling with Python. 9th Python in Science Conference, 2010.

187 Vallat R. Pingouin: statistics in Python. *J Open Source Softw* 2018; **3**: 1026.

188 Waskom ML. seaborn: statistical data visualization. *J Open Source Softw* 2021; **6**: 3021.

189 Yakupov R, Lei J, Hoffmann MB, Speck O. False fMRI activation after motion correction. *Hum Brain Mapp* 2017; **38**: 4497–510.

190 Penny WD, Friston KJ, Ashburner JT, Kiebel SJ, Nichols TE. Statistical Parametric Mapping: The Analysis of Functional Brain Images. Elsevier, 2011.

191 Friston KJ, Williams S, Howard R, Frackowiak RSJ, Turner R. Movement-Related effects in fMRI time-series. *Magn Reson Med* 1996; **35**: 346–55.

192 Havsteen I, Ohlhues A, Madsen KH, Nybing JD, Christensen H, Christensen A. Are Movement Artifacts in Magnetic Resonance Imaging a Real Problem?—A Narrative Review. *Front Neurol* 2017; **8**: 232.

193 James JS, Rajesh P, Chandran AV, Kesavadas C. fMRI paradigm designing and post-processing tools. *Indian J Radiol Imaging* 2014; **24**: 13–21.

194 Ashburner J, Friston KJ. Unified segmentation. *NeuroImage* 2005; **26**: 839–51.

195 Raslau FD, Lin LY, Andersen AH, Powell DK, Smith CD, Escott EJ. Peeking into the Black Box of Coregistration in Clinical fMRI: Which Registration Methods Are Used and How Well Do They Perform? *Am J Neuroradiol* 2018; **39**: 2332–9.

196 Salimi-Khorshidi G, Douaud G, Beckmann CF, Glasser MF, Griffanti L, Smith SM. Automatic denoising of functional MRI data: Combining independent component analysis and hierarchical fusion of classifiers. *NeuroImage* 2014; **90**: 449–68.

197 Park B, Byeon K, Park H. FuNP (Fusion of Neuroimaging Preprocessing) Pipelines: A Fully Automated Preprocessing Software for Functional Magnetic Resonance Imaging. *Front Neuroinformatics* 2019; **13**: 5.

198 Friston KJ, Fletcher P, Josephs O, Holmes A, Rugg MD, Turner R. Event-related fMRI: characterizing differential responses. *NeuroImage* 1998; **7**: 30–40.

199 Uga M, Dan I, Sano T, Dan H, Watanabe E. Optimizing the general linear model for functional near-infrared spectroscopy: an adaptive hemodynamic response function approach. *Neurophotonics* 2014; **1**: 15004.

200 Gaser C, Dahnke R, Kurth K, Luders E, Alzheimer's Disease Neuroimaging Initiative. CAT - A Computational Anatomy Toolbox for the Analysis of Structural MRI Data. *NeuroImage Rev* https://www.semanticscholar.org/paper/CAT-A-Computational-Anatomy-Toolbox-for-the-of-MRI-Gaser-Dahnke/2682c2c5f925da18f465952f1a5c904202ab2693 (accessed Jan 12, 2022).

201 Rorden C, Brett M. Stereotaxic Display of Brain Lesions. *Behav Neurol* 2000; **12**: 191–200.

202 Eickhoff SB, Stephan KE, Mohlberg H, *et al.* A new SPM toolbox for combining probabilistic cytoarchitectonic maps and functional imaging data. *NeuroImage* 2005; **25**: 1325–35.

203 Eickhoff SB, Heim S, Zilles K, Amunts K. Testing anatomically specified hypotheses in functional imaging using cytoarchitectonic maps. *NeuroImage* 2006; **32**: 570–82.

204 Eickhoff SB, Paus T, Caspers S, *et al.* Assignment of functional activations to probabilistic cytoarchitectonic areas revisited. *NeuroImage* 2007; **36**: 511–21.

205 Geyer S, Schleicher A, Zilles K. Areas 3a, 3b, and 1 of Human Primary Somatosensory Cortex: 1. Microstructural Organization and Interindividual Variability. *NeuroImage* 1999; **10**: 63–83.

206 Geyer S, Schormann T, Mohlberg H, Zilles K. Areas 3a, 3b, and 1 of Human Primary Somatosensory Cortex: 2. Spatial Normalization to Standard Anatomical Space. *NeuroImage* 2000; **11**: 684–96.

207 Grefkes C, Geyer S, Schormann T, Roland P, Zilles K. Human Somatosensory Area 2: Observer-Independent Cytoarchitectonic Mapping, Interindividual Variability, and Population Map. *NeuroImage* 2001; **14**: 617–31.

208 Eickhoff SB, Schleicher A, Zilles K, Amunts K. The Human Parietal Operculum. I. Cytoarchitectonic Mapping of Subdivisions. *Cereb Cortex* 2006; **16**: 254–67.

209 Eickhoff SB, Amunts K, Mohlberg H, Zilles K. The Human Parietal Operculum. II. Stereotaxic Maps and Correlation with Functional Imaging Results. *Cereb Cortex* 2006; **16**: 268–79.

210 Lenz FA, Treede R-D, Baumgartner U. Nociceptive Processing in the Secondary Somatosensory Cortex. In: Gebhard GF, Schmidt RF, eds. Encyclopedia of Pain. Berlin, Heidelberg: Springer, 2013.

211 Yushkevich PA, Piven J, Hazlett HC, *et al.* User-guided 3D active contour segmentation of anatomical structures: Significantly improved efficiency and reliability. *NeuroImage* 2006; **31**: 1116–28.

212 Ahrens J, Geveci B, Law C. Paraview: An end-user tool for large data visualization. *Vis Handb* 2005; **717**.

213 Ayachit U. The paraview guide: a parallel visualization application. Kitware, Inc., 2015.

214 Hinke RM, Hu X, Stillman AE, *et al.* Functional magnetic resonance imaging of Broca's area during internal speech. *NeuroReport* 1993; **4**: 675–8.

215 Binder JR, Rao SM, Hammeke TA, *et al.* Lateralized Human Brain Language Systems Demonstrated by Task Subtraction Functional Magnetic Resonance Imaging. *Arch Neurol* 1995; **52**: 593–601.

216 Jansen A, Menke R, Sommer J, *et al.* The assessment of hemispheric lateralization in functional MRI—Robustness and reproducibility. *NeuroImage* 2006; **33**: 204–17.

217 Seghier ML. Laterality index in functional MRI: methodological issues. *Magn Reson Imaging* 2008; **26**: 594–601.

218 Detre JA, Maccotta L, King D, *et al.* Functional MRI lateralization of memory in temporal lobe epilepsy. *Neurology* 1998; **50**: 926–32.

219 Tervaniemi M, Hugdahl K. Lateralization of auditory-cortex functions. *Brain Res Brain Res Rev* 2003; **43**: 231–46.

220 Seghier ML, Vuilleumier P. Functional neuroimaging findings on the human perception of illusory contours. *Neurosci Biobehav Rev* 2006; **30**: 595–612.

221 Bertolino A, Blasi G, Caforio G, *et al.* Functional lateralization of the sensorimotor cortex in patients with schizophrenia: effects of treatment with olanzapine. *Biol Psychiatry* 2004; **56**: 190–7.

222 Brumer I, Vita ED, Ashmore J, Jarosz J, Borri M. Implementation of clinically relevant and robust fMRI-based language lateralization: Choosing the laterality index calculation method. *PLOS ONE* 2020; **15**: e0230129.

223 Desmond JE, Sum JM, Wagner AD, *et al.* Functional MRI measurement of language Lateralization in Wada-tested patients. *Brain* 1995; **118**: 1411–9.

224 Branco DM, Suarez RO, Whalen S, *et al.* Functional MRI of memory in the hippocampus: Laterality indices may be more meaningful if calculated from whole voxel distributions. *NeuroImage* 2006; **32**: 592–602.

225 Abbott DF, Waites AB, Lillywhite LM, Jackson GD. fMRI assessment of language lateralization: An objective approach. *NeuroImage* 2010; **50**: 1446–55.

226 Bradshaw AR, Bishop DVM, Woodhead ZVJ. Methodological considerations in assessment of language lateralisation with fMRI: a systematic review. *PeerJ* 2017; **5**: e3557.

227 Nadkarni TN, Andreoli MJ, Nair VA, *et al.* Usage of fMRI for pre-surgical planning in brain tumor and vascular lesion patients: Task and statistical threshold effects on language lateralization. *NeuroImage Clin* 2015; **7**: 415–23.

228 Matsuo K, Chen S-HA, Tseng W-YI. AveLI: A robust lateralization index in functional magnetic resonance imaging using unbiased threshold-free computation. *J Neurosci Methods* 2012; **205**: 119–29.

229 Benjamini Y, Hochberg Y. Controlling the False Discovery Rate: A Practical and Powerful Approach to Multiple Testing. *J R Stat Soc Ser B Methodol* 1995; **57**: 289–300.

230 Hilton B, Gardner EL, Jiang Z, *et al.* Establishing Diagnostic Criteria for Degenerative Cervical Myelopathy [AO Spine RECODE-DCM Research Priority Number 3]. *Glob Spine J* 2022; **12**: 55S-63S.

231 Zipser CM, Margetis K, Pedro KM, *et al.* Increasing awareness of degenerative cervical myelopathy: a preventative cause of non-traumatic spinal cord injury. *Spinal Cord* 2021; **59**: 1216–8.

232 Behrbalk E, Salame K, Regev GJ, Keynan O, Boszczyk B, Lidar Z. Delayed diagnosis of cervical spondylotic myelopathy by primary care physicians. *Neurosurg Focus* 2013; **35**: E1.

233 Pope DH, Mowforth OD, Davies BM, Kotter MRN. Diagnostic Delays Lead to Greater Disability in Degenerative Cervical Myelopathy and Represent a Health Inequality. *Spine* 2020; **45**: 368–77.

234 Grodzinski B, Stubbs DJ, Davies BM. Most degenerative cervical myelopathy remains undiagnosed, particularly amongst the elderly: modelling the prevalence of degenerative cervical myelopathy in the United Kingdom. *J Neurol* 2023; **270**: 311–9.

235 Fouyas IP, Statham PFX, Sandercock PAG. Cochrane Review on the Role of Surgery in Cervical Spondylotic Radiculomyelopathy. *Spine* 2002; **27**: 736–47.

236 Yamada T. Somatosensory Evoked Potentials. In: Aminoff MJ, Daroff RB, eds. Encyclopedia of the Neurological Sciences (Second Edition). Oxford: Academic Press, 2014: 230–8.

237 Martina ISJ, Koningsveld R van, Schmitz PIM, Meché FGA van der, Doorn PA van. Measuring vibration threshold with a graduated tuning fork in normal aging and in patients with polyneuropathy. *J Neurol Neurosurg Psychiatry* 1998; **65**: 743–7.

238 Jütten K, Mainz V, Schubert GA, *et al.* Cortical volume reductions as a sign of secondary cerebral and cerebellar impairment in patients with degenerative cervical myelopathy. *NeuroImage Clin* 2021; **30**: 102624.

239 Akter F, Yu X, Qin X, *et al.* The Pathophysiology of Degenerative Cervical Myelopathy and the Physiology of Recovery Following Decompression. *Front Neurosci* 2020; **14**: 138.

240 Tu J, Vargas Castillo J, Das A, Diwan AD. Degenerative Cervical Myelopathy: Insights into Its Pathobiology and Molecular Mechanisms. *J Clin Med* 2021; **10**: 1214.

241 Kriz J, Kozak J, Zedka M. Primary motor cortex inhibition in spinal cord injuries. *Neuro Endocrinol Lett* 2012; **33**: 431–41.

242 Krishna V, Andrews H, Varma A, Mintzer J, Kindy MS, Guest J. Spinal Cord Injury: How Can We Improve the Classification and Quantification of Its Severity and Prognosis? *J Neurotrauma* 2014; **31**: 215–27.

243 Maier IL, Hofer S, Joseph AA, *et al.* Quantification of spinal cord compression using T1 mapping in patients with cervical spinal canal stenosis – Preliminary experience. *NeuroImage Clin* 2019; **21**: 101639.

244 Shabani S, Kaushal M, Budde M, Schmit B, Wang MC, Kurpad S. Comparison between quantitative measurements of diffusion tensor imaging and T2 signal intensity in a large series of cervical spondylotic myelopathy patients for assessment of disease severity and prognostication of recovery. *J Neurosurg Spine* 2019; **31**: 473–9.

245 Shabani S, Kaushal M, Budde MD, Wang MC, Kurpad SN. Diffusion tensor imaging in cervical spondylotic myelopathy: a review. *J Neurosurg Spine* 2020; **33**: 65–72.

246 Nukala M, Abraham J, Khandige G, Shetty BK, Rao A pol arjun. Efficacy of diffusion tensor imaging in identification of degenerative cervical spondylotic myelopathy. *Eur J Radiol Open* 2018; **6**: 16–23.

247 d'Avanzo S, Ciavarro M, Pavone L, *et al.* The Functional Relevance of Diffusion Tensor Imaging in Patients with Degenerative Cervical Myelopathy. *J Clin Med* 2020; **9**: 1828.

248 Harris JE, Eng JJ. Individuals with the Dominant Hand Affected following Stroke Demonstrate Less Impairment Than Those with the Nondominant Hand Affected. *Neurorehabil Neural Repair* 2006; **20**: 380–9.

249 Kemlin C, Moulton E, Samson Y, Rosso C. Do Motor Imagery Performances Depend on the Side of the Lesion at the Acute Stage of Stroke? *Front Hum Neurosci* 2016; **10**: 321.

250 Mattay VS, Callicott JH, Bertolino A, *et al.* Hemispheric control of motor function: a whole brain echo planar fMRI study. *Psychiatry Res Neuroimaging* 1998; **83**: 7–22.

251 Barber AD, Srinivasan P, Joel SE, Caffo BS, Pekar JJ, Mostofsky SH. Motor "Dexterity"?: Evidence that Left Hemisphere Lateralization of Motor Circuit Connectivity Is Associated with Better Motor Performance in Children. *Cereb Cortex* 2012; **22**: 51–9.

252 Moulton E, Galléa C, Kemlin C, *et al.* Cerebello-Cortical Differences in Effective Connectivity of the Dominant and Non-dominant Hand during a Visuomotor Paradigm of Grip Force Control. *Front Hum Neurosci* 2017; **11**: 511.

253 Andersen KW, Siebner HR. Mapping dexterity and handedness: recent insights and future challenges. *Curr Opin Behav Sci* 2018; **20**: 123–9.

254 Mori S, Tournier J-D, editors. Introduction to diffusion tensor imaging and higher order models, 2nd edition. Amsterdam ; Boston: Elsevier/Academic Press, 2014.

255 Makin TR, Cramer AO, Scholz J, *et al.* Deprivation-related and use-dependent plasticity go hand in hand. *eLife* 2013; **2**: e01273.

256 Hahamy A, Sotiropoulos SN, Henderson Slater D, Malach R, Johansen-Berg H, Makin TR. Normalisation of brain connectivity through compensatory behaviour, despite congenital hand absence. *eLife* 2015; **4**: e04605.

257 Rüber T, Lindenberg R, Schlaug G. Differential adaptation of descending motor tracts in musicians. *Cereb Cortex N Y N 1991* 2015; **25**: 1490–8.

258 Angstmann S, Madsen KS, Skimminge A, Jernigan TL, Baaré WFC, Siebner HR. Microstructural asymmetry of the corticospinal tracts predicts right-left differences in circle drawing skill in right-handed adolescents. *Brain Struct Funct* 2016; **221**: 4475–89.

259 Langer N, Hänggi J, Müller NA, Simmen HP, Jäncke L. Effects of limb immobilization on brain plasticity. *Neurology* 2012; **78**: 182–8.

260 Blatow M, Nennig E, Durst A, Sartor K, Stippich C. fMRI reflects functional connectivity of human somatosensory cortex. *NeuroImage* 2007; **37**: 927–36.

261 Eickhoff SB, Grefkes C, Fink GR, Zilles K. Functional Lateralization of Face, Hand, and Trunk Representation in Anatomically Defined Human Somatosensory Areas. *Cereb Cortex* 2008; **18**: 2820–30.

262 Lamp G, Goodin P, Palmer S, Low E, Barutchu A, Carey LM. Activation of Bilateral Secondary Somatosensory Cortex With Right Hand Touch Stimulation: A Meta-Analysis of Functional Neuroimaging Studies. *Front Neurol* 2019; **9**: 1129.

263 Tamè L, Braun C, Lingnau A, *et al.* The contribution of primary and secondary somatosensory cortices to the representation of body parts and body sides: an fMRI adaptation study. *J Cogn Neurosci* 2012; **24**: 2306–20.

264 Brodoehl S, Klingner C, Stieglitz K, Witte OW. Age-related changes in the somatosensory processing of tactile stimulation—An fMRI study. *Behav Brain Res* 2013; **238**: 259–64.

265 Wang J, Meng H-J, Ji G-J, *et al.* Finger Tapping Task Activation vs. TMS Hotspot: Different Locations and Networks. *Brain Topogr* 2020; **33**: 123–34.

266 Wang C, Ellingson BM, Oughourlian TC, Salamon N, Holly LT. Evolution of brain functional plasticity associated with increasing symptom severity in degenerative cervical myelopathy. *eBioMedicine* 2022; **84**. DOI:10.1016/j.ebiom.2022.104255.

267 Jain N, Catania KC, Kaas JH. Deactivation and reactivation of somatosensory cortex after dorsal spinal cord injury. *Nature* 1997; **386**: 495–8.

268 Kaas JH, Rothemund Y. Reorganization of somatosensory and motor cortex following peripheral nerve or spinal cord injury in primates. In: Reprogramming the Cerebral Cortex. Oxford: Oxford University Press, 2006.

269 Jain N, Florence SL, Qi HX, Kaas JH. Growth of new brainstem connections in adult monkeys with massive sensory loss. *Proc Natl Acad Sci U S A* 2000; **97**: 5546–50.

270 Dhillon RS, Parker J, Syed YA, *et al.* Axonal plasticity underpins the functional recovery following surgical decompression in a rat model of cervical spondylotic myelopathy. *Acta Neuropathol Commun* 2016; **4**: 89.

271 Zhao R, Song Y, Guo X, *et al.* Enhanced Information Flow From Cerebellum to Secondary Visual Cortices Leads to Better Surgery Outcome in Degenerative Cervical Myelopathy Patients: A Stochastic Dynamic Causal Modeling Study With Functional Magnetic Resonance Imaging. *Front Hum Neurosci* 2021; **15**: 632829.

272 Riemann BL, Lephart SM. The Sensorimotor System, Part I: The Physiologic Basis of Functional Joint Stability. *J Athl Train* 2002; **37**: 71–9.

273 Brasil-Neto JP, Valls-Solè J, Pascual-Leone A, *et al.* Rapid modulation of human cortical motor outputs following ischaemic nerve block. *Brain* 1993; **116**: 511–25.

274 Zhang Q, Zhou X, Li Y, Yang X, Abbasi QH. Clinical Recognition of Sensory Ataxia and Cerebellar Ataxia. *Front Hum Neurosci* 2021; **15**: 639871.

275 Sensinger JW, Dosen S. A Review of Sensory Feedback in Upper-Limb Prostheses From the Perspective of Human Motor Control. *Front Neurosci* 2020; **14**: 345.

276 Amoruso E, Dowdall L, Kollamkulam MT, *et al.* Intrinsic somatosensory feedback supports motor control and learning to operate artificial body parts. *J Neural Eng* 2022; **19**: 016006.

277 Strominger NL, Demarest RJ, Laemle LB. Motoneurons and Motor Pathways. In: Strominger NL, Demarest RJ, Laemle LB, eds. Noback's Human Nervous System, Seventh Edition: Structure and Function. Totowa, NJ: Humana Press, 2012: 191–203.

278 Turner BO, Paul EJ, Miller MB, Barbey AK. Small sample sizes reduce the replicability of task-based fMRI studies. *Commun Biol* 2018; **1**: 1–10.

279 Marek S, Tervo-Clemmens B, Calabro FJ, *et al.* Reproducible brain-wide association studies require thousands of individuals. *Nature* 2022; **603**: 654–60.

280 Puig J, Blasco G, Alberich-Bayarri A, *et al.* Resting-State Functional Connectivity Magnetic Resonance Imaging and Outcome After Acute Stroke. *Stroke* 2018; **49**: 2353–60.

281 Benjamin CF, Walshaw PD, Hale K, *et al.* Presurgical language fMRI: Mapping of six critical regions. *Hum Brain Mapp* 2017; **38**: 4239–55.

282 Constable RT. Challenges in fMRI and Its Limitations. In: Faro SH, Mohamed FB, eds. Functional MRI: Basic Principles and Clinical Applications. New York, NY: Springer, 2006: 75–98.

283 Uludağ K, Blinder P. Linking brain vascular physiology to hemodynamic response in ultra-high field MRI. *NeuroImage* 2018; **168**: 279–95.

284 Raj D, Anderson AW, Gore JC. Respiratory effects in human functional magnetic resonance imaging due to bulk susceptibility changes. *Phys Med Biol* 2001; **46**: 3331–40.

285 Alfaro-Almagro F, McCarthy P, Afyouni S, *et al.* Confound modelling in UK Biobank brain imaging. *NeuroImage* 2021; **224**: 117002.

286 Duncan NW, Northoff G. Overview of potential procedural and participant-related confounds for neuroimaging of the resting state. *J Psychiatry Neurosci JPN* 2013; **38**: 84–96.

287 Botvinik-Nezer R, Holzmeister F, Camerer CF, *et al.* Variability in the analysis of a single neuroimaging dataset by many teams. *Nature* 2020; **582**: 84–8.

288 Schluppeck D, Francis S. Somatosensory Processing. In: Toga AW, ed. Brain Mapping. Waltham: Academic Press, 2015: 549–52.

289 White LE, Andrews TJ, Hulette C, *et al.* Structure of the human sensorimotor system. I: Morphology and cytoarchitecture of the central sulcus. *Cereb Cortex N Y N 1991* 1997; **7**: 18–30.

290 Stricsek G, Gillick J, Rymarczuk G, Harrop JS. Managing the Complex Patient with Degenerative Cervical Myelopathy: How to Handle the Aging Spine, the Obese Patient, and Individuals with Medical Comorbidities. *Neurosurg Clin N Am* 2018; **29**: 177–84.

291 Jannelli G, Nouri A, Molliqaj G, Grasso G, Tessitore E. Degenerative Cervical Myelopathy: Review of Surgical Outcome Predictors and Need for Multimodal Approach. *World Neurosurg* 2020; **140**: 541–7.

7. Appendix

7.1. Supplementary Information

7.1.1. Supplementary Tables

Table 9: Clinical parameters acquired for the degenerative cervical myelopathy patients.

Subject	1	2	3	4	5	6	7	8	9
Age	74	65	45	66	49	57	44	37	64
Gender	m	m	m	m	f	m	m	m	f
Handedness	r	r	r	r	r	r	r	r	r
Extent of stenosis (nr. of segments)	3	2	2	1	1	1	1	3	1
Symptomatic time (months)	8	42	17	24	5	6	43	62	216
JOA score	10	14	14	16.5	16	14	10	13.5	12
Motor upper JOA	1	3	3	4	4	4	3	1.5	2.5
Motor lower JOA	3	4	3	4	4	3	2.5	4	3
Sensory JOA	4	5	5	5.5	5	4	2.5	5	3.5
Bladder dysfunction (JOA)	2	2	3	3	3	3	2	3	3
DASH score	33	20	53	6	26	38	43	18	16
SF-12 physical	38.10541	50.39502	28.49005	55.25834	41.59427	22.07675	32.1348	41.54321	42.76227
SF-12 mental	58.16266	61.23345	40.53534	60.69717	51.98225	57.17757	58.22272	36.36907	62.75756
6MWT (meters)	506	350	537	540	460	370	420	720	505
Paresthesia left upper extremity	1	1	0	1	0	1	1	1	1
Paresthesia right upper extremity	1	1	1	0	1	1	1	1	1
Paresthesia left lower extremity	0	0	0	0	0	0	1	0	0
Paresthesia right lower extremity	0	0	0	0	0	0	1	0	0
Hypoesthesia left upper extremity	0	1	0	0	0	0	1	1	0
Hypoesthesia right upper extremity	1	1	1	0	0	1	1	0	0
Hypoesthesia left lower extremity	0	0	0	0	0	0	1	0	0
Hypoesthesia right lower extremity	0	0	1	0	0	1	1	0	0
Allodynia left upper extremity	0	0	0	0	0	1	0	0	0
Allodynia right upper extremity	0	0	0	0	0	0	0	0	0
Allodynia left lower extremity	0	0	0	0	0	0	0	0	0
Allodynia right lower extremity	0	0	0	0	0	0	0	0	0
Impaired sensation of temperature l.u.e.	0	0	0	0	0	1	1	0	0
Impaired sensation of temperature r.u.e.	1	0	0	0	0	1	1	0	0
Impaired sensation of temperature l.l.e.	1	0	0	0	0	1	1	0	0
Impaired sensation of temperature r.l.e.	1	0	1	0	0	1	1	0	0
Proprioception left upper extremity	5/5	5/5	5/5	5/5	5/5	5/5	5/5	5/5	5/5
Proprioception right upper extremity	5/5	5/5	5/5	5/5	5/5	5/5	5/5	5/5	5/5
Proprioception left lower extremity	5/5	5/5	5/5	5/5	5/5	5/5	3/5	5/5	5/5
Proprioception right lower extremity	4/5	5/5	5/5	5/5	5/5	5/5	4/5	5/5	5/5
Pallesthesia left radial styloid proc.	5/8	7/8	5.5/8	8/8	8/8	8/8	8/8	6/8	5/8
Pallesthesia right radial styloid proc.	0/8	7/8	5/8	7/8	8/8	8/8	5/8	7/8	5/8
Pallesthesia left medial malleolus	0/8	4/8	5/8	7/8	8/8	4/8	6/8	4/8	5/8
Pallesthesia right medial malleolus	0/8	7/8	4/8	8/8	8/8	6/8	4/8	6/8	6/8
Increased reflexes upper extremity	0	1	0	0	0	0	0	1	0
Reduced reflexes upper extremity	0	0	0	0	0	0	1	0	0
Increased reflexes lower extremity	1	0	0	0	0	0	0	0	1

Reduced reflexes lower extremity	0	0	1	1	0	0	1	0	0
Positive Trömner sign	0	1	0	0	0	0	0	0	0
Positive Babinski sign	0	0	0	0	0	0	0	0	0
Strength left upper extremity (MRCS)	5/5	3/5	4+/5	5/5	5/5	5/5	5/5	4/5	5/5
Strength right upper extremity (MRCS)	3/5	5/5	5/5	5/5	4+/5	5/5	5/5	5/5	4/5
Strength left lower extremity (MRCS)	5/5	5/5	5/5	5/5	5/5	5/5	5/5	5/5	5/5
Strength right lower extremity (MRCS)	5/5	5/5	5/5	5/5	5/5	5/5	5/5	5/5	5/5
Increased muscle tone	1	1	0	0	0	0	0	1	0
Reduced muscle tone	0	0	0	0	0	0	0	0	1
Grip force left hand (kPa)	60	40	100	100	35	85	65	80	50
Grip force right hand (kPa)	50	80	100	75	30	80	90	100	50
Positive Romberg sign	0	0	0	0	0	0	1	0	0
Positive Unterberger stepping test	0	0	0	0	0	0	-	1	-
NHPT forwards lh (sec)	33	19	14	14	13	26	17	16	14
NHPT forwards rh (sec)	75	15	15	17	16	28	17	13	16
NHPT backwards lh (sec)	8	8	6	7	6	7	6	7	5
NHPT backwards rh (sec)	20	6	6	6	6	8	7	5	7
mITI paced FTT lh (sec)	0.2364	0.3030	0.3069	0.3295	0.3263	0.2963	0.2818	0.3334	0.4736
mITI paced FTT rh (sec)	0.3004	0.2846	0.2861	0.3392	0.3202	0.2972	0.3017	0.3199	0.4520
mITI max. speed FTT lh (sec)	0.2754	0.2534	0.2079	0.1858	0.1863	0.1905	0.2134	0.1618	0.2205
mITI max. speed FTT rh (sec)	0.3877	0.2240	0.1725	0.1847	0.1766	0.1818	0.1888	0.1540	0.1858
SSEP latency N33 left (ms)	40.4	36.6	36.8	31.6	35.3	35.8	-	32.6	51.0
SSEP latency N33 right (ms)	45.4	34.4	31.5	36.0	37.1	41.4	-	32.1	59.0
SSEP latency P40 left (ms)	45.9	42.4	43.1	36.9	40.5	47.1	-	40.8	62.0
SSEP latency P40 right (ms)	50.1	39.6	42.1	40.0	40.1	48.8	-	39.8	73.8
SSEP latency P60 left (ms)	59.6	59.2	59.9	55.6	63.4	66.2	-	59.0	96.3
SSEP latency P60 right (ms)	62.5	60.8	55.7	65.7	60.1	68.2	-	58.2	110.0
Side difference lat. N33 (ms)	5.0	2.2	5.3	4.4	1.8	5.6	-	0.6	8.0
Side difference lat. P40 (ms)	4.8	2.8	1.0	3.1	0.4	1.7	-	1.0	11.8
Side difference lat. P60 (ms)	2.9	1.6	4.2	10.1	3.3	2.0	-	0.8	13.7

Table 10: Clinical parameters acquired for the healthy control subjects.

Subject	**1**	**2**	**3**	**4**	**5**	**6**	**7**	**8**	**9**
Age	67	71	67	58	52	45	54	34	62
Gender	m	m	m	f	m	m	m	m	f
Handedness	r	r	r	r	r	r	r	r	r
6MWT (meters)	563	420	550	585	720	690	720	680	557
Paresthesia left upper extremity	0	0	0	0	0	0	0	0	0
Paresthesia right upper extremity	0	0	0	0	0	0	0	0	0
Paresthesia left lower extremity	0	0	0	0	0	0	0	0	0
Paresthesia right lower extremity	0	0	0	0	0	0	0	0	0
Hypoesthesia left upper extremity	0	0	0	0	0	0	0	0	0
Hypoesthesia right upper extremity	0	0	0	0	0	0	0	0	0
Hypoesthesia left lower extremity	0	0	0	0	0	0	0	0	0
Hypoesthesia right lower extremity	0	0	0	0	0	0	0	0	0
Allodynia left upper extremity	0	0	0	0	0	0	0	0	0
Allodynia right upper extremity	0	0	0	0	0	0	0	0	0
Allodynia left lower extremity	0	0	0	0	0	0	0	0	0
Allodynia right lower extremity	0	0	0	0	0	0	0	0	0

Impaired sensation of temperature l.u.e.	0	0	0	0	0	0	0	0	0
Impaired sensation of temperature r.u.e.	0	0	0	0	0	0	0	0	0
Impaired sensation of temperature l.l.e.	0	0	0	0	0	0	0	0	0
Impaired sensation of temperature r.l.e.	0	0	0	0	0	0	0	0	0
Proprioception left upper extremity	5/5	5/5	5/5	5/5	5/5	5/5	5/5	5/5	5/5
Proprioception right upper extremity	5/5	5/5	5/5	5/5	5/5	5/5	5/5	5/5	5/5
Proprioception left lower extremity	5/5	5/5	5/5	5/5	5/5	5/5	5/5	5/5	5/5
Proprioception right lower extremity	5/5	5/5	5/5	5/5	5/5	5/5	5/5	5/5	5/5
Pallesthesia left radial styloid proc.	7/8	7/8	8/8	6/8	7/8	7/8	8/8	8/8	6/8
Pallesthesia right radial styloid proc.	7/8	7/8	8/8	7/8	7/8	7/8	8/8	7/8	7/8
Pallesthesia left medial malleolus	6/8	8/8	7/8	6/8	5/8	8/8	8/8	8/8	6/8
Pallesthesia right medial malleolus	6/8	8/8	7/8	4/8	6/8	8/8	8/8	8/8	7/8
Increased reflexes upper extremity	0	0	0	0	0	0	0	0	0
Reduced reflexes upper extremity	0	0	0	0	0	0	0	0	0
Increased reflexes lower extremity	0	0	0	0	0	0	0	0	0
Reduced reflexes lower extremity	0	0	0	0	0	0	0	0	0
Positive Trömner sign	0	0	0	0	0	0	0	0	0
Positive Babinski sign	0	0	0	0	0	0	0	0	0
Strength left upper extremity (MRCS)	5/5	5/5	5/5	5/5	5/5	5/5	5/5	5/5	5/5
Strength right upper extremity (MRCS)	5/5	5/5	5/5	5/5	5/5	5/5	5/5	5/5	5/5
Strength left lower extremity (MRCS)	5/5	5/5	5/5	5/5	5/5	5/5	5/5	5/5	5/5
Strength right lower extremity (MRCS)	5/5	5/5	5/5	5/5	5/5	5/5	5/5	5/5	5/5
Increased muscle tone	0	0	0	0	0	0	0	0	0
Reduced muscle tone	0	0	0	0	0	0	0	0	0
Grip force left hand (kPa)	80	85	70	85	90	120	70	65	50
Grip force right hand (kPa)	90	80	70	80	75	135	70	65	50
Positive Romberg sign	0	0	0	0	0	0	0	0	0
Positive Unterberger stepping test	0	0	0	0	0	0	0	0	0
NHPT forwards lh (sec)	15	21	15	14	11	15	14	13	13
NHPT forwards rh (sec)	17	20	18	15	15	13	14	15	13
NHPT backwards lh (sec)	6	8	5	6	5	7	6	5	5
NHPT backwards rh (sec)	5	8	6	8	5	5	6	6	5
mITI paced FTT lh (sec)	0.3999	0.3049	0.3881	0.2868	0.3972	0.3091	0.1712	0.3127	0.1544
mITI paced FTT rh (sec)	0.4046	0.2800	0.3961	0.2082	0.4225	0.2473	0.1544	0.3189	0.2799
mITI max. speed FTT lh (sec)	0.2050	0.2309	0.1725	0.2393	0.1634	0.1538	0.1797	0.2000	0.1860
mITI max. speed FTT rh (sec)	0.1822	0.2084	0.1694	0.1972	0.1611	0.1557	0.1711	0.1811	0.1563

Table 11: Behavioral finger tapping results. This table shows the mean intertap intervals (mITI, sec) and the coefficients of variation (CoV) of the mITI during the visually paced finger tapping test (FTT) and the FTT at maximum speed without pacing.

		DCM patients		**Control subjects**		**P-value**	
		mITI	CoV	mITI	CoV	mITI	CoV
Visually paced FTT	Left hand	0.32 ± 0.06	0.13 ± 0.06	0.33 ± 0.08	0.14 ± 0.06	0.7755	0.8320
	Right hand	0.32 ± 0.05	0.15 ± 0.07	0.30 ± 0.09	0.14 ± 0.09	0.5822	0.9335
Maximum speed FTT	Left hand	0.21 ± 0.04	0.19 ± 0.07	0.19 ± 0.03	0.15 ± 0.08	0.2514	0.2552
	Right hand	0.21 ± 0.07	0.21 ± 0.27	0.18 ± 0.02	0.10 ± 0.03	0.2288	0.2374

Table 12: Number of significantly activated voxels in patients suffering from degenerative cervical myelopathy. This table lists the number of significantly activated voxels ($p \leq 0.05$, FWE corrected) within bihemispheric primary (S1) and secondary (S2) somatosensory cortex resulting from the single subject analysis.

	Task (somatosensory stimulation)			
DCM patient	Left hand	Right hand	Left foot	Right foot
1	0	10	0	0
2	73	110	122	55
3	0	0	0	0
4	19	26	25	40
5	8	16	10	5
6	0	7	0	0
7	164	418	47	36
8	32	170	1	11
9	46	46	64	11

Table 13: Number of significantly activated voxels in control subjects. This table lists the number of significantly activated voxels ($p \leq 0.05$, FWE corrected) within bihemispheric primary (S1) and secondary (S2) somatosensory cortex resulting from the single subject analysis.

	Task (somatosensory stimulation)			
Control subject	Left hand	Right hand	Left foot	Right foot
1	191	205	105	132
2	208	163	303	170
3	0	0	15	0
4	375	301	253	150
5	152	283	114	93
6	5	111	0	1
7	0	56	1	2
8	79	382	37	49
9	67	59	14	29

Table 14: Local maxima regarding the task condition “somatosensory stimulation of the left hand”.

ROI	DCM Patients						Control subjects						ED
	MNI-coordinate			T-value	P-value		MNI-coordinate			T-value	P-value		
	x	y	z		uncorrected	FWE-c.	x	y	z		uncorrected	FWE-c.	(mm)
S1 left	-54	-25	38	3.78	≤ 0.001	0.829	-57	-22	38	4.46	≤ 0.001	0.240	4.24
S2 left	-	-	-	-	-	-	-54	-28	20	4.31	≤ 0.001	0.349	-
BA 1 left	-	-	-	-	-	-	-	-	-	-	-	-	-
BA 2 left	-54	-25	38	3.78	≤ 0.001	0.829	-57	-22	38	4.46	≤ 0.001	0.240	4.24
BA 3a left	-	-	-	-	-	-	-	-	-	-	-	-	-
BA 3b left	-51	-22	35	3.39	≤ 0.001	0.989	-57	-19	35	3.79	≤ 0.001	0.826	6.71
S1 right	-	-	-	-	-	-	39	-31	65	5.83	≤ 0.001	**0.003***	-
S2 right	48	-22	20	4.08	≤ 0.001	0.559	54	-22	20	5.98	≤ 0.001	**0.002***	6
BA 1 right	-	-	-	-	-	-	39	-31	65	5.83	≤ 0.001	**0.003***	-
BA 2 right	-	-	-	-	-	-	30	-40	62	5.16	≤ 0.001	**0.032***	-
BA 3a right	-	-	-	-	-	-	-	-	-	-	-	-	-
BA 3b right	-	-	-	-	-	-	39	-31	59	4.93	≤ 0.001	0.066	-

Table 15: Local maxima regarding the task condition “somatosensory stimulation of the right hand”.

ROI	DCM Patients						Control subjects						ED
	MNI-coordinate			T-value	P-value		MNI-coordinate			T-value	P-value		
	x	y	z		uncorrected	FWE-c.	x	y	z		uncorrected	FWE-c.	(mm)
S1 left	-54	-25	38	5.88	≤ 0.001	**0.003***	-27	-43	68	7.14	≤ 0.001	**≤ 0.001***	44.19
S2 left	-51	-28	20	5.52	≤ 0.001	**0.01***	-57	-28	20	7.17	≤ 0.001	**0.001***	6
BA 1 left	-30	-37	68	4.70	≤ 0.001	0.127	-27	-40	68	6.70	≤ 0.001	**≤ 0.001***	4.24
BA 2 left	-54	-25	38	5.88	≤ 0.001	**0.003***	-27	-43	68	7.14	≤ 0.001	**≤ 0.001***	44.19
BA 3a left	-33	-34	53	3.38	≤ 0.001	0.990	-54	-19	29	3.55	≤ 0.001	0.957	35.24
BA 3b left	-51	-22	35	4.50	≤ 0.001	0.219	-57	-19	35	5.02	≤ 0.001	**0.049***	6.71
S1 right	-	-	-	-	-	-	-	-	-	-	-	-	-
S2 right	-	-	-	-	-	-	60	-25	23	4.17	≤ 0.001	0.472	-
BA 1 right	-	-	-	-	-	-	-	-	-	-	-	-	-
BA 2 right	-	-	-	-	-	-	-	-	-	-	-	-	-
BA 3a right	-	-	-	-	-	-	-	-	-	-	-	-	-
BA 3b right	-	-	-	-	-	-	-	-	-	-	-	-	-

Table 16: Local maxima regarding the task condition “somatosensory stimulation of the left foot”.

ROI	DCM Patients						Control subjects						ED
	MNI-coordinate			T-value	P-value		MNI-coordinate			T-value	P-value		
	x	y	z		uncorrected	FWE-c.	x	y	z		uncorrected	FWE-c.	(mm)
S1 left	-54	-25	38	3.97	≤ 0.001	0.658	-54	-25	38	5.14	≤ 0.001	**0.034***	0
S2 left	-	-	-	-	-	-	-57	-22	20	5.44	≤ 0.001	**0.013***	-
BA 1 left	-	-	-	-	-	-	-	-	-	-	-	-	-
BA 2 left	-54	-25	38	3.97	≤ 0.001	0.658	-54	-25	38	5.14	≤ 0.001	**0.034***	0
BA 3a left	-	-	-	-	-	-	-	-	-	-	-	-	-
BA 3b left	-51	-22	35	3.49	≤ 0.001	0.972	-57	-19	35	4.43	≤ 0.001	0.261	-
S1 right	-	-	-	-	-	-	12	-40	68	4.46	≤ 0.001	0.242	-
S2 right	-	-	-	-	-	-	54	-25	20	5.38	≤ 0.001	**0.016***	-
BA 1 right	-	-	-	-	-	-	-	-	-	-	-	-	-
BA 2 right	-	-	-	-	-	-	21	-40	68	4.12	≤ 0.001	0.515	-
BA 3a right	-	-	-	-	-	-	-	-	-	-	-	-	-
BA 3b right	-	-	-	-	-	-	12	-40	68	4.46	≤ 0.001	0.242	-

Table 17: Local maxima regarding the task condition “somatosensory stimulation of the right foot”.

ROI	DCM Patients						Control subjects						ED
	MNI-coordinate			T-value	P-value		MNI-coordinate			T-value	P-value		
	x	y	z		uncorrected	FWE-c.	x	y	z		uncorrected	FWE-c.	(mm)
S1 left	-54	-25	38	3.51	≤ 0.001	0.969	-54	-25	38	6.22	≤ 0.001	**0.001***	0
S2 left	-48	-34	20	3.93	0.001	0.705	-57	-28	20	6.56	≤ 0.001	**0.001***	10.82
BA 1 left	-	-	-	-	-	-	-21	-40	74	4.49	≤ 0.001	0.222	-
BA 2 left	-54	-25	38	3.51	≤ 0.001	0.969	-54	-25	38	6.22	≤ 0.001	**0.001***	0
BA 3a left	-	-	-	-	-	-	-9	-37	68	4.23	≤ 0.001	0.416	-
BA 3b left	-9	-40	74	3.44	≤ 0.001	0.996	-9	-40	74	4.90	≤ 0.001	0.071	0
S1 right	-	-	-	-	-	-	-	-	-	-	-	-	-
S2 right	-	-	-	-	-	-	57	-22	20	4.17	≤ 0.001	0.464	-
BA 1 right	-	-	-	-	-	-	-	-	-	-	-	-	-
BA 2 right	-	-	-	-	-	-	-	-	-	-	-	-	-
BA 3a right	-	-	-	-	-	-	-	-	-	-	-	-	-
BA 3b right	-	-	-	-	-	-	-	-	-	-	-	-	-

Table 18: Functional hemispheric lateralization of cortical response.

	DCM Patients	Control subjects	P-value	
ROI	**mean AveLI ± SD**	**mean AveLI ± SD**	**uncorrected**	**FDR corrected**
Somatosensory stimulation of the left hand				
S1	-0.13 ± 0.63	-0.32 ± 0.42	0.446	0.659
S2	-0.04 ± 0.58	-0.05 ± 0.56	0.971	0.989
Whole hemisphere	0.09 ± 0.35	-0.08 ± 0.31	0.288	0.581
BA 1	-0.38 ± 0.70	-0.67 ± 0.31	0.271	0.581
BA 2	-0.04 ± 0.74	-0.17 ± 0.54	0.680	0.811
BA 3a	0.28 ± 0.77	0.05 ± 0.69	0.519	0.711
BA 3b	-0.04 ± 0.65	-0.20 ± 0.55	0.584	0.758
Somatosensory stimulation of the right hand				
S1	0.89 ± 0.08	0.76 ± 0.18	0.059	0.328
S2	0.82 ± 0.16	0.74 ± 0.23	0.351	0.581
Whole hemisphere	0.33 ± 0.23	0.26 ± 0.26	0.529	0.715
BA 1	0.72 ± 0.42	0.69 ± 0.27	0.837	0.926
BA 2	0.88 ± 0.12	0.82 ± 0.15	0.345	0.581
BA 3a	0.94 ± 0.10	0.69 ± 0.35	0.054	0.317
BA 3b	0.91 ± 0.12	0.84 ± 0.13	0.274	0.581
Somatosensory stimulation of the left foot				
S1	0.49 ± 0.52	0.27 ± 0.39	0.321	0.581
S2	0.16 ± 0.67	0.34 ± 0.30	0.490	0.690
Whole hemisphere	0.15 ± 0.31	0.00 ± 0.25	0.284	0.581
BA 1	0.36 ± 0.60	-0.07 ± 0.38	0.085	0.426
BA 2	0.50 ± 0.60	0.29 ± 0.48	0.550	0.734
BA 3a	0.66 ± 0.41	0.60 ± 0.55	0.767	0.888
BA 3b	0.63 ± 0.47	0.45 ± 0.30	0.354	0.581
S1	0.49 ± 0.52	0.27 ± 0.39	0.321	0.581
Somatosensory stimulation of the right foot				
S1	0.62 ± 0.32	0.74 ± 0.14	0.322	0.581
S2	0.53 ± 0.40	0.78 ± 0.15	0.106	0.432
Whole hemisphere	0.27 ± 0.22	0.28 ± 0.19	0.942	0.982
BA 1	0.25 ± 0.74	0.55 ± 0.23	0.253	0.581
BA 2	0.60 ± 0.38	0.83 ± 0.12	0.102	0.432
BA 3a	0.74 ± 0.52	0.92 ± 0.12	0.345	0.581
BA 3b	0.64 ± 0.50	0.82 ± 0.16	0.319	0.581

7.1.2. Supplementary Figures

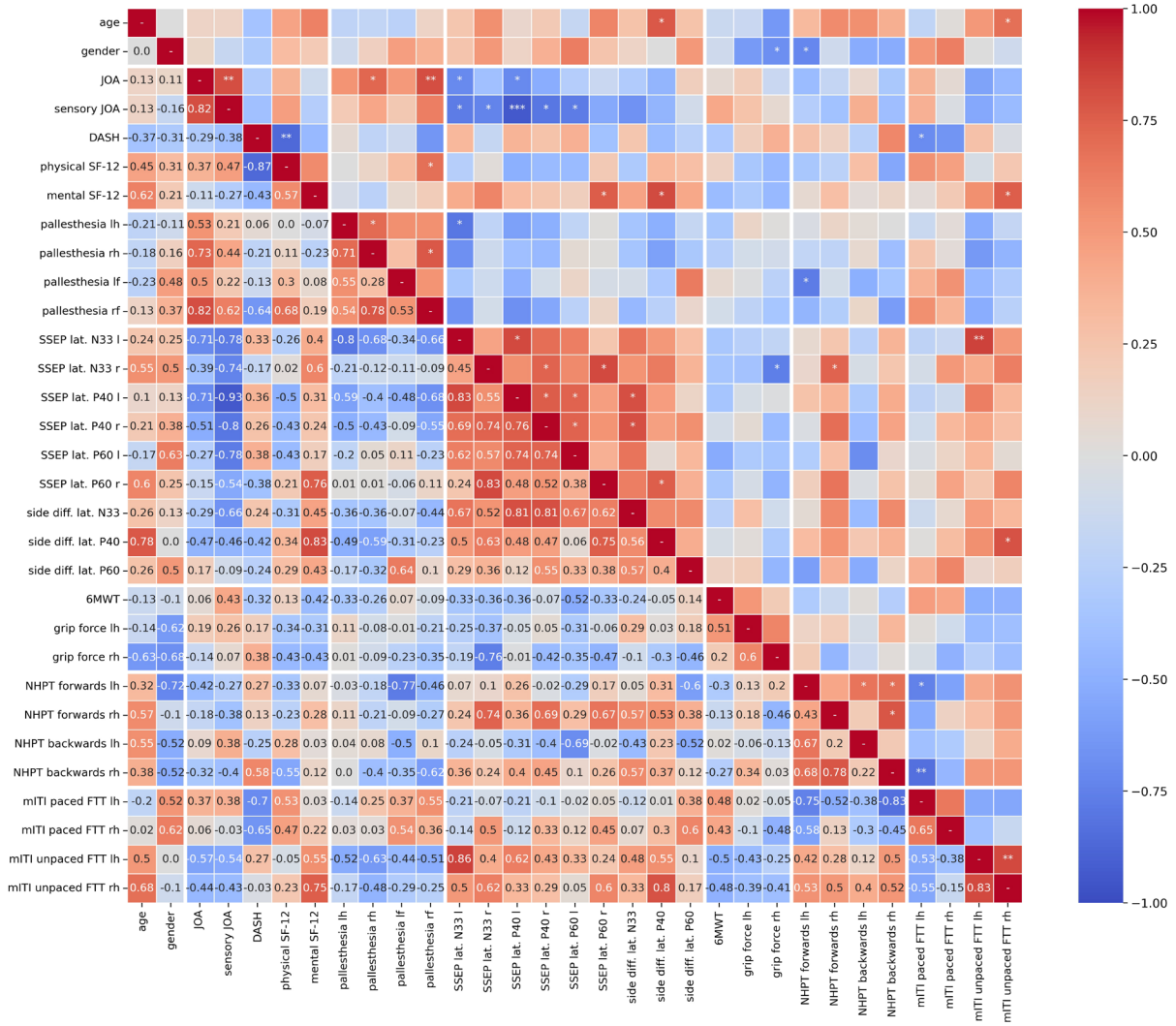

Figure 21: Correlation of clinical and demographic parameters. Spearman correlation was calculated pair-wise between the parameters acquired from the patients. The spearman correlation coefficients for each pair of parameters are given in the lower triangle of the correlation matrix. In the upper triangle, significant correlations are labeled as follows: *p ≤ 0.05, **p ≤ 0.01, ***p ≤ 0.001. Abbreviations: 6MWT (Six-Minute Walk Test), DASH (Disabilities of the Arm, Shoulder and Hand questionnaire), diff. (difference), FTT (Finger Tapping Test), JOA (Japanese Orthopaedic Association score), lat. (latency), lf (left foot), lh (left hand), mITI (mean intertap interval), NHPT (Nine-Hole Peg Test), rh (right hand), rf (right foot), SF-12 (Short Form 12 score).

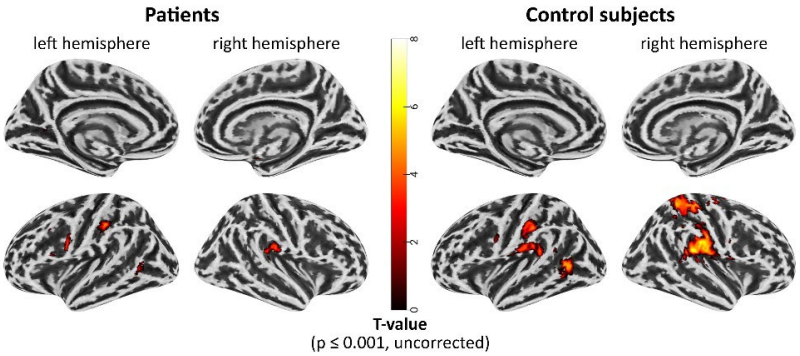

(a) Somatosensory stimulation of the left hand.

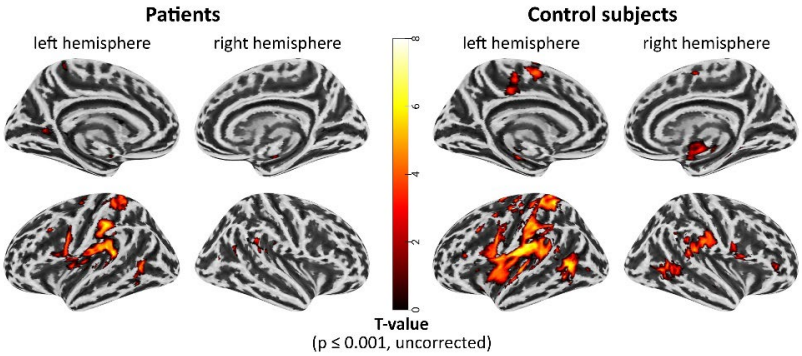

(b) Somatosensory stimulation of the right hand.

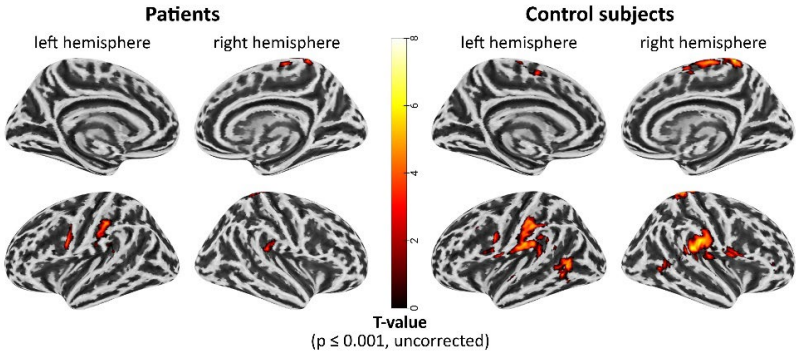

(c) Somatosensory stimulation of the left foot.

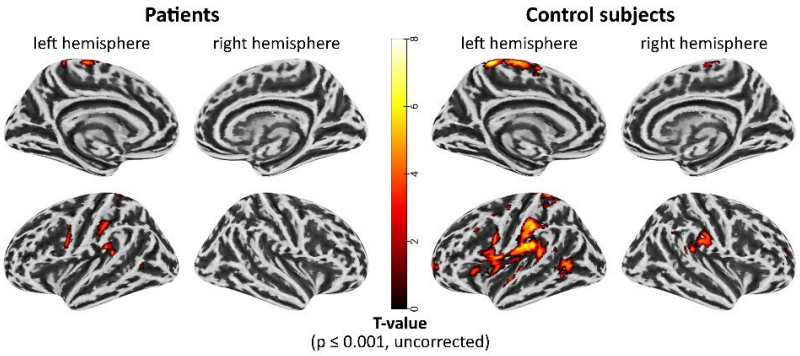

(d) Somatosensory stimulation of the right foot.

Figure 22: Blood oxygen level dependent responses to tactile stimuli at the group level. The inflated surface renderings show the effect of each task condition provided by the analysis of variance (ANOVA) ($p \leq 0.001$, no mask applied).

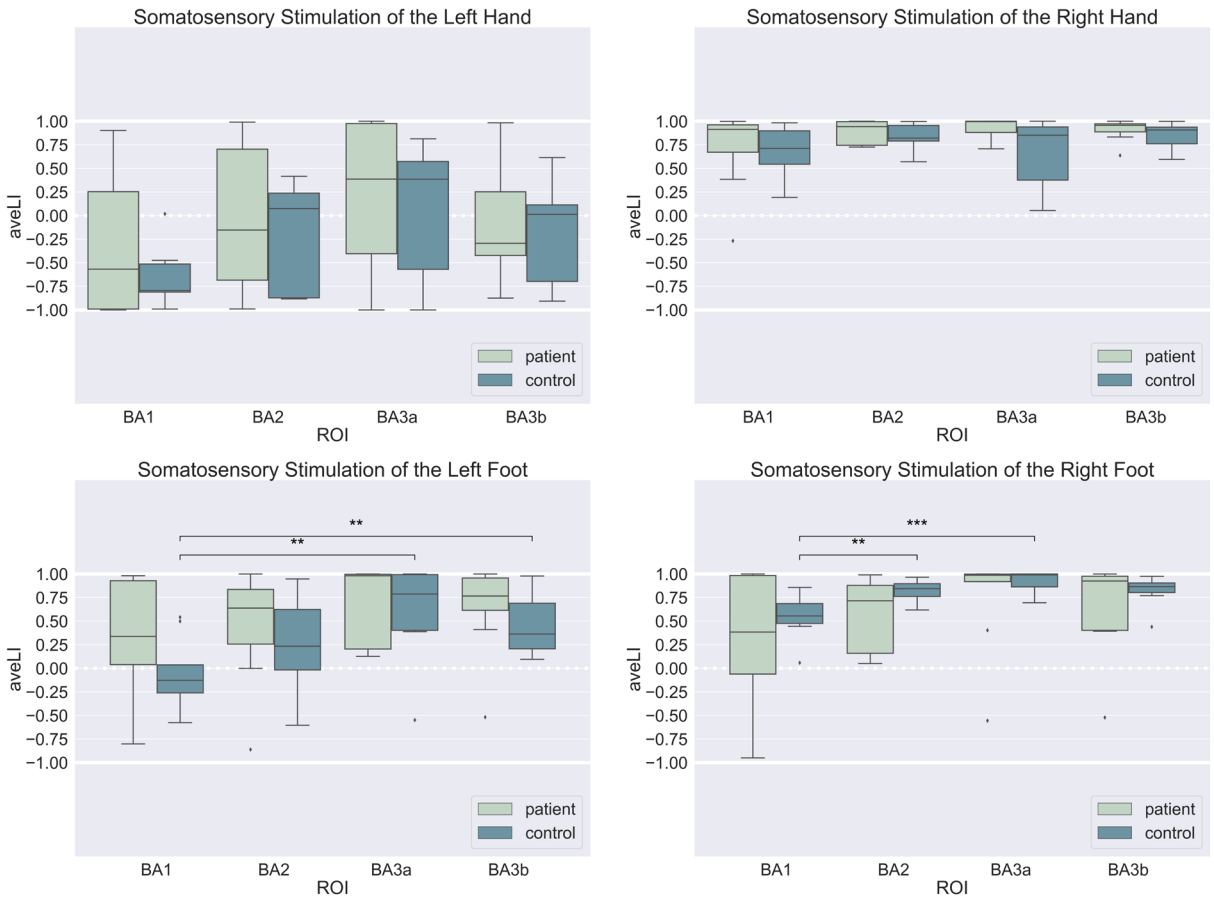

Figure 23: Hemispheric lateralization in the Brodmann areas of the primary somatosensory cortex. Average lateralization indices (AveLIs) are demonstrated for every group (patients: green, controls: blue), task condition and region of interest (ROI), respectively. Positive values indicate a lateralization of blood oxygen level dependent (BOLD) activity to the left hemisphere while negative values indicate a right hemispheric lateralization (*p ≤ 0.05, **p ≤ 0.01, ***p ≤ 0.001).

7.2. List of Figures

7.3. List of Tables

8. List of Publications

Conference Proceedings:

Oral Presentations:

Hams, L., Nettekoven, C., Kabbasch, C., Zdunczyk, A., Vajkoczy, P., Goldbrunner, R., Weiß Lucas, C. (2023). "Pre- and Postsurgical Functional Adaptations within the Somatosensory Cortex in Degenerative Cervical Myelopathy". 74th Annual Meeting of the German Society of Neurosurgery (DGNC), 25 - 28 June 2023, Tübingen/Stuttgart.

Nettekoven, C., Hams, L., Lichtenstein, T., Zdunczyk, A., Vajkoczy, P., Goldbrunner, R., Weiß Lucas, C. (2022). "Cortical Plasticity of Motor and Somatosensory Areas in Degenerative Cervical Myelopathy". 73rd Annual Meeting of the German Society of Neurosurgery (DGNC), 29 May - 1 June 2022, Cologne.

Hams, L., Nettekoven, C., Lichtenstein, T., Zdunczyk, A., Vajkoczy, P., Goldbrunner, R., Weiß Lucas, C. (2021). "Functional processing of somatosensory stimuli in degenerative cervical myelopathy". 1. Tagungswoche der Sektionen der Deutschen Gesellschaft für Neurochirurgie, 27 September - 1 October 2021, Göttingen.

Hams, L., Nettekoven, C., Lichtenstein, T., Zdunczyk, A., Vajkoczy, P., Goldbrunner, R., Weiß Lucas, C. (2021). "Adaptation of the somatosensory cortex in patients suffering from degenerative cervical myelopathy". 72nd Annual Meeting of the German Society of Neurosurgery (DGNC), 6-9 June 2021, Erfurt (digital).

Hams, L., Nettekoven, C., Lichtenstein, T., Zdunczyc, A., Vajkoczy, P., Goldbrunner, R., Weiß Lucas, C. (2021). "How Degenerative Cervical Myelopathy Affects Functional Imaging Correlates of the Somatosensory Cortex". 65th Congress of the German Society of Clinical Neurophysiology and Functional Imaging (DGKN), 10-12 March 2021, Frankfurt on the Main (digital).

Poster Presentation:

Nettekoven, C., Hams, L., Lichtenstein, T., Zdunczyk, A., Vajkoczy, P., Goldbrunner, R., Weiß Lucas, C. (2022). "Functional Adaptations of the Sensorimotor Cortex in Degenerative Cervical Myelopathy". 66th Congress of the German Society of Clinical Neurophysiology and Functional Imaging (DGKN), 10-12 March 2022, Würzburg.